Doctoral Dissertation (Shinshu University)

Synthesis and characterization of two-way shape memory polymers

双方向形状記憶ポリマーの創製と性能評価に関する研究

September 2020

Jin Hui

Abstract

Shape memory polymers (SMPs) have drawn increasing attention because they can respond to specific external stimulus by changing their own shape. They are many types of stimulus methods, such as temperature, electricity, magnetism, water, UV light and pH. SMPs can be formed from a permanent shape to a temporary shape that have their many novel properties and great potential are expected to have applications in actuators and sensors, biomedical devices, aerospace technology and textiles. The types of the shape memory effect (SME) include the one-way shape memory effect (1W-SME), two-way shape memory effect (2W-SME) and multi-shape memory effect (multi-SME). One-way shape memory polymers (1W-SMPs) only remember their shape upon external stimulus and programming once leads to only one shape memory cycle, which limits their application as actuators and for artificial intelligence. More than one programmed shape in the steady state representation of the shape memory cycle is known as multi-SME, multi-shape memory polymers also show the 1W-SME.

In recent years, two-way shape memory polymers (2W-SMPs) have attracted considerable interest because they are fully reversible following exposure to external stimuli without the necessity of reprogramming. Several pioneering works have contributed to production of materials with two-way shape memory behavior, including laminated polymer composites, liquid crystal elastomers, and crosslinked crystalline polymers. Laminated polymer composites comprising two layers bonded with an adhesive agent are limited by the weak interlayer strength and cyclicity. Furthermore,

the complicated synthesis of liquid crystal elastomers is still challenge, which limits their mass production. Thermal crosslinking reaction using a crosslinking agent to crosslink semicrystalline polymers has attracted much attention because of the good two-way shape memory reversibility, low cost, and simple synthesis process.

The aim of this research is to synthesize a novel two-way shape memory materials using thermal crosslinking reaction which exhibits the full two-way shape memory reversibility following exposure to external stimuli of temperature. The finding for this study will contribute to their application as soft material actuators and artificial muscles in various fields.

The three significant parts in this dissertation are given as follows:

(1)PEVA/BPO two-way (reversible) chemically crosslinked semi-crystalline shape memory polymers with various crosslinking densities from poly(ethylene-co-vinyl acetate) (PEVA) and various contents of benzoyl peroxide (BPO) were synthesized by thermally crosslinking reaction via micro twin-screw extruder and hot-pressing machine. PEVA containing various contents of BPO —i.e., 0wt% to 14wt%, are indicated by PEVA-B0 to PEVA-B14. The network properties related to the two-way shape memory behavior of PEVA/BPO samples were determined by the gel content. The gel content increased markedly from 69.77% to 91.25% with an increase in the BPO content from 1 wt% to 4 wt%, whereas it increased slowly from 91.25% to 95.82% as the BPO content increased from 4 wt% to 12 wt% because at higher gel contents there is a smaller change in the gel content with increasing BPO content. The developed materials were capable of reversible shape change, and we ensured that the "switch on"

temperature, which triggers shape change, was within a reasonable range. The recovery ratio (R_{rec}) increased markedly as the BPO content increased from 4 wt% to 10 wt%. Each PEVA-B10 (PEVA with 10wt% BPO) sample had optimal actuation performance and an excellent recovery ratio of over 99%. The non-crosslinked sample (PEVA-B0) did not recover during the heating, and did not exhibit two-way shape memory behavior. PEVA-B1 demonstrated weak two-way shape memory behavior and did not exhibit good thermomechanical recyclability. These results indicate that the crosslinking using BPO plays an important role in ensuring samples return to their original shape, and the PEVA/BPO compositions with high crosslinking densities had significantly elevated recovery ratios. As a result, the developed PEVA/BPO materials were adequately soft and had good mechanical properties, even at large deformation.

(2) The 2W-SME of PEVA/BPO polymers has been achieved under both constant stress and stress-free conditions. The relationship between the initial prestretching strain ($R_{prestretch}$) and recovery strain (R_{rec}) was the main reason for achievement of the stress-free 2W-SME of PEVA/BPO polymers. Furthermore, three different types of stress-free two-way shape memory behavior were observed during the TMA cycles: the ideal stress-free 2W-SME ($R_{rec} = R_{prestretch}$), the weak stress-free 2W-SME ($R_{rec} > R_{prestretch}$), and no stress-free 2W-SME ($R_{rec} < R_{prestretch}$), which can be controlled by varying R_{rec} using different setting temperature (T_{set}) during the recovery process. More importantly, the two-way shape memory driving force and recovery force, as one of the key indicators for two-way shape memory materials, was investigated, and they significantly change depending on the BPO content. The clear two-way shape memory

performance with clear driving and recovery force was observed for PEVA-B10. The sample with high BPO content shows excellent high-temperature creep resistant performance. A highly crosslinked structure can suppress viscous flow and provides sufficient force to allow the sample to recover its initial shape after crystal melting. Therefore, the PEVA/BPO samples are able to contract during heating. 2D-WAXS and DSC tests indicated that the crystalline structure led to oriented growth of crystals under applied stress, and crystallization led to elongation upon cooling.

(3) Two-way reversible shape memory PEVA/BPO foams with porous three-dimensional structures were fabricated using a salt-leaching and thermo-crosslinking technology. Various pore sizes of PEVA/BPO porous foam were obtained using different NaCl particle sizes. The different reversible shape changes in various pore size of PEVA/BPO foam upon exposure at low/high temperature under constant compression conditions were investigated using thermomechanical analysis (TMA). The ideal two-way shape memory performance can be clearly observed in the large pore size sample PEVA/BPO-450 under the same prestreching strain at the crosslinking temperature of 200 °C. The morphology was characterized by scanning electron micron microscopy (SEM) and X-ray microcomputed tomography scanning (μCT) analysis. The compression behavior of PEVA/BPO foam was also investigated. These properties of two-way reversible shape memory PEVA/BPO foams could qualify their use as lightweight porous actuators in artificial intelligence and aerospace applications.

Contents

Contents

Chapter 1

General Introduction

。

1 General Introduction

1.1 Shape memory polymers (SMPs)

1.1.1 Introduction

Shape memory polymers (SMPs) as a new class of smart materials can respond to specific external stimuli [1-9], such as temperature [10-12], water [13-16], light [17-19], electric filed [20-23], magnetic field [24-27], solution [28, 29] and pH [30, 31]. SMPs have the ability to memorize a permanent shape, be manipulated and fixes to a temporary and dormant shape under specific conditions, they are soft materials that have the advantages of light weight and excellent active deformation, and they have drawn considerable research interest in last few years because of their applications in actuators [32] and sensors [33], and in aerospace technology [34], textiles [35], and biomedical applications [36, 37] (**Figure 1.1**).
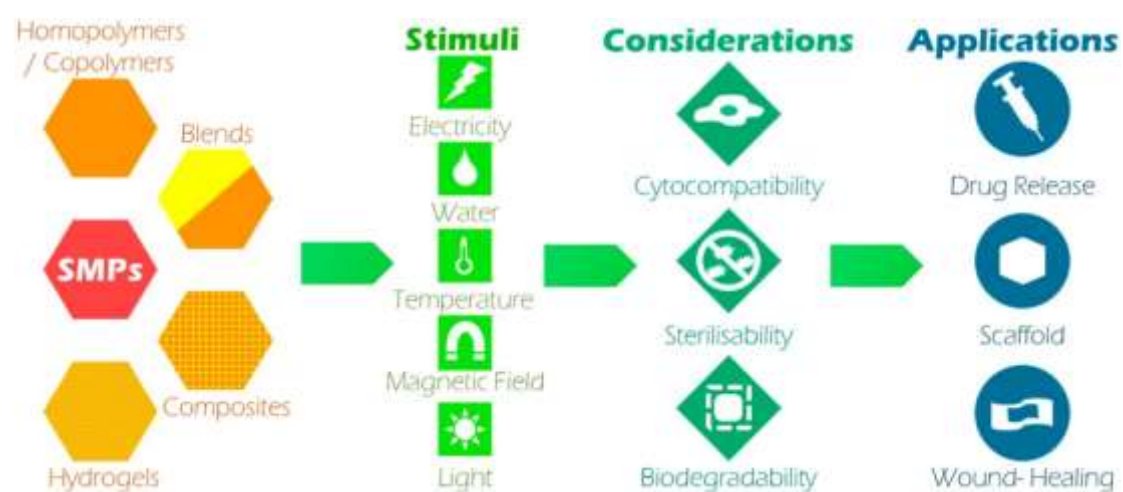
Figure 1.1 A review of shape memory polymers (SMPs) [158].

1.1.2 Various stimulation of SMPs

1.1.2.1 Temperature stimulation

SMPs can significantly change their shape upon variation of environmental conditions such as temperature. In the past decade, many researchers have explored on the mechanism, shape recovery and thermo-mechanical properties of SMPs. Temperature stimulation is the most common, basic and direct way to trigger shape change. The capacity of shape memory effect (SME) has resulted in rapid development of thermo-responsive SMPs based on deployable space structures and medical devices. Lendlein et al. reported that a series of degradable thermoplastic polymers, which served as structural concept to tailor macroscopic properties with different molecular parameters, were applied for potential applications [38, 39].

1.1.2.2 Electric stimulation

SMPs with electrically conductive carbon materials as fillers such as carbon nanotubes, carbon black, carbon nanofibers or graphite, enabled electrically conductive SMPs [40, 41]. If a voltage is applied to the conductive SMPs filled with enough electrically conductive ingredients, resistive joule heating may heat the materials to trigger the SME. The internal resistive joule heating method by electricity, as compared with direct external-heating, has many advantages such as convenient, uniform heating, and remotely controllable. The conductive fillers can also improve the thermal conductivity of SMPs which contribute to a fast response. This electricity triggered SME is especially useful for applications where direct heating is not possible such as

self-deployable aerospace structures, implanted biomedical devices, actuators and sensors.

1.1.2.3 Magnetism stimulation

The magnetically induced shape recovery of shape memory polymer composites could be realized by incorporating magnetic nanoparticles in SMPs. The magnetic particles improved the mechanical properties and also enabled the induction of the SME in an alternating magnetic field [42]. In general, the incorporated magnetic particles consisted of iron, iron oxide, nickel, or cobalt compounds and could generally heat in an alternating magnetic field by hysteresis losses, eddy current losses or other relaxation losses depending on the nature and size of the particle. Magnetic driving is a typical approach without direct contact, and this heating method is highly suitable for medical instruments such as implanted shape memory polymer supporters [43].

1.1.2.4 Light stimulation

Light-induced stimulation of SMPs has been realized through the incorporation of reversible photoreactive molecular switches [44, 45]. This stimulation is independent of any temperature effects and must be differentiated from the indirect actuation of the thermally induced shape memory effect. For light-induced SMPs, the infrared laser stimulation of the SMP is interesting for sensor and actuator system as well as for medical applications. There are mainly two mechanisms in light induced SMPs, photochemical reactions leading to deformation and employment of particles that can covert light to heat.

1.1.2.5 Solution/Water stimulation

Additionally, solvent can serve as a method of stimulating the shape recovery process. The doped solutions reported to drive shape memory polymers include a shape memory polymer with a glass state transformation and a hydrogen bond-locked shape memory polymer. Water driven actuation of SMPs was first brought up in 2005 by Huang [13]. The mechanism has attracted board attention since then. In general, water or solvent molecules could infiltrate into the SMPs. Due to the plasticizing effect of water or solvent on SMPs and increase of the flexibility of macromolecules, glass transition temperature drops upon addition of even a low amount of water. When glass transition temperature approaches to the environment temperature, the recovery process of water-induced SMPs is triggered.

1.1.3 Type of shape memory effect (SME)

1.1.3.1 One-way shape memory effect (1W-SME)

Scientist once thought that one-way shape memory effect (1W-SME) was not good enough for many applications because they were the most simple and common SME for SMPs, and they were only remembering their shape upon external stimulus, and programming once leads to only one shape memory cycle, which limits their applications as actuators or for artificial intelligence. Thus, they began to explore two-way shape memory effect (2W-SME) of polymers. 1W-SME has their original shapes predefined in the manufacturing process, while temporary shapes can be varied based on different shape memory programming processes. There are several types of current

evaluation methods for characterizing 1W-SME, such as cyclic tensile investigation [46], strain recovery process [47], bending tests [48] and shrinkage determination[49]. Considerable effort has been devoted to determining the factors that may have an influence on the shape memory performance of SMPs of 1W-SME. Different influence factors have been studied using common 1W-SME system (shape memory polymer polyurethane (SMPU) and SMPU ionomers), including the segment contents [50, 51], the molecular weight and crystallization of soft segments [52], ionic group contents [53], thermo-mechanical cyclic conditions (i.e., deformation and fixing speed [54] and maximum strain [46]), and processing conditions [55].

1.1.3.2 Multi-shape memory effect (multi-SME)

Recently, it has been reported that polymers with a broad thermomechanical transition temperature range can demonstrate a multi-shape memory effect (multi-SME), where multi-SME can remember more than two temporary shapes. Xie et al. used the board glass transition (T_g) of T_g-type polymers to demonstrate multi-SME. They also systematically investigated the influence of thermomechanical conditions on these multi-SME [56]. All of these publications on multi-SME will not only meet the requirements of increasingly complex applications but will also further stimulate the development of shape memory functions of SMPs.

1.1.3.3 Two-way shape memory effect (2W-SME)

In recent years, two-way shape memory polymers (2W-SMPs) have attracted considerable interest because they exhibit reversible changes of shape with change in

external stimuli without the necessity of reprogramming that is required for many applications, such as actuators and artificial muscles. In addition to classical approaches such as shape memory alloys (SMAs), many polymeric materials and approaches are under active investigation, including liquid crystal elastomers (LCEs), crosslinked crystalline polymers and laminated polymer composites.

1.1.4 Application of SMPs

1.1.4.1 Application of SMPs in aerospace technology

Because of their stable single-deformation ability, shape memory materials have attracted board attention in all kinds of aerospace expansion structures. Fiber-reinforced SMPs due to the low mass, high toughness and large deformation, could be made into matrices of large expansion structures [57] (such as reflective antennas), which achieved the combination of driving devices and structural materials. It has now been proven that epoxy resin-based and cyanate ester-based SMPs have good tolerance of the outer-space environment. Furthermore, because of their outstanding thermo-dynamic properties (especially the tolerance of high and low temperature cycling) and stable chemical properties, polyimide-based SMPs have been identified as ideal candidates for future applications of SMPs in space.

1.1.4.2 Application of SMPs in smart textiles

Shape memory polymer fibers can be obtained by moist spinning, melt spinning or electric spinning to develop smart textiles that respond to thermal stimulus [58]. SMPs can be used for smart textiles, clothing and related products in the form of shape

memory fibers, shape memory yarns and shape memory fabrics [59, 60]. Shape memory finishing chemicals and technologies for cotton fabrics, wool fabrics and garment finishing was investigated. Shape memory finishing fabrics can be produced with coating shape memory emulsion or combining shape memory film. When washed in hot water or dried at temperatures higher than T_g, their wrinkles will disappear and they can recover the original flat shape. It is also expected that the smart fibers may be used for novel fiber sensors or advanced medical usage.

Significant progress has been made in the manufacture of textile fibers from SMPs through common spinning methods. It is easy to make a polymer fiber, as long as the polymer has adequate molecular weight, sufficient viscosity or a suitable melting point, but it is difficult to make a fiber for textiles. The durability, elongation, tactile properties and processability of fibers are the main factors that influence their final end uses. Shape memory polymer fibers include micro fibers, nanofibers [61] and non-wovens [62].

1.1.4.3 Application of SMPs in biomedical applications

SMPs have been of interest to the medical field from the beginning, which can be dated back to the fourth decade of the last century. Compared with metal materials, polymers offer suitable recovery force as well as good biological adaptability. Many SMPs also have the ability to be decomposed in the body, such as polyurethane [63], polycaprolactone [64], polyether urethane [65], and polylactic acid [66, 67]. SMPs and their composite materials have been used in many biomedical instruments, as described in the reports of prototypes and experiments. Their uses include thrombus cleaners, surgical sutures, intravascular stents, aneurysm occludes and orthodontic fixers (**Figure**

1.2).

A polymer vascular stent with an SMPs as the drug delivery system, the use of applications of this polymer stent was demonstrated in pre-trials. The use of the SMPs stent as a drug delivery system leads to significant reduction of restenosis and thrombosis. An improved biological tolerance in general is expected when using biocompatible shape memory polymer materials. A piece of original curved SMPs is straightened and then inserted into a living cell. Upon absorbing moisture inside the cell, the SMPs recovers its original shape. As the recovery strain in solid or porous SMPs is on an order of hundred percent, it becomes possible to make cell or sub-cell sized machines using the thermo/moisture-responsive SMPs and then deliver the machines into living cells for operation controlled by an outside laser beam.
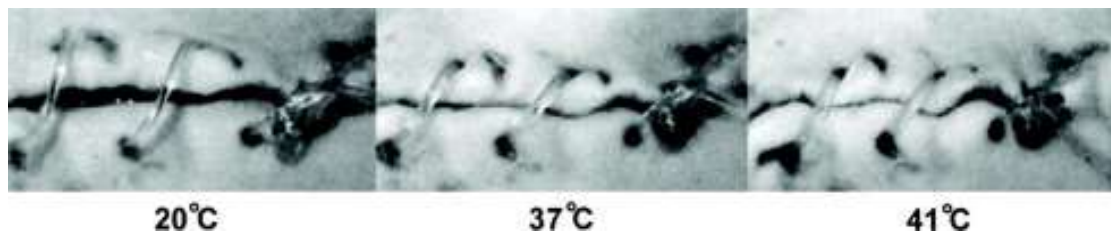
Figure 1.2 Degradable shape-memory suture for wound closure. The photo series from the animal experiment shows (top to bottom) the shrinkage of the fiber while the temperature increases from 20 °C to 41 °C [36].

1.1.4.4 Other applications

Some of deployable structures are as follow: thermally insulated deployable shelters, hubs, prefabricated walls, slabs, access denial barriers and walls, automatic disassembly of electronic products [68, 69], reusable shape-memory polymer mandrel [70]. SMPs packaging of thermal sensitive products, and sensors/drug/food air delivery

systems. A potential application is to use four dimensions (4D) printing of SMPs, which have unique or even irreplaceable advantages in many fields. For example, through the rational design shapes of application, efficiency of production and transportation can be improved. Another example is the production of soft drive components, and 4D print product can be used directly without the need to introduce complex mechanical components.

SMPs have been used in automobile engineering, and many interesting products have been developed. Some interesting applications of SMPs include seat assemblies, reconfigurable storage bins, energy absorbing assemblies, tunable vehicle structures, hood assemblies, releasable fastener systems, airflow control devices, adaptive lens assemblies and morphable automotive body molding [71-74]. During the development of morphing aircraft, finding a proper skin under certain criteria is crucial. Generally, a wing skin is necessary, especially for the wing of a morphing aircraft. Researchers focus their works on investigating proper types of materials that are currently available to be used as a skin material for a morphing wing. In this case, the SMPs show more advantages for this application. It becomes flexible when heated to a certain degree, and then returns to a solid state when the stimulus is terminated. Since SMPs hold the ability to change its elastic modulus, they could potentially be used in the mentioned concept designs.

1.2 Two-way shape memory polymers (2W-SMPs)

1.2.1 Introduction

In recent years, 2W-SMPs have attracted considerable interest because they are fully reversible following exposure to external stimuli without the necessity of reprogramming that is required for many applications, such as actuators, sensors, and artificial intelligence. 2W-SME has been studied systematically on LCEs. One of the possible applications of shape-memory LCEs is the development of responsive smart actuators [82, 157]. Thermal-active crosslinked semi-crystalline polymers can also show 2W-SME under constant stress and stress-free conditions [83-97]. The underlying two-way shape memory mechanism is that cooling induced crystallization of semi-crystalline polymer films results in elongation under a tensile load, subsequent heating to melt the network yields contraction (shape recovery).

1.2.2 Type of 2W-SMPs

1.2.2.1 Two-way shape memory laminates

Several pioneering works have contributed to production of materials with two-way shape memory behavior, including two-way shape memory laminates [75-80], LCEs [81, 82], and crosslinked crystalline polymers [83-98]. Much research has concentrated on developing 2W-SME using composite technologies. The previous two-way shape memory polymer laminated composites mainly focused on SMAs and polymer composites. Laminated polymer composites comprising two layers bonded with an adhesive agent are limited by the weak interlayer strength and cyclicity. In the two-way shape memory materials by laminating an SMPs with elastic polymer, the 2W-SME was ascribed to the release of elastic strain of SMPs layer upon heating, and the

recovery of elastic strain induced by the bending force of elastic polymer layer upon cooling. The modulus of SMPs and SMAs change significantly at the switching or phase transition temperature. If they are laminated together, the unbalance of the internal stress in the composites as a result of changing environmental temperature can produce the driving force for the 2W-SME.

1.2.2.2 Liquid crystal elastomers (LCEs)

Thermo-sensitivity in two-way LCEs resulted from a coupling between the liquid crystalline ordering of mesogenic moieties and the elastic properties of the polymer. When a LCEs is heated toward the anisotropic–isotropic phasetransition temperature, the mesogens become disordered, and the film generally contracts. When the temperature is lowered below the phase-transition temperature, the LCEs will expand back to its original size [99-101]. However, the complicated synthesis of LCEs is still challenge, which limits their mass production. Liquid crystal two-way shape memory elastomers are able to produce high strain up to 300%, and they are still costly in addition to their unstable shape changing behavior.

1.2.2.3 Crosslinked crystalline polymers

Thermal crosslinking is an effective way of achieving two-way shape memory behaviors because of the good two-way shape memory reversibility, low cost, and simple synthesis process.

Mather's group reported two-way reversible shape memory in a semi-crystalline network. They investigated crosslinked poly(cyclooctene) (PCO) [76, 77], and its related

2W-SME by varying the concentration of the crosslinking agent dicumyl peroxide (DCP). Lendlein and co-workers [85, 86] reported preparation and characterization of crosslinked semi-crystalline polymers exhibiting two-way reversible shape memory behavior. Crosslinking of poly(ethylene-*co*-vinyl acetate) (PEVA) resulted in free-standing reversible temperature actuators with various vinyl acetate contents and crosslinking densities, which allow physical adjustment of the actuation temperature [87]. Crosslinked blends of the two crystallizable polymers poly(ε-carpolactone) (PCL) and PEVA resulted in noncontinuously responding polymeric actuators [88]. Pandini et al. reported the 2W-SMPs response of semi-crystalline PCL based on polymer networks [89]. In addition, they recently reported nonwoven fibrous mats based on semi-crystalline networks prepared from crosslinked PCL (cPCL) by combining electrospinning and sol-gel reactions and investigated the two-way shape memory behavior [90]. Xie and co-workers [91] and Qian et al. [92] both used semi-crystalline PEVA crosslinked by DCP to synthesize a 2W-SMPs. The findings of Xie's group showed how crosslinking affects the 2W-SME in different ways to the 1W-SME. Dong et al. discussed the two-way shape memory properties and corresponding structural origin of cPCL with different gel contents obtained by using different weight percentages of benzoyl peroxide (BPO) [93].

Several interesting studies have been conducted on PEVA or PEVA/PCL blends crosslinked with DCP. The examples include research into non-continuously responding polymeric actuators [88], the triple-shape effect [102, 103], shape-memorizing micro-optics [98], two-level shape changes of polymeric micro cuboids and two-way

shape memory artificial muscle [96].

1.2.3 Two-way shape memory crystalline polymers under constant stress conditions

1.2.3.1 Chemically crosslinked crystalline polymers

2W-SME can be achieved in semi-crystalline polymer networks, the 2W-SME under constant stress was first reported by Chung et al. in 2008 [83]. 2W-SMPs are based on the principle of crystallization-induced elongation (CIE) that occurs during cooling and melting-induced contraction (MIC) during heating under constant stress. During cooling to low temperature under constant stress, the CIE was attributed to the formation of crystallites in the load direction. When heated from low temperature to high temperature, the increased elongation caused by the CIE can be reversed by the MIC. Thus, by applying a constant stress, crystals are formed along a single preferred orientation in these systems, and the semi-crystalline phase shows reversible shape changing. The mechanism of CIE was investigated by wide-angle X-ray diffraction (WAXD) techniques, and the results suggested that by increasing the stress, crystallization was promoted increasingly along the uniaxial axis, thus leading to greater elongation.

Subsequently, a series of systems based on semi-crystalline PCL segment, such as the polyhedral oligomeric silsesquioxane (POSS)/PCL networks [105], SMPU [106], and chemically cPCL [107], have been shown to exhibit their 2W-SME under an appropriate

13

constant tensile load. Westbrook et al. [84] investigated and developed a one-dimensional constitutive model to describe the main mechanism of observed shape memory effect which is due to stretch induced crystallization. Subsequent research has found that cPCL [89, 108], crosslinked poly(ethylene-co-vinyl acetate) (cPEVA) [91, 92], and crosslinked polyethylenes (cPE) [109, 110] exhibited 2W-SME under constant stress conditions. Tao Xie group synthesized semi-crystalline PEVA crosslinked by DCP, it was found that a reversible shape transition could be stimulated using temperature, and how crosslinking affected 2W-SME in different ways to 1W-SME.

1.2.3.2 Physically crosslinked crystalline polymers

Bothe et al. [111] reported the phase-segregated poly(ester urethane) (PEU) exhibits two-way shape changes under various constant stresses. Most distinct actuation (expansion on cooling and contraction on heating) can be detected between +60 °C and −20 °C when the maximum stress applied during a thermo-mechanical pretreatment approached the point where deformation-induced crystallization of the poly(1,4-butylene adipate) (PBA) soft segment sets in. The driving forces for the strain-related two-way shape changes consist of PBA crystallization and PBA melting-induced entropy elasticity. At low constant stresses (<1.5 MPa), entropy elasticity also contributes to specimen expansion on cooling. Hong et al. [112] reported novel findings showing that two-way shape memory behavior can be imparted to SMPU using a thermo-mechanical treatment, i.e., imposing a constant stress on them after their temporary shaping.

1.2.4 Two-way shape memory crystalline polymers under stress-free conditions

1.2.4.1 Polymer laminates

Two-way shape memory polymer composites based on pure polymeric materials by layer techniques (similar to bimetals) were reported [75]. Hu et al. achieved reversible bending and unbending behavior in pure shape memory polymer composites prepared using two types of one-way shape memory polymer films [113]. The driving force of the 2W-SME resulted from a combination of the recovery force in the shape memory polymer layers during heating and the elasticity or stiffness of the other polymer layers. Most recently, Qi et al. developed a pure two-way shape memory polymer laminated composite by embedding pre-stretched SMPs into an elastomeric matrix. This resultant composite can show 2W-SME in response to changes in temperature, without a constant external load. A transversal actuation of 10% in actuator length was achieved [114]. This work indicates that 2W-SME can be more simply performed in SMPs. Compared with two-way SMAs and polymer laminated composites, these shape memory polymer composites are capable of much larger recoverable strains, and their reversible deformation is easily controlled by their hardness, thickness and deformation ratio of the shape memory polymer layers. Moreover, their 2W-SME can be simply performed without any external stress.

1.2.4.2 Chemically crosslinked crystalline polymers

Sheiko et al. [97] presented a general strategy for enabling reversible shape transformation in semi-crystalline shape memory materials, which exhibits two-way reversible shape memory behavior under stress-free conditions. Shape reversibility is achieved through partial melting of a crystalline scaffold which secures memory of a temporary shape by leaving a latent template for recrystallization. This behavior is neither mechanically nor structurally constrained, thereby allowing for multiple switching between encoded shapes without applying any external force, which was demonstrated for different shapes including hairpin, coil, origami, and a robotic gripper. Lendlein and coworkers [87] reported temperature-memory polymer actuators (TMPAs) based on cross-linked copolymer networks exhibiting a broad melting temperature range (ΔT_m) are presented, which are capable of a long-term temperature-memory enabling more than 250 cyclic thermally controlled actuations with almost constant performance. Chen qian et al. [92] proposed semi-crystalline SMPs exhibit 2W-SME under constant stresses and stress-free conditions through CIE upon cooling and MIC upon heating.

1.2.4.3 Physically crosslinked crystalline polymers

Bothe et al. reported a thermoplastic polyurethane elastomer completely stress-free, bidirectional motion. They applied training, consisting of extensive tensile deformation in the specimen's viscoelastic state, initiating deformation-induced crystallization. Once unloaded, thermo-reversible specimen expansion and contraction

could be detected. Maiti et al. [116] reported 2W-SMPs in polyurethane and to assign two functions to two different structural domains which are connected to each other in an alternative manner at the molecular level. The soft segments of the polyurethane acts as actuator domains which expand during cooling to fixed temperature (T_{fix}) and collapse on heating at intermediate temperature (T_{rev}), and the hard segments not only act as geometry determining domains which provide a skeleton at T_{rev} but also help to crystallize the actuator domains on cooling.

1.2.5 Application of 2W-SMPs

2W-SMPs shows the full reversibility upon external stimuli without the necessity of reprogramming that required for many applications. In recent years, actuators utilizing 2W-SMPs as a gripper and release system for remote and precise manipulation of small objects have attracted considerable interest [87, 97, 117]. 2W-SMPs under constant stress and laminated composites, which are good candidate to achieve bending actuation [118, 119]. The smart textile applications of actively moving polymers being developed rapidly have drawn wide attention, which summarized from the fiber spinning (including wet spinning, melt spinning and electro-spinning), fabric manufacturing, shape memory finishing technologies and water vapor permeability investigation [120]. The functionality, combined with the good biocompatibility of 2W-SMPs, is a good candidate for biomedical applications because they are fully reversible following exposure to external stimuli without the necessity of reprogramming. The development of 2W-SMPs and two-way reversible shape memory composites opens the possibility of incorporating 2W-SMPs into device design, which can lead to vast

technological improvements in the biomedical field.

1.3 Shape memory polymer foams

1.3.1 Introduction

Shape memory polymer foams with three-dimensional (3D) porous structures has been extensively investigated for aerospace, biomedical [121, 122] and self-healing [123-125] applications. A wide range of applications [126, 127] can be expected due to the materials' low mass, highly compressible, and self-deployable qualities, such as solar sail, and foldable microcars and airplane wings for specific flight requirements. Numerous methods were used in fabricate porous foam, such as gas foaming, particulate leaching, electro-spinning, phase separation, emulsion templating, and solid-state foaming.

Due to lightweight with a significant shape recovery, shape memory polymer foams can be used for quick molding into a particular shape [138]. Porous SMPs have a unique advantage as biomaterials because they can be implanted via minimally invasive procedures and undergo geometric changes after implantation [137]. For tissue engineering applications, porous SMPs can be designed to serve as self-fitting scaffolds for tissue growth. Some stimulus– responsive hydrogels are also considered to be porous SMPs.

1.3.2 Synthesis of shape memory foams

1.3.2.1 Particulate leaching

Particle leaching is a fabrication technique that provides porous scaffolds with

well-interconnected cells [128, 129]. It consists of leaching solid particles out of a polymer system. Salt particles, with a fixed diameter, are mixed into the polymer and solvent solution to ensure uniform distribution. The solvent is then removed via airdrying, vacuum-drying, or freeze-drying, leaving behind the salt particles embedded into the polymer matrix. The polymer and solid composite were further immersed in water to dissolve the salt particles, leaving behind a porous, interconnected polymer scaffold. The porosity and cell size are dependent on the particle concentration and diameter, respectively.

Most particle leaching techniques use salts, however, other particles such as sugar, ammonium chloride, sucrose, starch, paraffin, and gelatin particles have also been reported [130, 131]. When the porous SMPs is manufactured by taking advantages of these capabilities, it is expected to be used as an intelligent material that is capable of heat insulation under high temperature conditions and shape memorization. Porous SMPs is manufactured generally by the process of chemical foaming. However, the salt leaching method is widely used to manufacture foam for biomaterials. This method makes the manufacturing process simple and helps to readily control the pore size and the foaming process does not include any chemical blowing agents [139, 140].

1.3.2.2 Gas foaming

Gas foaming of polymers is a process that is widely used in industry for the preparation of e.g. expanded polystyrene, polyvinyl chloride foams, but it can also be applied for the preparation of scaffolds. Foaming can be carried out by reacting the components or releasing the gas which is a product of the thermal degradation of the

gas-foaming agent. This technique is rarely used for the fabrication of scaffolds, because it is hard to control pore diameter and the average pore diameter is too large to allow adequate cell proliferation [134]. Another method of foaming polymer is introducing gas into the melted polymer. The melted polymer is pressurized at high pressure with gases such as carbon dioxide, flu form, and nitrogen [135, 136]. This creates a scaffold with a pore diameter ranging from 500 to 2000 μm. Gas foaming does not require the use of organic solvents, which is a huge advantage. The main disadvantage is the difficulty in controlling the size and interconnection of pores, because large, closed pores can be created inside the polymer structure during the foaming process.

1.3.2.3 Solid-state foaming

The solid-state foaming process has been studied to generate microcellular foams for biomedical applications. There are two basic steps in the solid-state foaming of thermoplastic polymers. The first step consists of saturation of the polymer with gas under high pressure. This step is normally carried out at room temperature. Given sufficient time for diffusion of gas into the polymer, the gas attains an equilibrium concentration that is consistent with the solubility of gas in the polymer and the gas pressure. In the second step, bubbles are nucleated in the gas–polymer system by creating a thermodynamic instability. This is achieved by either a sudden drop in pressure or sudden increase in temperature [141, 142]. Both strategies suddenly reduce the solubility of the gas, driving the gas out of the polymer matrix and into nucleated bubbles. One consequence of dissolving gas in the polymer is plasticization, reducing the polymer's glass transition temperature [143]. After saturation, the temperature of the

gas-saturated polymer only needs to be raised to the glass transition temperature of the gas–polymer system to nucleate bubbles. The pore sizes that have been achieved range from sub-micrometers to a few hundred micrometers. However, the disadvantage of the process is that the foams it produces are mostly close-pored and not suitable for tissue engineering applications.

1.3.2.4 Emulsion templating

In recent years, highly porous polymer foams with an interconnected pore network structure obtained from high internal phase emulsion templates have gained increasing interest because of their unique properties such as high porosity and high degree of pore interconnectivity. High internal phase emulsions (HIPEs) are concentrated systems possessing a large volume of internal, or dispersed phase. The volume fraction is above 0.74, resulting in deformation of the dispersed phase droplets into polyhedral, which are separated by thin films of continuous phase. HIPEs have been known in the literature for many years and are frequently encountered in the cosmetic and food industries [144].

In the 1960s, the first descriptions of preparing polymer foams using HIPEs was reported [145]. Polymerized high internal phase emulsions (polyHIPEs) are materials prepared by polymerizing the continuous phase of an HIPEs. In most cases, this is the oil (organic) phase while water (aqueous) phase is the droplet phase. However, oil in water and even non aqueous HIPEs are known as precursors for porous polymer preparation. Recently, extensive reviews of polyHIPEs preparation have been published, which confirm a growing interest in the field [146-148].

1.3.3 Two-way shape memory polymer foams

The one-way shape memory polymer foam has its own drawback that the programming step requires an external force for each cycle [149-154]. The two-way shape memory polymer foam showing full reversibility exposure to external stimuli in every cycle was potentially applied in a wide range of applications, including lightweight porous polymeric actuators, sensors, and artificial intelligence. Mather and coworkers proposed shape memory poly(ε-caprolactone)-co-poly(ethylene glycol) foams. Their foam with salts could be UV cured and exhibited reversible actuation in compressed [155]. Lendlein and coworkers proposed water-blown polyurethane foams that showed a reversible shape memory effect [156]. Despite the importance of two-way shape memory polymer foams, few relevant researchers have focused on this material.

1.3.4 Two-way shape memory polymer foams characterization

In porous polymeric substrates, cell size, homogeneity, open and closed structure and membrane thickness are all important factors that influence material behavior. Modulus, shape recovery capability, and environmental response, in addition to other properties, are highly dependent on cell structure. X- ray micro-computed tomography scanning (μCT), scanning electron micron microscopy (SEM), and optical microscopy (OM) are generally used in cell structure analysis. Pore interconnectivity is an important parameter that defines the openness of a porous structure, while it can be estimated qualitatively from two-dimensional SEM images [132].

The density of polymeric porous materials is arguably the most influential of all

physical attributes on mechanical properties. High-density porous materials exhibit significantly different mechanical behavior than to low-density porous materials, and density is also highly influential over environmental response to porous materials after introduction to new environments. The characterization of porous shape memory polymer materials includes both bulk material properties as well as three-dimensional structure analysis.

The SME is achieved, typically, in one-way, thermally actuated SMPs by heating or cooling polymers at about a thermal transition temperature (T_{trans}) to enable some combination of geometric programming, shape fixity, and shape recovery. T_{trans} may be a glass transition (T_g), crystalline melt transition (T_m), or some other transition, such as a supramolecular or ionomeric dissociation [133]. Differential scanning calorimetry (DSC) is one of the most widely reported experimental methods used to characterize polymeric thermal transitions. For amorphous shape memory polymer foams, DSC can be used to predict the temperature at which shape recovery will begin—the onset of the T_g—and can also be used to calculate percent crystallinity and enthalpies of melting or fusion for semi-crystalline SMPs.

Dynamic mechanical analysis (DMA) can be employed to measure numerous temperature and frequency-dependent properties of polymers, including glassy and rubbery modulus, which are very important properties for porous SMPs.

One of the major reasons for interest in shape memory polymer foams is their ability to be compacted to a higher density (smaller volume) state that can then be actuated to a lower density (larger volume) state. Consequently, thermo-mechanical

shape memory characterization of these materials is mostly done in the compressive mode, although tensile tests.

1.3.5 Potential application of two-way shape memory polymer foams

The two-way shape memory polymer foam showing full reversibility exposure to external stimuli in every cycle was potentially applied in porous polymeric actuators, aerospace and biomedical applications. Potential biomedical applications include scaffolds for filling bone defects, hemostatic sponges, soft tissue scaffolds, and drug-delivery platforms. Shape memory polymer foam have been proposed for applications in space. Large structures used in space such as solar sails, solar arrays, sunshields and radar antennas require heavy and space consuming mechanical mechanisms for deployment and control. New designs are being developed for low mass, low launch volume deployable two-way shape memory structures. Two-way shape memory porous foams, upon exposure to an external stimulus to induce actuation and recovery may as a potential issue, such use a removable thermal blanket capable of converting solar radiation to thermal energy to provide the heat needed for deployment.

1.4 Purpose and significance of research

The purpose of this study is to synthesize two-way (reversible) chemically crosslinked semi-crystalline shape memory polymers with various crosslinking densities from poly(ethylene-co-vinyl acetate) (PEVA) and various contents of benzoyl peroxide (BPO). The developed materials were capable of reversible shape change, and we ensured that the "switch on" temperature, which triggers shape change, was within

a reasonable range. The samples (PEVA/BPO soft materials) with high crosslinking densities had optimal actuation performance and an excellent recovery ratio of over 99%. BPO as a common crosslinker can crosslink PEVA by combining with the acetate group, which endows the PEVA/BPO with the ability of actuation and shape recovery. The 2W-SME was achieved under both constant stress and stress-free conditions. The developed PEVA/BPO materials were adequately soft and had good mechanical properties, even at large deformation. Therefore, the significance of this investigation can potentially useful as soft material actuators, sensors, and artificial intelligence or for other applications Two-way reversible shape memory polymer foams with porous three-dimensional structures were prepared using salt-leaching technology based on benzoyl peroxide (BPO) thermo-crosslinked poly(ethylene-co-vinyl acetate) (PEVA). This finding of the two-way shape memory PEVA/BPO foams may contribute to their applications as lightweight porous actuators in artificial intelligence and aerospace application, among others.

1.5 Outline of dissertation

In our research, in order to develop novel two-way reversible shape memory materials with an excellent recovery ratio and actuation performance, we synthesized PEVA/BPO two-way (reversible) chemically crosslinked semi-crystalline shape memory polymers and its foams. For two-way shape memory PEVA/BPO polymers, we found that the BPO crosslinker was key with regard to shape recovery, and the PEVA/BPO compositions with high crosslinking densities had significantly elevated recovery ratios. The 2W-SME is achieved under both constant stress and stress-free

conditions. We investigated the formation conditions of the stress-free 2W-SME. The tunable two-way shape memory driving force and recovery force of PEVA with different BPO contents were investigated by thermomechanical cycles. For two-way shape memory PEVA/BPO foams, we found that the different reversible shape changed in various pore sizes of PEVA/BPO foams upon exposure at low/high temperatures under constant compression conditions. Various pore sizes of PEVA/BPO porous foam were obtained using different NaCl particle sizes, and their morphology of two-way shape memory PEVA/BPO porous foams with different pore sizes were observed.

The thesis is comprised of five subsequent chapters: general introduction; three main studies including experimental, results and discussion, conclusions; summary for this dissertation.

In chapter 1, an overview of SMPs, 2W-SMPs and shape memory polymer foams is introduced in three sections which included shape memory type, structures, synthesis and their applications.

In chapter 2, two-way (reversible) chemically crosslinked semi-crystalline shape memory polymers with various crosslinking densities from poly(ethylene-co-vinyl acetate) (PEVA) and various contents of benzoyl peroxide (BPO) were synthesized via a thermo-crosslinked technology. Two-way shape memory behavior, mechanical properties, and crosslinked network have been investigated.

In chapter 3, the different stress conditions of two-way chemically crosslinked semi-crystalline shape memory PEVA/BPO polymers have been discussed. The formation conditions of the stress-free 2W-SME, the two-way driving force and

recovery force of PEVA with different BPO contents was investigated by thermomechanical cycles.

In chapter 4, we synthesized two-way shape memory PEVA/BPO foams with different interconnected pores using a salt-leaching technology and thermo-crosslinking technology. The morphology, porous structure and two-way shape memory behavior of PEVA/BPO foams have been discussed.

In chapter 5, all the works was summarized and its conclusion was presented.

Reference

[1] Behl. M, Razzaq. M. Y, Lendlein. A. Multifunctional Shape-Memory Polymers. *Adv. Mater.* 2010, *22*, 3388-3410.

[2] Meng. H, Li. G. A review of Stimulus-Responsive Shape Memory Polymer Composites. *Polymer* 2013, *54*, 2199-2221.

[3] Mu. T, Liu. L, Lan. X, Liu. Y, Leng. J. Shape Memory Polymer for Composites. *Compos. Sci. Technol.* 2018, *160*, 169-198.

[4] Liu. C, Qin. H, Mather. P. T. Review of Progress in Shape-Memory Polymers. *J. Mater. Chem.* 2007, *17*, 1543-1558.

[5] Du. L, Xu. Z. Y, Fan. C. J, Xiang. G, Yang. K. K, Wang. Y. Z. A Fascinating Metallo-Supramolecular Polymer Network with Thermal/Magnetic/Light-Responsive Shape-Memory Effect Anchored by Fe_3O_4 Nanoparticles. *Macromolecules* 2018, *51*, 705-715.

[6] Li. W, Liu. Y, Leng. J. Shape Memory Polymer Nanocomposite with Multi-Stimuli Response and Two-Way Reversible Shape Memory Behavior. *RSC Adv.* 2014, *4*, 61847-61854.

[7] Hu. J, Zhu. Y, Huang. H, Lu. J. Recent advances in shape–memory polymers: Structure, mechanism, functionality, modeling and applications. *Prog. Polym. Sci*. 2012, *37(12)*, 1720-1763.

[8] Ratna. D, Karger-Kocsis. J. Recent advances in shape memory polymers and composites: a review. *J. Mater. Sci.* 2008, *43(1)*, 254-269.

[9] Leng. J, Lan. X, Liu. Y, Du. S. Shape-memory polymers and their composites:

stimulus methods and applications. *Pro. Mater Sci*. 2011. *56(7)*, 1077-1135.

[10] Lendlein. A, Schmidt. A. M, Schroeter. M. Langer. R. Shape-Memory Polymer Networks from Oligo (ϵ-caprolactone) dimethacrylates. *J. Polym. Sci. Part A: Polym. Chem.* 2005, *43,* 1369-1381.

[11] Ohki. T, Ni. Q. Q, Ohsako. N, Iwamoto. M. Mechanical and Shape Memory Behavior of Composites with Shape Memory Polymer. *Compo. Part A-Appl. Sci. Manuf.* 2004, *35*, 1065-1073.

[12] Wu. J, Yuan. C, Ding. Z, Isakov. M, Mao. Y, Wang. T, Qi. H. J. Multi-shape active composites by 3D printing of digital shape memory polymers. *Sci. Rep.* 2016, *6*, 24224.

[13] Huang. W. M, Yang. B, An. L, Li. C, Chan. Y. S. Water-Driven Programmable Polyurethane Shape Memory Polymer: Demonstration and Mechanism. *Appl. Phys. Lett.* 2005, *86*, 114105.

[14] Ma. M, Guo. L, Anderson. D. G, Langer. R. Bio-inspired polymer composite actuator and generator driven by water gradients. *Science* 2013, *339(6116)*, 186-189.

[15] Yang. B, Huang. W. M, Li. C, Li. L, Chor. J. H. Qualitative separation of the effects of carbon nano-powder and moisture on the glass transition temperature of polyurethane shape memory polymer. *Scripta Mater.* 2005, *53(1)*, 105-107.

[16] Yang. B, Huang. W. M, Li. C, Li. L. Effects of moisture on the thermomechanical properties of a polyurethane shape memory polymer. *Polymer* 2006, *47(4)*, 1348-1356.

[17] Lendlein. A, Jiang. H, Jünger. O, Langer. R. Light-Induced Shape-Memory Polymers. *Nature* 2005, *434*, 879.

[18] Iqbal. D, Samiullah. M. H. Photo-responsive shape-memory and shape-changing liquid-crystal polymer networks. *Materials* 2013, *6(1)*, 116-142.

[19] Zhang. X, Zhou. Q, Liu. H, Liu. H. UV light induced plasticization and light activated shape memory of spiropyran doped ethylene-vinyl acetate copolymers. *Soft Matter* 2014, *10(21)*, 3748-3754.

[20] Liu. Y, Lv. H, Lan. X, Leng. J, Du. S. Review of Electro-Active Shape-Memory Polymer Composite. *Compos. Sci. Technol.* 2009, *69*, 2064-2068.

[21] Zhang. Z. X, Wang. W. Y, Yang. J. H, Zhang. N, Huang. T, Wang. Y. Excellent Electroactive Shape Memory Performance of EVA/PCL/CNT Blend Composites with Selectively Localized CNTs. *J. Phys. Chem. C.* 2016, *120*, 22793-22802.

[22] Melvin. G. J. H, Ni. Q. Q, Natsuki. T. Bending actuation and charge distribution behavior of polyurethane/carbon nanotube electroactive nanocomposites. *Polym. Compos.* 2016, *37(1)*, 262-269.

[23] Park. J. M, Kim. S. J, Jang. J. H, Wang. Z, Kim. P. G, Yoon. D. J, DeVries. K. L. Actuation of electrochemical, electro-magnetic, and electro-active actuators for carbon nanofiber and Ni nanowire reinforced polymer composites. *Compos. Part. B-Eng.* 2008, *39(7)*, 1161-1169.

[24] Razzaq. M. Y, Behl. M, Kratz. K, Lendlein. A. Multifunctional Hybrid Nanocomposites with Magnetically Controlled Reversible Shape-Memory Effect. *Adv. Mater.* 2013, *25*, 5730-5733.

[25] Schmidt. A. M. Electromagnetic Activation of Shape Memory Polymer Networks Containing Magnetic Nanoparticles. *Macromol Rapid Commun.* 2006, *27*, 1168-1172.

[26] Kumar. U. N, Kratz. K, Wagermaier. W, Behl. M, Lendlein. A. Non-contact actuation of triple-shape effect in multiphase polymer network nanocomposites in alternating magnetic field. *J. Mater. Chem.* 2010, *20(17)*, 3404-3415.

[27] Zrinyi. M. Intelligent polymer gels controlled by magnetic fields. *Colloid. Polym. Sci.* 2000, *278(2)*, 98-103.

[28] Lv. H. B, Liu. Y. J, Zhang. D. X, Leng. J. S. Du. S. Y. Solution-responsive shape-memory polymer driven by forming hydrogen bonding. *Adv. Mater. Res.* (Vol. 47, pp. 258-261). 2008, Trans Tech Publications.

[29] Morton. M. Solution theory of polymer. 1987.

[30] Han. X. J, Dong. Z. Q, Fan. M. M, Liu. Y, Li. J. H, Wang. Y. F, Zhang. S. pH-Induced Shape-Memory Polymers. *Macromol Rapid Commun.* 2012, *33*, 1055-1060.

[31] Feil. H, Bae. Y. H, Feijen. J, Kim. S. W. Mutual influence of pH and temperature on the swelling of ionizable and thermosensitive hydrogels. *Macromolecules* 1992, *25(20)*, 5528-5530.

[32] Song. J. J, Chang. H. H, Naguib. H. E. Biocompatible Shape Memory Polymer Actuators with High Force Capabilities. *Eur. Polym. J.* 2015, *67*, 186-198.

[33] Kunzelman. J, Chung. T, Mather. P. T, Weder. C. Shape Memory Polymers with Built-in Threshold Temperature Sensors. *J. Mater. Chem.* 2008, *18*, 1082-1086.

[34] Liu. Y, Du. H, Liu. L, Leng. J. Shape memory polymers and their composites in aerospace applications: a review. *Smart Mater. Struct.* 2014, *23(2)*, 023001.

[35] Hu. J, Chen. S. A Review of Actively Moving Polymers in Textile Applications. *J. Mater. Chem.* 2010, *20*, 3346-3355.

[36] Lendlein. A, Langer. R. Biodegradable, elastic shape-memory polymers for potential biomedical applications. *Science* 2002, *296(5573)*, 1673-1676.

[37] Ward Small. I. V, Singhal. P, Wilson. T. S, Maitland. D. J. Biomedical Applications of Thermally Activated Shape Memory Polymers. *J. Mater. Chem.* 2010, *20*, 3356-3366.

[38] Baer. G, Wilson. T. S, Matthews. D. L, Maitland. D. J. Shape-memory behavior of thermally stimulated polyurethane for medical applications. *J. Appl. Polym. Sci.* 2007, *103(6)*, 3882-3892.

[39] Shi. Y, Yoonessi. M, Weiss. R. A. High temperature shape memory polymers. *Macromolecules* 2013, *46(10)*, 4160-4167.

[40] Cho. J. W, Kim. J. W, Jung. Y. C, Goo. N. S. Electroactive shape-memory polyurethane composites incorporating carbon nanotubes. *Macromol. Rapid. Commun.* 2005, *26(5)*, 412-416.

[41] Koerner. H, Price. G, Pearce. N. A, Alexander. M, Vaia. R. A. Remotely a ctuated polymer nanocomposites—stress-recovery of carbon-nanotube-filled t hermoplastic elastomers. *Nat Mater.* 2004, *3(2)*, 115.

[42] Vialle. G, Di Prima. M, Hocking. E, Gall. K, Garmestani. H, Sanderson. T, Arzberger. S. C. Remote activation of nano magnetite reinforced shape memory

polymer foam. *Smart Mater. Struct.* 2009, *18(11)*, 115014.

[43] Kumar. U. N, Kratz. K, Heuchel. M, Behl. M, Lendlein. A. Shape-Memory Nanocomposites with Magnetically Adjustable Apparent Switching Temperatures. *Adv. Mater.* 2011, *23(36)*, 4157-4162.

[44] Jiang. H. Y, Kelch. S, Lendlein. A. Polymers move in response to light. *Adv. Mater.* 2006, *18(11)*, 1471-1475.

[45] Yu. Y, Ikeda. T. Photodeformable polymers: A new kind of promising smart material for micro-and nano-applications. *Macromol. Chem. Phys.* 2005, *206(17)*, 1705-1708.

[46] Kim. B. K, Lee. S. Y, Xu. M. Polyurethanes having shape memory effects. *Polymer* 1996, *37(26)*, 5781-5793.

[47] Li. F, Zhang. X, Hou. J, Xu. M, Luo. X, Ma. D, Kim. B. K. Studies on thermally stimulated shape memory effect of segmented polyurethanes. *J. Appl. Polym. Sci.* 1997, *64(8)*, 1511-1516.

[48] Lin. J. R, Chen. L. W. Study on shape-memory behavior of polyether-based polyurethanes. I. Influence of the hard-segment content. *J. Appl. Polym. Sci.* 1998, *69(8)*, 1563-1574.

[49] Kumar. S, Pandya. M. V. Thermally recoverable crosslinked polyethylene. *J. Appl. Polym. Sci.* 1997, *64(5)*, 823-829.

[50] Ji. F. L, Hu. J. L, Han. J. P. Shape memory polyurethane-ureas based on isophorone diisocyanate. *High Perform. Polym.* 2011, *23(3)*, 177-187.

[51] Chen. S, Hu. J, Liu. Y, Liem. H, Zhu. Y, Liu. Y. Effect of SSL and HSC on

morphology and properties of PHA based SMPU synthesized by bulk polymerization method. *J. Poly. Sci., Part B: Polym. Phys.* 2007, *45(4)*, 444-454.

[52] Lendlein. A, Schmidt. A. M, Langer. R. AB-polymer networks based on oligo (ε-caprolactone) segments showing shape-memory properties. *PNAS* 2001, *98(3)*, 842-847.

[53] Zhu. Y, Hu. J, Yeung. K. W, Choi. K. F, Liu. Y, Liem. H. Effect of cationic group content on shape memory effect in segmented polyurethane cationomer. *J. Appl. Polym. Sci.* 2007, *103(1)*, 545-556.

[54] Hu. J. L, Ji, F. L, Wong. Y. W. Dependency of the shape memory properties of a polyurethane upon thermomechanical cyclic conditions. *Polym. Int.* 2005, *54(3)*, 600-605.

[55] Hu. J. L, Zeng. Y. M, Yan. H. J. Influence of processing conditions on the microstructure and properties of shape memory polyurethane membranes. *Text. Res. J.* 2003, *73(2)*, 172-178.

[56] Li. J, Xie. T. Significant impact of thermo-mechanical conditions on polymer triple-shape memory effect. *Macromolecules*, 2010, *44(1)*, 175-180.

[57] Dong. Y, Fu. Y, Ni, Q. Q. In-situ grown silica/water-borne epoxy shape memory composite foams prepared without blowing agent addition. *J. Appl. Polym. Sci.* 2015, *132(39)*.

[58] Ji. F, Zhu. Y, Hu. J, Liu. Y, Yeung. L. Y, Ye. G. Smart polymer fibers with shape memory effect. *Smart Mater. Struct.* 2006, *15(6)*, 1547.

[59] Mondal. S, Hu. J. L. Temperature stimulating shape memory polyurethane for

smart clothing. Indian *J. Fiber. Text. Res.* 2006, *31(66)*, 71.

[60] Kobayashi. K, Hayashi. S. *U.S. Patent No.* 1992, *5,098,776*. Washington, DC: U.S. Patent and Trademark Office.

[61] Cha. DI. Kim HY, Lee KH, Jung YC, Cho JW, Chun BC. Electrospun nonwovens of shape-memory polyurethane block copolymers. J. Appl. Polym. Sci. 2005, *96*, 460–5.

[62] Zhuo HT, Hu JL, Chen SJ. Study of the thermal properties of shape memory polyurethane nanofibrous nonwoven. *J. Mate. Sci.* 2011, *46*, 3464–9.

[63] A Metcalfe. A, Desfaits. A. C, Salazkin. I, Yahia. L. H, Sokolowski. W. M, Raymond. J. Cold hibernated elastic memory foams for endovascular interventions. *Biomaterials* 2003, *24(3)*, 491-497.

[64] Lendlein. A, Langer. R. Biodegradable, elastic shape-memory polymers for potential biomedical applications. *Science* 2002, *296(5573)*, 1673-1676.

[65] Mohr. R, Kratz. K, Weigel. T, Lucka-Gabor. M, Moneke. M, Lendlein. A. Initiation of shape-memory effect by inductive heating of magnetic nanoparticles in thermoplastic polymers. *PNAS* 2006, *103(10)*, 3540-3545.

[66] C. Min, W. Cui, J. Bei. Biodegradable shape-memory polymerdpolylactideco- poly (glycolide-co-caprolactone) multiblockcopolymer, *Polym. Adv. Technol.* 2005, *16 (8)*, 608-615.

[67] Zheng. X, Zhou. S, Li. X, Weng. J. Shape memory properties of poly (D, L-lactide)/hydroxyapatite composites. *Biomaterials* 2006, *27(24)*, 4288-4295.

[68] Hussein. H, Harrison. D. Investigation into the use of engineering polymers as

acutators to produce 'automatic disassembly'of electronic products. 2004, Wiley-VCH, p. 35-49.

[69] Chiodo. J. D, Harrison. D. J, Billett. E. H. An initial investigation into active disassembly using shape memory polymers. *Proc. Inst. Mech. Eng. B: J. Eng. Manuf.* 2001, *215(5)*, 733-741.

[70] Everhart MC, Nickerson DM, Hreha RD. High-temperature reusable shape memory polymer mandrels. Smart structures and materials: industrial and commercial applications of smart structures technologies. *Proceedings SPIE*, 2006, *6171*, 61710K:1-10.

[71] Browne. A. L, Johnson. N. L. *U.S. Patent No. 7,* 2007, *309*, *104*. Washington, DC: U.S. Patent and Trademark Office.

[72] Browne. A. L, Johnson. N. L, Cafeo. J. A, Mayer. R. R, Aase. J. H. *U.S. Patent No. 8,* 2011, *061,550*. Washington, DC: U.S. Patent and Trademark Office.

[73] Browne. A. L, Johnson. N. L, Namuduri. C. S. *U.S. Patent No. 6,* 2005, *944,920*. Washington, DC: U.S. Patent and Trademark Office.

[74] Browne. A. L, Aase. J. H, Johnson. N. L, Keefe. A. C. *U.S. Patent No. 7,* 2007, *275,846*. Washington, DC: U.S. Patent and Trademark Office.

[75] Chen. S, Hu. J, Zhuo. H. Properties and Mechanism of Two-Way Shape Memory Polyurethane Composites. *Compos. Sci. Technol.* 2010, *70*, 1437-1443.

[76] Ge. Q, Westbrook. K. K, Mather. P. T, Dunn. M. L, Qi. H. J. Thermomechanical behavior of a Two-Way Shape Memory Composite Actuator. *Smart Mater. Struct.* 2013, *22*, 055009.

[77] Westbrook. K. K, Mather. P. T, Parakh. V, Dunn. M. L, Ge. Q, Lee. B. M, Qi. H. J. Two-Way Reversible Shape Memory Effects in a Free-Standing Polymer Composite. *Smart Mater. Struct.* 2011, *20*, 065010.

[78] Zhang. C. S, Ni. Q. Q. Bending Behavior of Shape Memory Polymer based Laminates. *Compos Struct.* 2007, *78*, 153-161.

[79] Wang. Z, Song. W, Ke. L, Wang. Y. Shape Memory Polymer Composite Structure with Two-Way Shape Memory Effects. *Mater. Lett.* 2012, *89*, 216-218.

[80] Tamagawa. H, Kikuchi. K, Nagai. G. Mechanical Characteristics of a Thermo-Responsive Two-Way Shape Change Polymeric Laminate. *Sensor Actuat A-Phys.* 2010, *163*, 356-362.

[81] Qin. H, Mather. P. T. Combined One-Way and Two-Way Shape Memory in a Glass-Forming Nematic Network. *Macromolecules* 2008, *42*, 273-280.

[82] Burke. K. A, Rousseau. I. A, Mather. P. T. Reversible Actuation in Main-Chain Liquid Crystalline Elastomers with Varying Crosslink Densities. *Polymer* 2014, *55*, 5897-5907.

[83] Chung. T, Romo-Uribe. A, Mather. P. T. Two-Way Reversible Shape Memory in a Semicrystalline Network. *Macromolecules* 2008, *41*, 184-192.

[84] Westbrook. K. K, Parakh. V, Chung. T, Mather. P. T, Wan. L. C, Dunn. M. L, Qi. H. J. Constitutive Modeling of Shape Memory Effects in Semicrystalline Polymers with Stretch Induced Crystallization. *J. Eng. Mater. Technol.* 2010, *132*, 041010.

[85] Behl. M, Kratz. K, Zotzmann. J, Nöchel. U, Lendlein. A. Reversible Bidirectional Shape-Memory Polymers. *Adv. Mater.* 2013, *25*, 4466-4469.

[86] Farhan. M, Chaganti. S. R, Nöchel. U, Kratz, K, Lendlein. A. Reversible Shape-Memory Properties of Surface Functionalizable, Crystallizable Crosslinked Terpolymers. *Polym. Adv. Technol.* 2015, *26*, 1421-1427.

[87] Behl. M, Kratz. K, Noechel. U, Sauter. T, Lendlein. A. Temperature-Memory Polymer Actuators. *PNAS* 2013, *110*, 12555-12559.

[88] Farhan. M, Rudolph. T, Nöchel,. U, Yan. W, Kratz. K, Lendlein. A. Noncontinuously responding Polymeric actuators. *ACS Appl. Mater. Interfaces.* 2017, *9*, 33559-33564.

[89] Pandini. S, Passera, S, Messori. M, Paderni. K, Toselli. M, Gianoncelli. A, Riccò, T. Two-Way Reversible Shape Memory Behavior of Crosslinked Poly (ε-Caprolactone). *Polymer* 2012, *53*, 1915-1924.

[90] Pandini. S, Agnelli. S, Merlettini. A, Chiellini. F, Gualandi. C, Paderni. K, Toselli, M. Multifunctional Electrospun Nonwoven Mats with Two-Way Shape Memory Behavior Prepared from Sol-Gel Crosslinked Poly (ε-Caprolactone). *Macromol. Mater. Eng.* 2008, *302*, 1600519.

[91] Li. J, Rodgers. W. R, Xie. T. Semi-Crystalline Two-Way Shape Memory Elastomer. *Polymer* 2011, *52*, 5320-5325.

[92] Qian. C, Dong. Y, Zhu. Y, Fu. Y. Two-Way Shape Memory Behavior of Semi-Crystalline Elastomer under Stress-Free Condition. *Smart Mater. Struct.* 2016, *25*, 085023.

[93] Huang. M, Dong. X, Wang. L, Zhao. J, Liu. G, Wang. D. Two-Way Shape Memory Property and its Structural Origin of Cross-Linked Poly (ε-Caprolactone). *RSC Adv.*

2014, *4*, 55483-55494.

[94] Dolynchuk. O, Kolesov. I, Jehnichen. D, Reuter. U, Radusch. H. J, Sommer. J. U. Reversible Shape-Memory Effect in Cross-Linked Linear Poly (ε-Caprolactone) under Stress and Stress-Free Conditions. *Macromolecules* 2017, *50*, 3841-3854.

[95] Han. J. L, Lai. S. M, Chiu. Y. T, Two-Way Multi-Shape Memory Properties of Peroxide Crosslinked EthyleneVinyl-Acetate Copolymer (EVA)/Polycaprolactone (PCL) blends. *Polym. Adv. Technol.* 2018, *29*, 2010-2024.

[96] Yang. Q, Fan. J, Li. G. Artificial Muscles Made of Chiral Two-Way Shape Memory Polymer Fibers. *Appl. Phys. Lett.* 2016, *109*, 183701.

[97] Zhou. J, Turner. S. A, Brosnan. S. M, Li. Q, Carrillo. J. M. Y, Nykypanchuk. D, Sheiko. S. S. Shapeshifting: Reversible Shape Memory in Semicrystalline Elastomers. *Macromolecules* 2014, *47*, 1768-1776.

[98] Xu. H, Yu. C, Wang. S, Malyarchuk. V, Xie. T, Rogers. J. A. Deformable, Programmable, and Shape-Memorizing Micro-Optics. *Adv. Funct. Mater.* 2013, *23*, 3299-3306.

[99] Thomsen. D. L, Keller. P, Naciri. J, Pink. R, Jeon. H, Shenoy, D, Ratna. B. R. Liquid crystal elastomers with mechanical properties of a muscle. *Macromolecules*, 2001, *34(17)*, 5868-5875.

[100] Li. M. H, Keller. P, Yang. J, Albouy. P. A. An artificial muscle with lamellar structure based on a nematic triblock copolymer. *Adv. Mater.* 2004, *16(21)*, 1922-1925.

[101] Bispo. M, Guillon. D, Donnio. B, Finkelmann. H. Main-chain liquid crystalline

elastomers: Monomer and cross-linker molecular control of the thermotropic and elastic properties. *Macromolecules* 2008, *41(9)*, 3098-3108.

[102]Nöchel. U, Kumar. U. N, Wang. K, Kratz. K, Behl. M, Lendlein. A. Triple-Shape Effect with Adjustable Switching Temperatures in Crosslinked Poly [ethylene-co-(vinyl acetate)]. *Macromol. Chem. Phys.* 2014, *215(24)*, 2446-2456.

[103]Zhang. Z. X, Wei. X, Yang. J. H, Zhang. N, Huang. T, Wang. Y, Gao. X. L. Triple-Shape Memory Materials Based on Cross-Linked Poly (ethylene vinyl acetate) and Poly (ε-caprolactone). *Ind. Eng. Chem. Res.* 2016, *55(47)*, 12232-12241.

[104]Liu. Y, Razzaq. M. Y, Rudolph. T, Fang. L, Kratz. K, Lendlein. A. Two-level shape changes of polymeric microcuboids prepared from crystallizable copolymer networks. *Macromolecules* 2017, *50(6)*, 2518-2527.

[105]Lee. K. M, Knight. P. T, Chung. T, Mather. P. T. Polycaprolactone− POSS chemical/physical double networks. *Macromolecules* 2008, *41(13)*, 4730-4738.

[106]Hong. S. J, Yu. W. R, Youk. J. H. Two-way shape memory behavior of shape memory polyurethanes with a bias load. *Smart Mater. Struct.* 2010, *19(3)*, 035022.

[107]Raquez. J. M, Vanderstappen. S, Meyer. F, Verge. P, Alexandre. M, Thomassin. J. M, Dubois. P. Design of Cross-Linked Semicrystalline Poly (ε-caprolactone)-Based Networks with One-Way and Two-Way Shape-Memory Properties through Diels–Alder Reactions. *Chemistry.: Eur. J.* 2011, *17(36)*, 10135-10143.

[108]Pandini. S, Baldi. F, Paderni. K, Messori. M, Toselli. M, Pilati. F, Riccò. T. One-way and two-way shape memory behaviour of semi-crystalline networks based on sol–gel cross-linked poly (ε-caprolactone). *Polymer* 2013, *54(16)*, 4253-4265.

[109]Dolynchuk. O, Kolesov. I, Androsch. R, Radusch. H. J. Kinetics and dynamics of two-way shape-memory behavior of crosslinked linear high-density and short-chain branched polyethylenes with regard to crystal orientation. *Polymer* 2015, *79*, 146-158.

[110]Kolesov. I, Dolynchuk. O, Jehnichen, D, Reuter. U, Stamm, M, Radusch. H. J. Changes of crystal structure and morphology during two-way shape-memory cycles in cross-linked linear and short-chain branched polyethylenes. *Macromolecules* 2015, *48(13)*, 4438-4450.

[111]Bothe. M, Pretsch. T. Two-way shape changes of a shape-memory poly (ester urethane). *Macromol. Chem. Phys.* 2012, *213(22)*, 2378-2385.

[112]Hong. S. J, Yu. W. R, Youk. J. H. Two-way shape memory behavior of shape memory polyurethanes with a bias load. *Smart Mater. Struct.* 2010, *19(3)*, 035022.

[113]Chen. S, Hu. J, Zhuo. H. Properties and mechanism of two-way shape memory polyurethane composites. *Compo. Sci. Technol.* 2010, *70(10)*, 1437-1443.

[114]Westbrook. K. K, Mather. P. T, Parakh. V, Dunn. M. L, Ge, Q, Lee. B. M, Qi. H. J. Two-way reversible shape memory effects in a free-standing polymer composite. *Smart Mater. Struct.* 2011, *20(6)*, 065010.

[115]Bothe. M, Pretsch. T. Bidirectional actuation of a thermoplastic polyurethane elastomer. *J. Mater. Chem. A*. 2013, *1(46)*, 14491-14497.

[116]Biswas. A, Aswal. V. K, Sastry. P. U, Rana. D, Maiti. P. Reversible bidirectional shape memory effect in polyurethanes through molecular flipping. *Macromolecules* 2016, *49(13)*, 4889-4897.

[117]Xu. Z, Ding. C, Wei. D. W, Bao. R. Y, Ke. K, Liu. Z, Yang. W. Electro and Light-Active Actuators Based on Reversible Shape-Memory Polymer Composites with Segregated Conductive Networks. *ACS App. Mater. Interfaces*. 2019, *11(33)*, 30332-30340.

[118]Gao. Y, Liu. W, Zhu. S. Polyolefin thermoplastics for multiple shape and reversible shape memory. *ACS App. Mater. Interfaces*. 2017, *9(5)*, 4882-4889.

[119]Huang Y. N, Fan L. F, Rong M. Z, Zhang M. Q, Gao Y. M. External Stress-Free Reversible Multiple Shape Memory Polymers. *ACS App. Mater. Interfaces*. 2019, *11(34)*, 31346-31355.

[120]Hu. J, Chen. S. A review of actively moving polymers in textile applications. *J. Mater. Chem*. 2010, *20(17)*, 3346-3355.

[121]Metcalfe. A, Desfaits. A. C, Salazkin. I, Yahia. L. H, Sokolowski. W. M, Raymond. J. Cold hibernated elastic memory foams for endovascular interventions. *Biomaterials*. 2003, *24(3)*, 491-497.

[122]De Nardo. L, Alberti. R, Cigada. A, Yahia. L. H, Tanzi. M. C, Farè. S. Shape memory polymer foams for cerebral aneurysm reparation: effects of plasma sterilization on physical properties and cytocompatibility. *Acta biomater*. 2009, *5(5)*, 1508-1518.

[123]Li. G, Uppu. N. Shape memory polymer based self-healing syntactic foam: 3-D confined thermomechanical characterization. *Compo. Sci. Technolo*. 2010, *70(9)*, 1419-1427.

[124]Li. G, Nettles. D. Thermomechanical characterization of a shape memory polymer

based self-repairing syntactic foam. *Polymer* 2010, *51(3)*, 755-762.

[125] Van Meerbeek. I. M, Mac Murray. B. C, Kim. J. W, Robinson. S. S, Zou. P. X, Silberstein. M. N, Shepherd. R. F. Morphing Metal and Elastomer Bicontinuous Foams for Reversible Stiffness, Shape Memory, and Self-Healing Soft Machines. *Adv. Mater.* 2016, *28(14)*, 2801-2806.

[126] Hasan. S. M, Nash. L. D, Maitland. D. J. Porous shape memory polymers: Design and applications. *J. Polym. Sci. Pol. Phys.* 2016, *54(14)*, 1300-1318.

[127] Fabrizio. Q, Loredana. S, Anna. S. E. Shape memory epoxy foams for space applications. *Mater. Lett.* 2012, *69*, 20-23.

[128] El-Kady. A. M, Rizk. R. A, El-Hady. B. M. A, Shafaa. M. W, Ahmed. M. M. Characterization, and antibacterial properties of novel silver releasing nanocomposite scaffolds fabricated by the gas foaming/salt-leaching technique. *JGEB* 2012, *10(2)*, 229-238.

[129] Okamoto. M, John. B. Synthetic biopolymer nanocomposites for tissue engineering scaffolds. *Prog. Polym. Sci.* 2013, *38(10-11)*, 1487-1503.

[130] Janik. H, Marzec. M. A review: Fabrication of porous polyurethane scaffolds. *Mater. Sci. Eng. C.* 2015, *48*, 586-591.

[131] Okamoto. M, John. B. Synthetic biopolymer nanocomposites for tissue engineering scaffolds. *Prog. Polym. Sci.* 2013, *38(10-11)*, 1487-1503.

[132] Zhang. D, Burkes. W. L, Schoener. C. A, Grunlan. M. A. Porous inorganic–organic shape memory polymers. *Polymer* 2012, *53(14)*, 2935-2941.

[133] Ware. T, Hearon. K, Lonnecker. A, Wooley K. L, Maitland D. J, Voit W. Triple-

shape memory polymers based on self-complementary hydrogen bonding. *Macromolecules* 2012, *45(2)*, 1062-1069.

[134] Kim. H. J, Park. I. K, Kim. J. H, Cho. C. S, Kim. M. S. Gas foaming fabrication of porous biphasic calcium phosphate for bone regeneration. *Tissue. Eng. Regen. Med.* 2012, *9(2)*, 63-68.

[135] Parks. K. L, Beckman. E. J. Generation of microcellular polyurethane foams via polymerization in carbon dioxide. II: Foam formation and characterization. *Polym. Eng. Sci.* 1996, *36(19)*, 2417-2431.

[136] Di Maio. E, Mensitieri. G, Iannace. S, Nicolais. L, Li. W, Flumerfelt. R. W. Structure optimization of polycaprolactone foams by using mixtures of CO2 and N2 as blowing agents. *Polym. Eng. Sci.* 2005, *45(3)*, 432-441.

[137] Zhang. D, George. O. J, Petersen. K. M, Jimenez-Vergara. A. C, Hahn. M. S, Grunlan. M. A. A bioactive "self-fitting" shape memory polymer scaffold with potential to treat cranio-maxillo facial bone defects. *Acta biomater.* 2014, *10(11)*, 4597-4605.

[138] Huang. W. M, Lee. C. W, Teo. H. P. Thermomechanical behavior of a polyurethane shape memory polymer foam. *J. Intel. Mat. Syst. Str.* 2006, *17(8-9)*, 753-760.

[139] Mikos. A. G, Sarakinos. G, Leite. S. M, Vacant. J. P, Langer. R. Laminated three-dimensional biodegradable foams for use in tissue engineering. *Biomaterials* 1993, *14(5)*, 323-330.

[140] Nam. Y. S, Yoon. J. J, Park. T. G. A novel fabrication method of macroporous

biodegradable polymer scaffolds using gas foaming salt as a porogen additive. *Journal of Biomedical Materials Research: An Official FFB, JSB, and The Australian Society for Biomaterials and the Korean Society for Biomaterials*, 2000, *53(1)*, 1-7.

[141]Kumar. V, Weller. J. E. A process to produce microcellular PVC. *Int. Polym. Proc.* 1993, *8(1)*, 73-80.

[142]Kumar. V, Weller. J. Production of microcellular polycarbonate using carbon dioxide for bubble nucleation. *J. Eng. Ind.* 1994, *116(4)*, 413-420.

[143]Chow. T. S. Molecular interpretation of the glass transition temperature of polymer-diluent systems. *Macromolecules* 1980, *13(2)*, 362-364.

[144]Lissant. K, editor. Emulsions and emulsion technology. CRC Press; 1974 Sep 1.

[145]Bartl VH, Von Bonin W. Über die Polymerisation in umgekehrter Emulsion. *Die Makromolekulare Chemie: Macromol. Chem. Phys.* 1962, 57*(1)*:74-95.

[146]Cameron. N. R. High internal phase emulsion templating as a route to well-defined porous polymers. *Polymer* 2005, *46(5)*, 1439-1449.

[147]Kimmins. S. D, Cameron. N. R. Functional porous polymers by emulsion templating: recent advances. *Adv. Funct. Mater.* 2011, *21(2)*, 211-225.

[148]Zhang. H, Cooper. A. I. Synthesis and applications of emulsion-templated porous materials. *Soft Matter*. 2005, *1(2)*, 107-113.

[149]Hearon, K, Singhal, P, Horn, J, Small IV, W, Olsovsky, C, Maitland, K. C, Maitland. D. J. Porous shape-memory polymers. *Polym. Rev.* 2013, *53(1)*, 41-75.

[150]Chung. S. E, Park. C. H. The thermoresponsive shape memory characteristics of

polyurethane foam. *J. Appl. Poly. Sci.* 2010, *117(4)*, 2265-2271.

[151]Zhang. D, Petersen. K. M, Grunlan. M. A. Inorganic–organic shape memory polymer (SMP) foams with highly tunable properties. *ACS Appl. Mater. Interfaces*. 2012, *5(1)*, 186-191.

[152]Squeo.E. A, Quadrini. F. Shape memory epoxy foams by solid-state foaming. *Smart Mater. Struct.* 2010, *19(10)*, 105002.

[153]Santo. L, Quadrini. F, Squeo. E. A, Dolce. F, Mascetti. G, Bertolotto. D, Zolesi. V. Behavior of shape memory epoxy foams in microgravity: experimental results of STS-134 mission. *Microgravity Sci. Tec.* 2012, *24(4)*, 287-296.

[154]Santo. L. Shape memory polymer foams. *Prog. Aerosp. Sci.* 2016, Feb 1;81:60-5.

[155]Baker. R. M, Henderson. J. H, Mather. P. T. Shape memory poly (ε-caprolactone)-co-poly (ethylene glycol) foams with body temperature triggering and two-way actuation. *J. Mater. Chem. B*. 2013, *1(38)*, 4916-4920.

[156]Zharinova. E, Heuchel. M, Weigel. T, Gerber. D, Kratz. K, Lendlein. A. Water-blown polyurethane foams showing a reversible shape-memory effect. *Polymers* 2016, *8(12)*, 412.

[157]Kolesov. I, Dolynchuk. O, Radusch. H. J. Shape-memory behavior of cross-linked semi-crystalline polymers and their blends. *Express Polym. Lett.* 2015, *9*(3).

[158]Chan. B. Q. Y, Low. Z. W. K, Heng. S. J. W, Chan. S. Y, Owh. C, Loh. X. J. Recent advances in shape memory soft materials for biomedical applications. *ACS Appl. Mater. Interfaces*. 2016, *8(16)*, 10070-10087.

Chapter 2

Two-way reversible shape memory polymer: Synthesis and characterization of benzoyl peroxide-crosslinked poly(ethylene-co-vinyl acetate)

2 Two-way reversible shape memory polymer: Synthesis and characterization of benzoyl peroxide-crosslinked poly(ethylene-co-vinyl acetate)

2.1 Introduction

In recent years, two-way shape memory polymers (2W-SMPs) [1-11] have attracted considerable interest because they are fully reversible following exposure to external stimuli without the necessity of reprogramming. Several pioneering works have contributed to the production of materials with two-way shape memory behavior. These include the development of laminated polymer composites [12-14], liquid crystal elastomers [15, 16], and crosslinked crystalline polymers [17-23] Laminated polymer composites comprising two layers bonded with an adhesive agent are limited by weak interlayer strength and cyclicity. Furthermore, the synthesis of liquid crystal elastomers is complicate, which limits mass production.

Thermal crosslinking is an effective way of achieving two-way shape memory behaviors. Example of thermally crosslinked systems include poly(ε-caprolactone) (PCL) with a mixture of crosslinking agents comprising dicumyl peroxide (DCP) and benzoyl peroxide (BPO) [17, 18], and poly(cyclooctene) (PCO) and poly(ethylene-co-vinyl acetate) (PEVA) with DCP [19-23]. There have been numerous studies on the shape memory properties of PEVA crosslinked with DCP [18-23]. Several interesting studies have been conducted on PEVA or PEVA/PCL blends crosslinked with DCP, Example

include research into non-continuously responding polymeric actuators [24], the triple-shape effect [25, 26], shape-memorizing micro-optics [27], and two-level shape changes of polymeric micro cuboids and two-way shape memory artificial muscle [28, 29].

In the present chapter, we synthesized high-performance two-way (reversible) shape memory polymers comprising BPO-crosslinked PEVA. We produced soft PEVA/BPO materials with high crosslinking densities and excellent shape memory recovery ratios. Tensile tests and thermomechanical analysis (TMA) are used to investigate shape memory effects and their mechanical properties. All the tests indicated that the PEVA/BPO materials developed in the present study exhibited actuation performance and high recover ability that could be controlled by temperature, and may therefore be applicable as soft actuators, artificial muscle, etc.

2.2 Experimental

2.2.1 Materials

Poly(ethylene-co-vinyl acetate) (PEVA) with 18 wt% weight percent (wt%) vinyl acetate was purchased from Sigma-Aldrich (Japan). Benzoyl peroxide (BPO, Acros Organics) was purchased from the Nippon Miractran Co., Ltd. (Japan).

2.2.2 Preparation of PEVA/BPO film

We fed PEVA containing various contents of BPO—i.e., 0wt% to 14wt%, indicated by PEVA-B0 to PEVA-B14 into a DSM compounder 15 micro twin-screw extruder (Xplore, Nederland). The constituents were then mixed at a rotation speed of 10 rpm for 10 min, and the temperatures of the three sections of the extruder were

individually set to 90 °C, 95 °C, and 100 °C. We then collected the extrudate cooled it

to 25 °C, and subjected it to a pressure of 10 MPa at 130 °C for 20 min in a hot-pressing

machine (**Figure 2.1**). The resulting PEVA/BPO films were 0.1 mm to 1 mm thick and

cut into dumb-bell shaped specimens for testing.
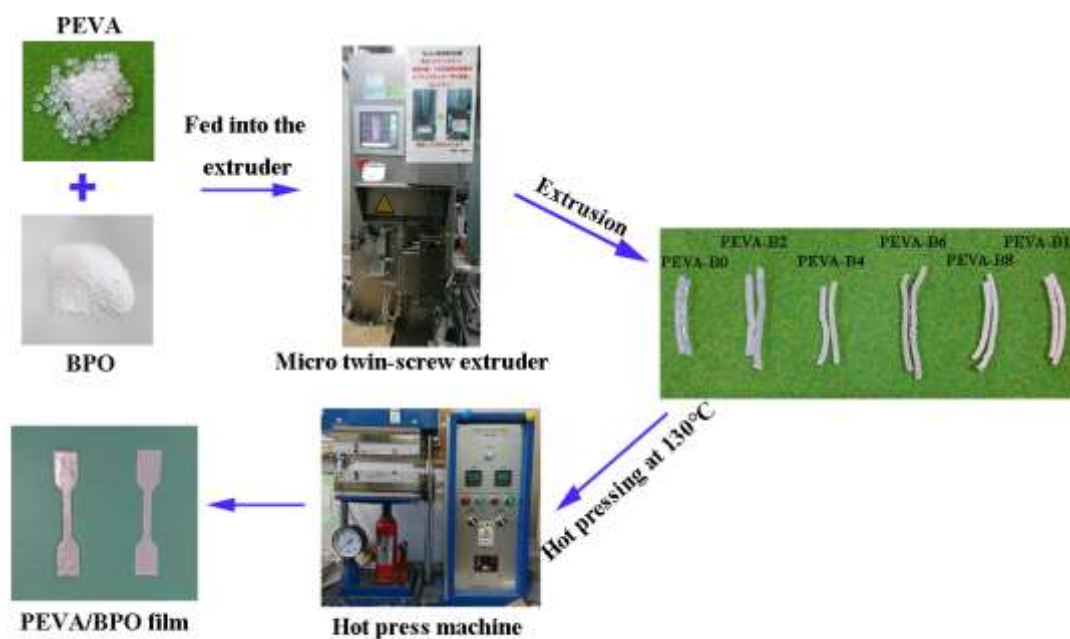
Figure 2.1 Schematic representation of the fabrication of a poly(ethylene-co-vinyl acetate)/benzoyl peroxide (PEVA/BPO) film.

2.2.3 Characterization

We determined the gel content using the solvent extraction method. Each

PEVA/BPO sample with a particular crosslinking density was cut into three specimens

(initial mass, m_0; 7 mm long and 6 mm wide), and the specimens were immersed in 20

mL of xylene at 85 °C for approximately 12 h to dissolve the non-crosslinked PEVA

fraction. Subsequently, the insoluble residue was washed with xylene, dried in a

vacuum oven at 85 °C for 12 h, and weighed (m_1). The gel content (*G)* was determined

gravimetrically using the following equation:

$$G = \frac{m1}{m0} *100\%$$

Eq. (2.1)

where G represents the weight fraction of the PEVA crosslinked with the BPO component in the sample.

We conducted tensile tests using a universal testing instrument (Tensile Tester, AND. Co. Japan). For the tensile test, the specimens were cut into the dumb-bel shape (JIS K6251-7, Figure 2.2). The tensile rate was 20 mm/min. The two-way shape memory properties of samples were determined through thermomechanical cycling, which was carried out using a TMA/SS6100 (SII Nano Technology Inc. Japan). The sample strips were 20 mm in length and 2 mm in width, and the samples were cooled from 90 °C to 25 °C for 22 min, cooling rate at about 3 °C/min, then heated to 90 °C for 22 min, heating rate at about 3 °C/min. In step 1, we heated the PEVA/BPO samples to 90 °C above their melting temperature (T_m) and applied 0.2 MPa of tension at a loading speed of 0.02 MPa/min, then maintained a constant stress of 0.2 MPa throughout the test. The stress applied to the samples with low BPO contents—e.g., PEVA-B0, PEVA-B1 was set to 0.02 MPa because these materials exhibited large viscous flow deformation above the T_m. In step 2, we cooled the samples to 25 °C below their crystallization temperature (T_c) under constant stress, then heated to 90 °C. We repeated this step three times.

We investigated the effect of the various crosslinking densities on the thermal properties of the films using an 8230 differential scanning calorimetry (DSC) system (Rigaku Corporation), with nitrogen as a purge gas at a flow rate of 30 mL/min. The

first heating trace was obtained over the range 20 °C to 110 °C at a rate of 10 K/min

using a sample weighing approximately 1 mg. The samples were then equilibrated for

2 min to clear the thermal history, cooled to 20°C, and maintained at 20 °C for 2 min.

Then second heating run from 20 °C to 110 °C was then recorded at the same rate of 10

K/min. The crystallization temperature (T_c) was determined from the peak of the

cooling curve, and the melting temperature (T_m) was determined from the second

heating curve. The crystallinity (X_c) of each sample was calculated using the following

equation:

$$X_c = (\Delta H_m / \Delta H_m^\infty) \times 100\% \qquad \text{Eq. (2.2)}$$

where ΔH_m is the melting enthalpy of the sample, calculated from the DSC trace

area between the melting curve trace and a linear baseline in the second heating run;

and ΔH_m^∞ is the equilibrium melting enthalpy of a pure crystal of linear polyethylene

(taken to equal 293J/g) [30].

We determined the storage modulus of the two-way shape memory polymer using

dynamic mechanical analysis (DMA) (ITK-DVA225; IT Measurement Control Co.) at

a frequency of 1 Hz. The samples were cut into rectangular strips (10 mm long and 2

mm wide). The temperature was increased from −80 °C to 120 °C at a rate of 3 °C/min,

and the displacement amplitude was 15 μm. The data were recorded at every one degree

Celsius.

2.3 Results and discussion

2.3.1 Determination of gel content

The crosslinked network properties of the PEVA/BPO samples tested by gel content measurement are shown in **Table 2.1** The gel content increased markedly from 69.77% to 91.25% with an increase in the BPO content from 1 wt% to 4 wt%, whereas it increased slowly from 91.25% to 95.82% as the BPO content increased from 4 wt% to 12 wt% because at higher gel contents there is a smaller change in the gel content with increasing BPO content.

Table 2.1 Characterization and thermal properties of poly(ethylene-co-vinyl acetate)/benzoyl peroxide (PEVA/BPO) samples

Sample	BPO[a] (wt%)	Gel content[b] (%)	ΔHm[c] (J/g)	T_m[d] (°C)	T_c[e] (°C)	X_c[f] (%)	E_1[g] (MPa)	E_2[h] (MPa)
PEVA-B0	0	0	66.95	84.4	68.2	22.85	33±1	1.1±0. 1
PEVA-B1	1	69.77	49.84	80.2	65.1	17.0	——	——
PEVA-B2	2	78.08	46.88	79.0	64.1	16.00	——	——
PEVA-B4	4	91.25	41.38	77.6	62.5	14.13	——	——
PEVA-B6	6	92.16	40.84	75.4	58.1	13.94	25±1	4.4±0.1
PEVA-B8	8	92.31	39.21	74.3	57.6	13.38	23±1	5.6±0. 1
PEVA-B10	10	94.79	35.71	70.8	53.8	12.19	16±1	6.5±0. 1
PEVA-B12	12	95.82	33.83	69.4	52.6	11.55	15±1	6.8±0.1

a) BPO (wt%) content crosslinked with PEVA
b) Gel content determined using the solvent extraction method in xylene
c) ΔHm: melting enthalpy calculated as the area under the curve of the PEVA melting peak
d) T_m: melting temperature peak of PEVA
e) T_c: crystallization temperature peak of PEVA
f) X_c: weight percent crystallinity of PEVA calculated from differential scanning calorimetry (DSC) melting enthalpies
g) E_1: initial Young's modulus determined by tensile tests
h) E_2: Average slope of stress and strain at the second part of the tensile curves

2.3.2 Tensile test and thermomechanical evaluation

The stress–strain curves of the PEVA/BPO samples are shown in **Figure 2.2a-b**, where the curves of (i)-(v) corresponding to PEVA-B0 to PEVA-B12. The stress-strain curves mainly consist of two parts with different slopes, marked as E_1 and E_2 (**Figure**

2.2a-b, Table 2.1). In the first part of the stress–strain curves—i.e., an elongation of less than approximately 10%—the initial Young's modulus (E_1) decreased as the BPO content increased, indicating that the materials had been softened by the addition of BPO. In the second part of the curves, the slope of E_2 increased markedly as the BPO content increased, and the materials, which were sufficiently soft, exhibited better mechanical properties at the breaking elongation of greater than approximately 200% during deformation **(Figure 2.2c)**.
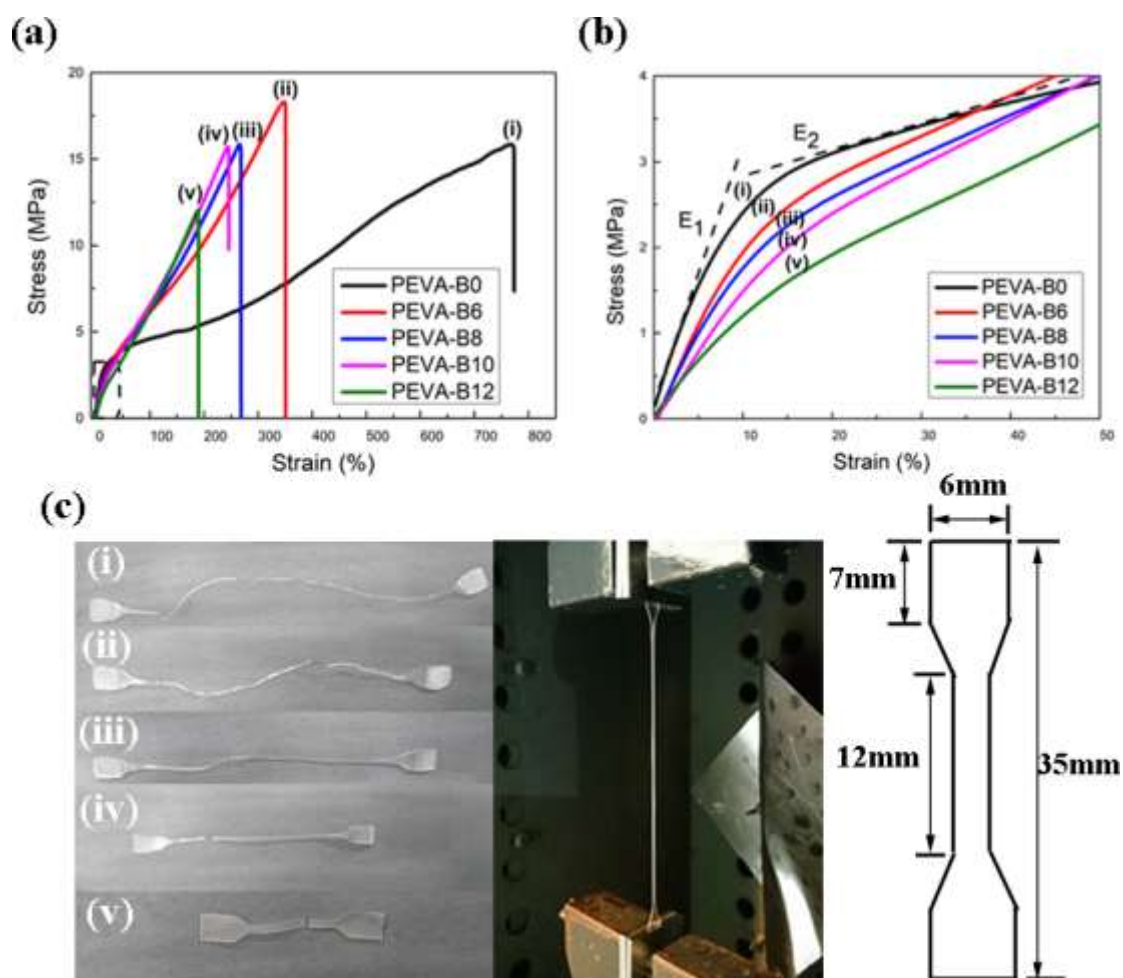

Figure 2.2 a: Stress–strain curves from static tensile tests of poly(ethylene-co-vinyl acetate)/benzoyl peroxide (PEVA/BPO) samples. b: Enlarged stress–strain curves at the initial stage of Fig. 1a. c: The deformation process of each sample with a particular BPO content.

This may have resulted from cooperation between the crosslinked network and the crystalline structure. A higher crosslinking density resulted in lower crystallinity (**X_c, Table 2.1**), and the crosslinked network increased with increasing BPO content (**Gel content, Table 2.1**). When the tensile strain of the samples was less than approximately 10%, the lower crystallinity made the greatest contribution to the reduction in the initial Young's modulus E_1 in the first part of the stress–strain curves. In contrast, in the second part of the stress–strain curves, which indicate deformation under a larger strain of between approximately 10% and 200%, the more crosslinked networks with greater BPO contents may have been more resistant to deformation because the crosslinked networks had begun to restrict the mobility of the molecular chains (see the slope of E_2).

The reversible shape memory cycle and the mechanism by which the reversible behavior occurred in the PEVA/BPO samples are represented in **Figure 2.3a-b**. We first heated the samples to 90 °C ($>T_m$) from 25 °C ($<T_c$). The melting temperature of corresponding crystalline phase we denote as T_m, which represent crystal-melting in the heating process (**Table 2.1**), then an external stress of 0 to 0.2 MPa was applied and maintained. The phase structure of the material may have changed from phase I to II, as represented schematically in **Figure 2.3b**. We then cooled the samples to 25 °C, and observed the elongation caused by the oriented crystal by cooling under an applied stress [19, 31], which corresponded to the transition from phase II to III. When the temperature was further increased above the T_m, the high temperature induced the contraction of the samples to their original shape as a result of crosslinking (phase III

to II). We found that the two-way shape memory behavior of PEVA/BPO samples occur in transition temperature between the T_c and T_m. The crystalline regions melt when the temperature reaches T_m, and the cross-linked structure in the PEVA which provide the driving force for the recovery of the deformation. The shape can be controlled between phase II and phase III only by changing temperature, which is two-way shape memory performance. **Figure 2.3c** illustrates the behavior of the PEVA-B10 sample under a constant weight of 862 mN at temperatures of 90 °C and 20 °C. The elongation of the sample during cooling was approximately 17%, and the sample almost recovered its original shape during heating.
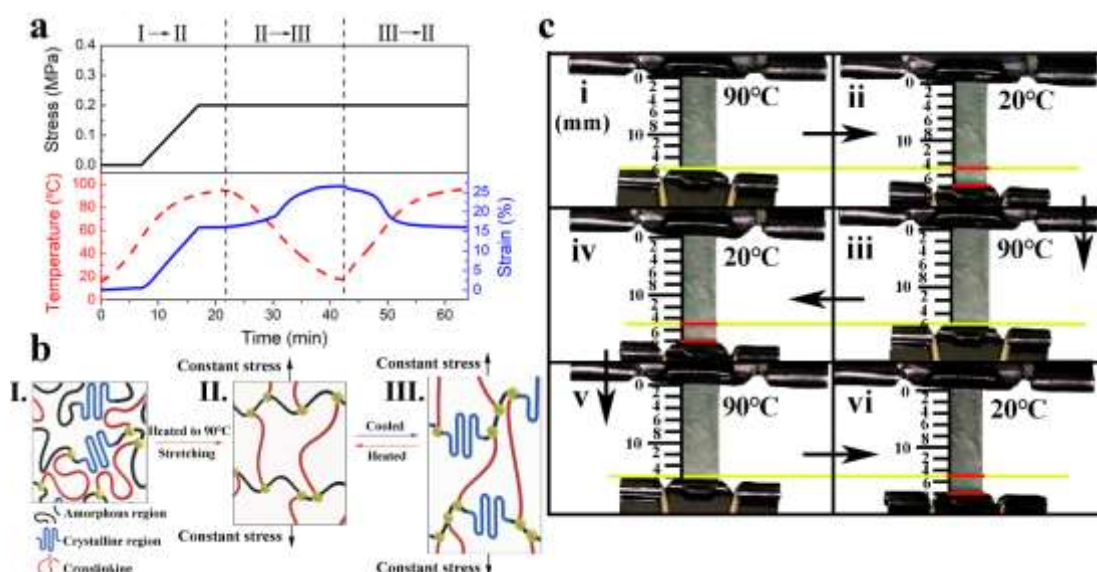
Figure 2.3 a: Two-way shape memory cycles for PEVA-B10. b: Mechanism of reversible behavior. c: Two-way behavior of PEVA-B10 at 90 °C and 20 °C under constant stress.

Table 2.2 shows the actuation strain calculated by $\varepsilon_{act} = (\varepsilon_L - \varepsilon_H) \times 100\%$, and the recovery ratio calculated by $R_{rec} = (\varepsilon_L - \varepsilon_{Hrec}) / (\varepsilon_L - \varepsilon_{H0}) \times 100\%$, where ε_{H0} is the pre-stretch at high temperatures, ε_L is the strain at low temperatures, ε_{Hrec} is the strain when the sample is reheated to 90 °C, and ε_H represents the strain at temperatures

above the crystal melting point in every cycle.

Table 2.2 Two-way shape memory of poly(ethylene-co-vinyl acetate)/benzoyl peroxide (PEVA/BPO) samples

	ε_{act} (%)			R_{rec} (%)		
Sample	1st cycle	2nd cycle	3rd cycle	1st cycle	2nd cycle	3rd cycle
PEVA-B1	——	——	——	——	——	——
PEVA-B2	——	——	——	——	——	——
PEVA-B4	10	9	9	57	58	57
PEVA-B6	10	10	10	86	84	83
PEVA-B8	10	10	10	99	98	97
PEVA-B10	12	12	12	99	99	99
PEVA-B12	10	10	11	99	99	99
PEVA-B14	11	11	11	99	99	98
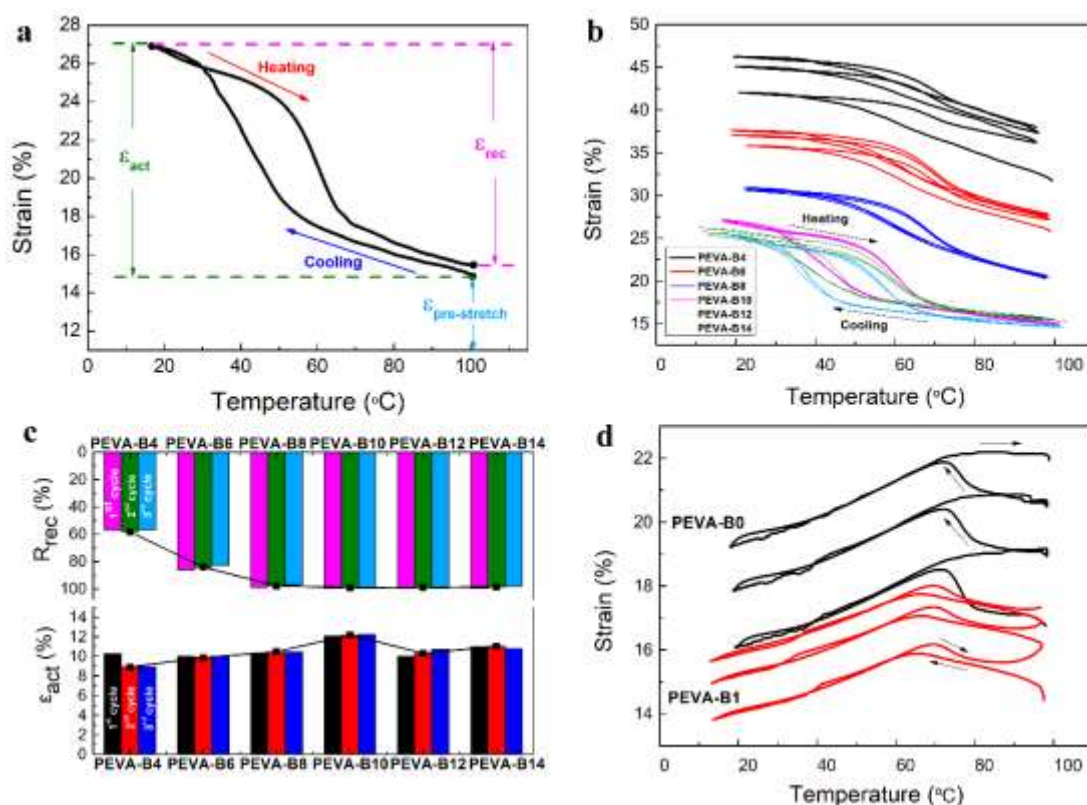
Figure 2.4 a: Definition of two-way shape memory process; b: Two-way shape memory behavior of samples with various benzoyl peroxide (BPO) contents of 4 wt% to 14 w% under 0.2 MPa; c: Actuation and recovery capabilities, the actuation strain (ε_{act}) represents crystallization leading to elongation upon cooling, the recovery ratio (R_{rec}) represents the recovery capabilities during heating; d: Two-way behavior of a low crosslinking density sample of 1 wt% BPO and a non-crosslinked sample under 0.02 MPa.

The definition of parameters and a deformation image of the two-way shape

memory process are shown in **Figure 2.4a**, and the two-way shape memory behavior

of samples with various BPO contents under a constant stress of 0.2 MPa over three

cycles is presented in **Figure 2.4b**. The recovery ratio (R_{rec}) increased markedly as the

BPO content increased from 4 wt% to 10 wt%, then remained at over 99%. The

actuation strain (ε_{act}) also increased to approximately 12% with the increasing BPO

content (**Figure 2.4c**). The high crosslink density sample PEVA-B10 had optimal

actuation performance and shape recovery, with actuation strains of 12% and shape

recovery ratios reaching 99%, and it exhibited excellent repeatable thermomechanical

performance and clear two-way shape memory reversibility **(Table 2.2)**. This may have

been because the plastic flow of the pristine PEVA was restrained by crosslinking

(Figure 2.6). **Figure 2.4d** shows the TMA results for a non-crosslinked sample and a

low-crosslinked sample with 1 wt% BPO under 0.02 MPa. The non-crosslinked sample

(PEVA-B0) did not recover during the heating, and did not exhibit two-way shape

memory behavior. PEVA-B1 demonstrated weak two-way shape memory behavior and

did not exhibit good thermomechanical recyclability. These results indicate that

crosslinking using BPO plays an important role in ensuring samples return to their

original shape.

2.3.3 Differential scanning calorimetry test

We investigated the degree of crystallinity, the melting temperature (T_m), and the

crystallization temperature (T_c) as transition temperature triggers of shape change using

differential scanning calorimetry (DSC). **Figure 2.5** shows the DSC traces of cooling

and heating runs for the PEVA/BPO samples. Various BPO contents resulted in the

different T_m, T_c, and crystallinity (X_c) values listed in **Table 2.1**. The decalescence peak

in the DSC curves correspond to the T_m, and the exothermic peak correspond to T_c.
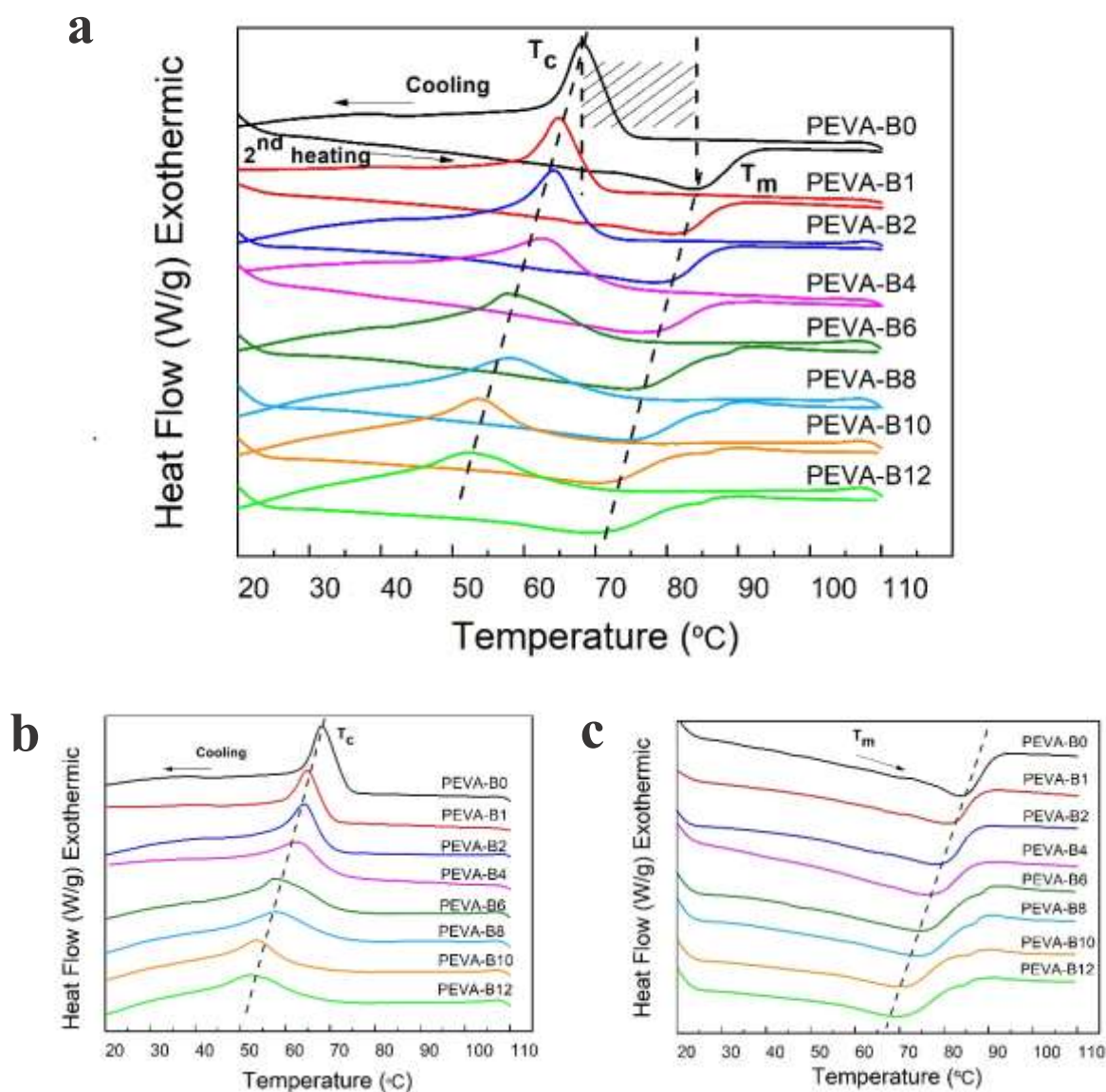
Figure 2.5 a: Differential scanning calorimetry (DSC) traces of poly(ethylene-co-vinyl acetate)/benzoyl peroxide (PEVA/BPO) samples: second heating and first cooling runs for PEVA cured with various amounts of BPO. b: PEVA/BPO samples first cooling runs. c: PEVA/BPO samples second heating runs.

The DSC test revealed that T_m, T_c, and X_c gradually decreased with increasing

BPO content. T_m decreased from 84.4 °C to 69.4 °C, and T_c followed the same trend,

decreasing from 68.2 °C to 52.6 °C. The higher the BPO content, the lower the X_c, which decreased from 22.85% to 11.55%, as shown in **Table 2.1**. The semi-crystalline PEVA/BPO polymer sample had a crosslinked structure; higher crosslinking density results in lower crystallinity as it becomes more difficult for the molecular chains to orient themselves within the network, and the growth of crystallites is restricted. The results show that the crosslinking reaction can affect the crystalline regions and control the transition temperature.

2.3.4 Dynamic mechanical analysis

The storage moduli of the PEVA/BPO films were determined from the DMA tests. The glass transition temperature (T_g) values of the PEVA samples at approximately −40 °C are shown in **Figure 2.6a**. The DMA analysis reveals that crosslinking influences the storage modulus above the melting temperature. The pristine PEVA exhibited viscous flow behavior above the melting temperature, and all the crosslinked PEVA samples tested (PEVA-B1–PEVA-B12) had a plateau in the rubbery modulus above the melting temperature. Crosslinking increased with increasing BPO content. This enhanced viscous flow suppression, restricting the movement of the molecular chains and extending the modulus plateau, making it wider and flatter owing to the high gel fraction.

The DMA curves of the loss factor (tan δ) values of the PEVA/BPO samples with various BPO contents are shown in **Figure 2.6b**. The intensity of the tan δ peak is used for the quantitative analysis of the amorphous phase of the polymer [32]. The results show that with the increase of the amount of BPO from 0wt% to 12wt%, the

height of the tan δ peak increased from 0.26 to 0.34, which may be attributed to the increase in the amorphous phase of the PEVA structure with increasing BPO content. The position and the size of the tan δ peak was not affected by the increases in BPO content. The tan δ value decreased with increasing crosslinking density within the region 90 °C to 115 °C.
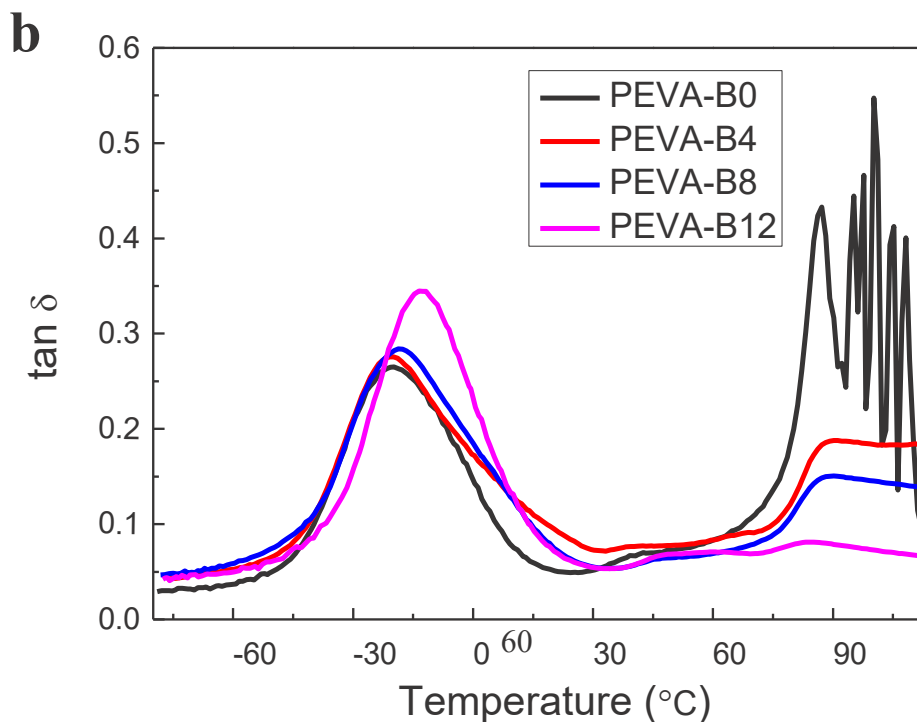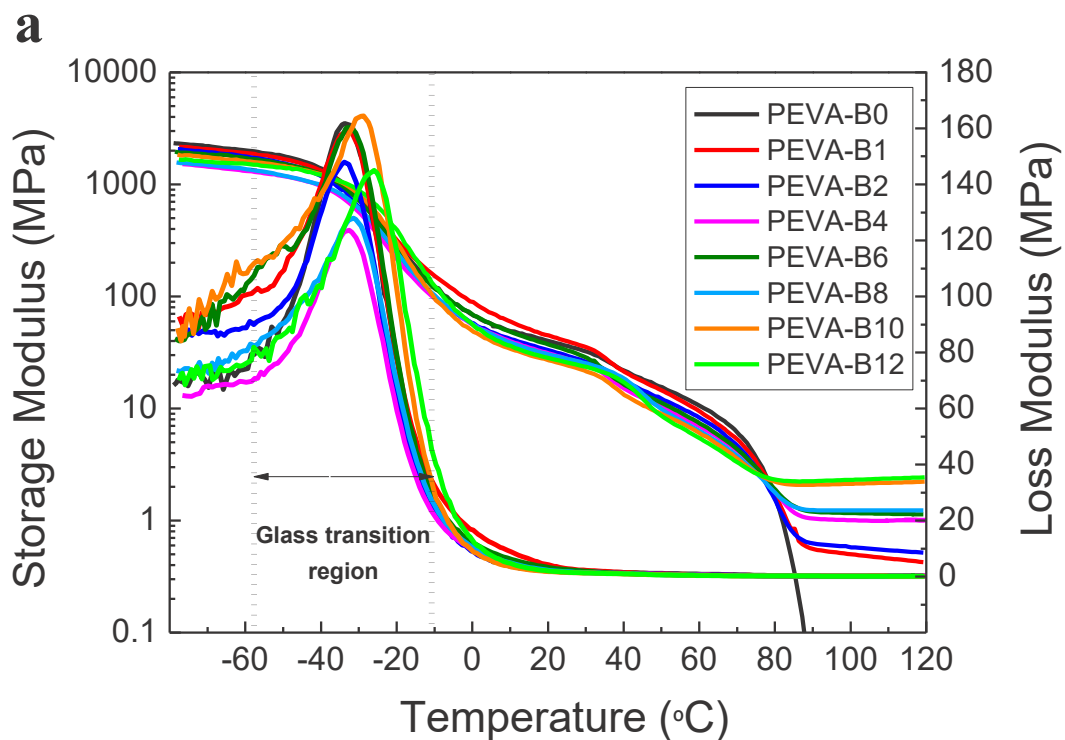
Figure 2.6 a: Dynamic mechanical analysis (DMA) curves of storage moduli of the poly(ethylene-co-vinyl acetate) (PEVA) benzoyl peroxide (BPO) samples with various BPO contents. b: Loss factor (tan δ) of the PEVA/BPO samples with various BPO contents.

2.3.5 Two-way shape memory multicycle evaluation

To evaluate the long-term two-way shape memory cycles of PEVA-B10 (PEVA with 10wt% BPO) with 20 cycles by using a TMA/SS6100 (SII Nano Technology Inc., Japan), as shown in **Figure 2.7**. In multicycle experiment, the two-way shape memory cycles of the PEVA-B10 sample shows good reversibility of two-way shape memory behavior and the two-way shape memory performance is stable.
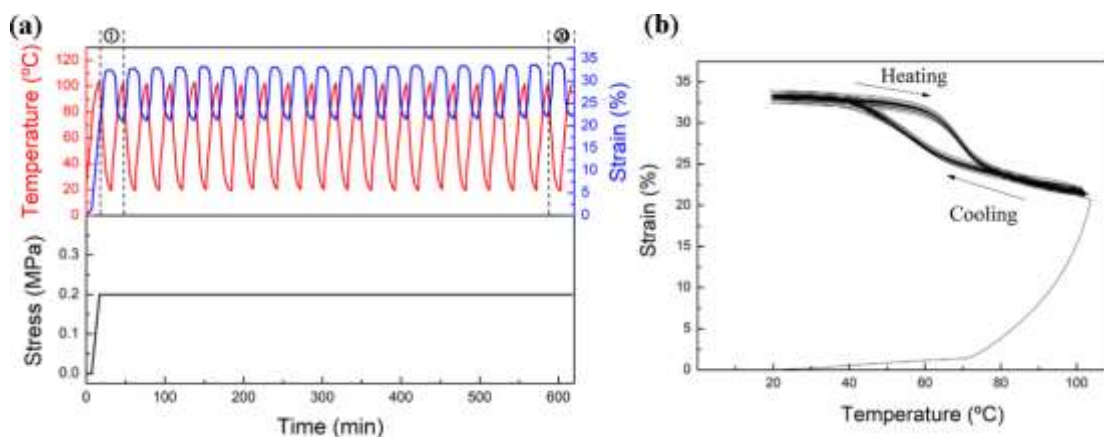
Figure 2.7 a: Consecutive two-way shape memory cycles for PEVA-B10 with 20 cycles; b: Temperature-strain curves of PEVA-B10 sample with 20 cycles.

2.4 Conclusion

We synthesized a two-way (reversible) shape memory polymer comprising BPO-crosslinked PEVA. The recovery ratios of the samples with high crosslinking densities were over 99%, and such samples almost completely recovered their original shapes. The BPO crosslinker was key with regard to shape recovery, and the PEVA/BPO

compositions with high crosslinking densities had significantly elevated recovery ratios. The PEVA/BPO materials developed in the present study were sufficiently soft and had improved mechanical properties, even when subjected to large deformation. The PEVA-B10 sample had an optimal actuation strain of 12% and a shape recovery ratio of 99%. These properties could qualify the materials for use as soft actuators or in artificial intelligence, amongst other application. Further studies should investigate the long-term two-way shape memory behavior for practical applications of actuators or sensors. We also want to apply this soft shape memory materials for the artificial filed in smart bioengineering.

Reference

[1] Huang. Y. N, Fan. L. F, Rong. M. Z, Zhang. M. Q, Gao. Y. M. External Stress-Free Reversible Multiple Shape Memory Polymers. *ACS Appl. Mater. Interfaces.* 2019, *11*, 31346-31355.

[2] Gao. Y, Liu. W, Zhu. S. Polyolefin Thermoplastics for Multiple Shape and Reversible Shape Memory. *ACS Appl. Mater. Interfaces.* 2017, *9*, 4882-4889.

[3] Wu. Y, Hu. J, Han. J, Zhu. Y, Huang. H, Li. J, Tang. B. Two-Way Shape Memory Polymer with "Switch-Spring" Composition by Interpenetrating Polymer Network. *J. Mater. Chem. A* 2014, *2*, 18816-18822.

[4] Lu. L, Li. G. One-way Multishape-Memory Effect and Tunable Two-Way Shape Memory Effect of Lonomer Poly(ethylene-co-methacrylic acid). *ACS Appl. Mater. Interfaces.* 2016, *8*, 14812-148263.

[5] Li. M, Guan. Q, Dingemans. T. J. High-Temperature Shape Memory Behavior of Semicrystalline Polyamide Thermosets. *ACS Appl. Mater. Interfaces.* 2018, *10*, 19106-19115.

[6] Wang. K, Jia. Y. G, Zhu. X. X. Two-Way Reversible Shape Memory Polymers Made of Cross-Linked Cocrystallizable Random Copolymers with Tunable Actuation Temperatures. *Macromolecules* 2017, *50*, 8570-8579.

[7] Xu. Z, Ding. C, Wei. D. W, Bao. R. Y, Ke. K, Liu. Z, Yang. W. Electro and Light Active Actuators Based on Reversible Shape-Memory Polymer Composites with Segregated Conductive Networks. *ACS Appl. Mater. Interfaces.* 2019, *11*, 30332-30340.

[8] Turner. S. A, Zhou. J, Sheiko. S. S, Ashby. V. S. Switchable Micropatterned Surface Topographies Mediated by Reversible Shape Memory. *ACS Appl. Mater. Interfaces*. 2014, *6*, 8017-8021.

[9] Tippets. C. A, Li. Q, Fu, Y. Donew, E, U.; Zhou, J.; Turner, S, A.; Lopez, R. Dynamic Optical Gratings Accessed by Reversible Shape Memory. *ACS Appl. Mater. Interfaces*. 2015, *7*, 14288-14293.

[10] Kolesov. I, Dolynchuk. O, Jehnichen. D, Reuter. U, Stamm. M, Radusch. H. J. Changes of Crystal Structure and Morphology during Two-way Shape-Memory Cycles in Cross-Linked Linear and Short-Chain Branched Polyethylenes. *Macromolecules* 2015, *48*, 4438-4450.

[11] Quitmann. D, Gushterow. N, Sadowski. G, Katzenberg. F, Tiller. J. C. Solvent-Sensitive Reversible Stress-Response of Shape Memory Natural Rubber. *ACS Appl. Mater. Interfaces*. 2013, *5*, 3504-3507.

[12] Chen. S, Hu. J, Zhuo. H, Zhu. Y. Two-way shape memory effect in polymer laminates. *Mater. Lett.* 2008, *62(25)*, 4088-4090.

[13] Tamagawa. H. Thermo-responsive two-way shape changeable polymeric laminate. *Mater. Lett.* 2010, *64(6)*, 749-751.

[14] Westbrook. K. K, Mather. P. T, Parakh. V, Dunn. M. L, Ge. Q, Lee. B. M, Qi. H. J. Two-way reversible shape memory effects in a free-standing polymer composite. *Smart Mater. Struct.* 2011, *20(6)*, 065010.

[15] Qin. H, Mather. P. T. Combined one-way and two-way shape memory in a glass-forming nematic network. *Macromolecules*, 2008, *42(1)*, 273-280.

[16] Burke. K. A, Rousseau. I. A, Mather. P. T. Reversible actuation in main-chain liquid crystalline elastomers with varying crosslink densities. *Polymer*. 2014, *55(23)*, 5897-5907.

[17] Pandini. S, Passera. S, Messori. M, Paderni. K, Toselli. M, Gianoncelli. A, Riccò, T. Two-way reversible shape memory behaviour of crosslinked poly (ε-caprolactone). *Polymer*, 2012, *53(9)*, 1915-1924.

[18] Huang. M, Dong. X, Wang. L, Zhao. J, Liu. G, Wang. D. Two-way shape memory property and its structural origin of cross-linked poly (ε-caprolactone). *RSC Advances*, 2014, *4(98)*, 55483-55494.

[19] Chung. T, Romo-Uribe. A, Mather. P. T. Two-way reversible shape memory in a semicrystalline network. *Macromolecules*, 2008, *41(1)*, 184-192.

[20] Behl. M, Kratz. K, Noechel. U, Sauter. T, Lendlein. A. (2013). Temperature-memory polymer actuators. *PNAS*. 2013, *110(31)*, 12555-12559.

[21] Li. J, Rodgers. W. R., Xie. T. Semi-crystalline two-way shape memory elastomer. *Polymer*, 2011, *52(23)*, 5320-5325.

[22] Kratz. K, Madbouly. S. A, Wagermaier. W, Lendlein. A. Temperature-Memory Polymer Networks with Crystallizable Controlling Units. *Adv. Mater.* 2011, *23(35)*, 4058-4062.

[23] Qian. C, Dong Y, Zhu. Y, Fu Y. Two-way shape memory behavior of semi-crystalline elastomer under stress-free condition. *Smart Mater. Struct.* 2016, *25(8)*, 085023.

[24] Farhan. M, Rudolph. T, Nöchel,. U, Yan. W, Kratz. K, Lendlein. A.

Noncontinuously responding Polymeric actuators. *ACS Appl. Mater. Interfaces.* 2017, *9*, 33559-33564.

[25] Nöchel. U, Kumar. U. N, Wang. K, Kratz. K, Behl. M, Lendlein. A. Triple-Shape Effect with Adjustable Switching Temperatures in Crosslinked Poly [ethylene-co-(vinyl acetate)]. *Macromol. Chem. Phys.* 2014, *215(24)*, 2446-2456.

[26] Zhang. Z. X, Wei. X, Yang. J. H, Zhang. N, Huang. T, Wang. Y, Gao. X. L. Triple-Shape Memory Materials Based on Cross-Linked Poly (ethylene vinyl acetate) and Poly (ε-caprolactone). *Industrial & Engineering Chemistry Research*, 2016, *55(47)*, 12232-12241.

[27] Xu. H, Yu. C, Wang. S, Malyarchuk. V, Xie. T, Rogers. J. A. Deformable, Programmable, and Shape-Memorizing Micro-Optics. *Adv. Funct. Mater.* 2013, *23*, 3299-3306.

[28] Liu. Y, Razzaq. M. Y, Rudolph. T, Fang. L, Kratz. K, Lendlein. A. Two-level shape changes of polymeric microcuboids prepared from crystallizable copolymer networks. *Macromolecules*, 2017, *50(6)*, 2518-2527.

[29] Yang. Q; Fan. J, Li. G. Artificial Muscles Made of Chiral Two-Way Shape Memory Polymer Fibers. *Appl. Phys. Lett.* 2016, *109*, 183701.

[30] Brogly. M, Nardin. M, Schultz. J. Effect of vinylacetate content on crystallinity and second-order transitions in ethylene—vinylacetate copolymers. *J. Appl. Polym. Sci.* 1997, *64(10)*, 1903-1912.

[31] Westbrook. K. K, Parakh. V, Chung. T, Mather. P. T, Wan. L. C, Dunn. M. L, Qi. H. J. Constitutive modeling of shape memory effects in semicrystalline polymers

with stretch induced crystallization. *J. Eng. Mater. Technol.* 2010, *132(4)*, 041010.

[32] Tsagaropoulos. G, Eisenberg. A. Dynamic mechanical study of the factors affecting the two glass transition behavior of filled polymers. Similarities and differences with random ionomers. *Macromolecules*, 1995, *28(18)*, 6067-6077.

Chapter 3

Two-way reversible shape memory properties of benzoyl peroxide crosslinked poly(ethylene-co-vinyl acetate) under different stress conditions

3 Two-way reversible shape memory properties of benzoyl peroxide crosslinked poly(ethylene-co-vinyl acetate) under different stress conditions

3.1 Introduction

Shape memory polymers (SMPs) are smart materials that can significantly change their shape upon exposure to an external stimulus [1-6], such as temperature [7, 8], water [9], light [10], electricity [11-13], magnetism [14, 15], and pH [16]. SMPs can be formed into soft materials that have the advantages of light weight and excellent active deformation, and they have potential uses in a wide range of applications, including as actuators [17] and sensors [18], and in aerospace technology [19], textiles [20], and biomedical applications [21, 22].

Compared with one-way shape memory polymers which every cycle need programming at once. Two-way shape memory polymers [23-33] exhibit the complete reversibility in heating and cooling that is required for many applications. Several pioneering works have contributed to production of materials with two-way shape memory behavior, including laminated composites [34-39], liquid crystal elastomers [40, 41], and crosslinked crystalline polymers [42-57]. Laminated polymer composites because its structural instability which limit by many applications. Furthermore, synthesis of liquid crystal elastomers is still challenge.

The thermal crosslinking reaction using a crosslinking agent to crosslink semi-

crystalline polymers has attracted much attention because of the good two-way shape memory reversibility, low cost, and simple synthesis process. Mather's group reported two-way reversible shape memory in a semi-crystalline network. They investigated crosslinked poly(cyclooctene) (PCO) [35, 36, 42, 43], and its related 2W-SME by varying the concentration of the crosslinking agent dicumyl peroxide (DCP). Lendlein and co-workers [44, 45] reported preparation and characterization of crosslinked semi-crystalline polymers exhibiting two-way reversible shape memory behavior. Crosslinking of poly(ethylene-*co*-vinyl acetate) (PEVA) resulted in free-standing reversible temperature actuators with various vinyl acetate contents and crosslinking densities, which allow physical adjustment of the actuation temperature [46]. Crosslinked blends of the two crystallizable polymers poly(ε-carpolactone) (PCL) and PEVA resulted in noncontinuously responding polymeric actuators [47]. Pandini et al. reported the two-way shape memory polymer response of semi-crystalline PCL based on polymer networks [48]. In addition, they recently reported nonwoven fibrous mats based on semi-crystalline networks prepared from crosslinked PCL (cPCL) by combining electrospinning and sol-gel reactions and investigated the two-way shape memory behavior [49]. Xie and co-workers [50] and Qian et al [51]. both used semi-crystalline PEVA crosslinked by DCP to synthesize a two-way shape memory polymer. The findings of Xie's group showed how crosslinking affects the 2W-SME in different ways to the 1W-SME. Dong et al. discussed the two-way shape memory properties and corresponding structural origin of cPCL with different gel contents obtained by using different weight percentages of benzoyl peroxide (BPO) [52]. Several interesting studies on reversible

shape memory in semi-crystalline polymers have also been performed [53-57].

In the previous chapter, we developed a two-way reversible shape memory polymer using PEVA with the crosslinker BPO. In this chapter, the 2W-SME of the developed PEVA/BPO materials was achieved under constant stress and stress-free conditions. We investigated the formation conditions of the stress-free 2W-SME and found that it is determined by the relationship between the initial prestretching strain ($R_{prestretch}$) and recovery strain (R_{rec}), and it can be controlled by using a different setting temperature (T_{set}). The tunable two-way shape memory driving force and recovery force of PEVA with different BPO contents was investigated by thermomechanical cycles. The developed materials with highly crosslinked structures exhibited excellent creep resistant performance at high temperature. The reason for sample contraction during heating is that the highly crosslinked structure can provide sufficient force to recover the initial shape after melting of the crystal. Two-way actuation behavior can be achieved, resulting in an oriented crystal by cooling under an applied stress.

3.2 Experimental

3.2.1 Materials

Poly(ethylene-co-vinyl acetate) (PEVA) with 18 wt% weight percent (wt%) vinyl acetate was purchased from Sigma-Aldrich (Japan). Benzoyl peroxide (BPO, Acros Organics) was purchased from the Nippon Miractran Co., Ltd. (Japan).

3.2.2 PEVA/BPO sample preparation

A micro twin-screw extruder (DSM Xplore Compounder 15, The Nederlands) was

preheated to ensure the uniformity and stability of the temperature in the whole cylinder. The temperatures of the three section of the extruder could be individually controlled, and they were set to 90 ℃ (feeding zone), 95 ℃ (melting zone), and 100 ℃ (metering zone). PEVA containing different BPO contents (2-10 wt%) was fed into the extruder hopper and mixed at a rotation speed of 10 rpm for 10 min. The extrudate was collected and cooled to room temperature. It was then pressed in a hot press machine to crosslink into films under a pressure of 10 MPa for 20 min at 130 °C. The resulting film thickness was 0.1–1 mm and the film was cut into dumb-bell-shaped specimens for testing.

3.2.3 Characterization

The effect of strain on the two-way shape memory performance was determined from the thermo-mechanical cycles obtained by thermomechanical analysis (TMA, TMA/SS6100, SII Nano Technology Inc., Japan). The maximum reversibility of the PEVA-B10 sample was confirmed in previous work [58]. For the two-way shape memory process under the stress-free condition, the dimensions of the PEVA-B10 (PEVA with 10 wt% BPO) samples were 10 mm in length, 2 mm in width, and 0.9 mm in thickness. The cooling-heating process was as follows. The PEVA-B10 samples were preheated to 100 ℃ and then 0.2 MPa (360 mN) stretching was applied. The samples were then cooled under 0.2 MPa, the stress was unloaded to 0 MPa, and the samples were reheated to 100 ℃ under the stress-free condition. This cooling-heating process was repeated for three cycles.

For the two-way shape memory process under the constant stress condition, the PEVA-B10 samples were 10 mm in length, 2 mm in width, and 0.9 mm in thickness.

The cooling-heating process was as follows. The PEVA-B10 sample was preheated to 100 °C, external stress of 0.1 MPa (180 mN) or 0.2 MPa (360 mN) was applied, and then the constant stress was maintained throughout the test. The sample was then cooled to 20 °C and heated to 100 °C without changing the stress. This process was repeated for three cycles.

The two-way shape memory driving force and recovery force behavior was investigated for PEVA with BPO contents of 0, 2, 4, 6, 8, 10 wt%, which are designated pristine PEVA, PEVA-B2, PEVA-B4, PEVA-B6, PEVA-B8, and PEVA-10, respectively. The samples were stretched to strain of 30% at high temperature and constant strain was maintained throughout the test. The samples were then cooled to 20 °C and heated to 100 °C for three cycles to observe the change of the driving force during cooling and recovery force during heating.

The high-temperature creep tests were performed using a universal testing machine with a heat furnace (Tensile Tester, AND. Co., Japan). The PEVA/BPO sample strips were 10 mm in length and 2 mm in width. The strips were tensioned to 0.2 MPa at a tensile speed of 60 mm/min, and then maintained at 0.2 MPa for 10 min to observe the creep behavior. The whole process was performed at a high temperature of 90 °C.

The crystalline structure changes of PEVA-B10 after cooling under the unstretched condition and different stress levels were investigated by two-dimensional wide-angle X-ray diffraction (2D-WAXS, SmartLab/ST/Hypix, Rigaku Corporation) using Cu Kα radiation (λ= 1.5418 Å) at 40 kV and 30 mA on a copper anode at room temperature. The exposure time was 30 min per sample and a collimator diameter of 100 μm was

72

used. The distance between the samples and the detector was 27 mm. Samples with a thickness of about 0.5 mm were used.

The PEVA-B10 sample showing the best two-way shape memory behavior was selected for 2D-WAXS and differential scanning calorimetry (DSC, DSC8230, Rigaku Corporation) tests. The sample was preheated to 100 °C, stretched at various stresses (0.4-0.8 MPa), and then the temperature was cooled to 20 °C (below the crystallization temperature) under fixed stress applied with the TMA/SS6100 analyzer at the same stretching speed as the 2W-SME experiment and equilibrated for 5 min. The unstretched sample was also subjected to this heating-cooling process with no applied stress. The samples were then removed from the clamps and fixed to the sample holder for the 2D-WAXS and DSC tests.

3.3 Results and discussion

3.3.1 Two-way shape memory behavior under stress-free condition

3.3.1.1 Design and demonstration of two-way actuation

The PEVA-B10 film was programmed to "V" and "M" shapes under prestress (9800 mN). The programming process is shown in **Figure 3.1b**. The initial "V" and "M" shapes at high temperature (hot water, 70 °C) transformed to temporary shapes at low temperature (cold water, 20 °C) under the stress-free condition (**Figure 3.1a(i) and (ii)**). The gripper sample with the same programming process can lift an object at high temperature and then release it at low temperature (**Figure 3.1a(iii)**). An initial stress of 0.2 MPa (360 mN) was used for the PEVA-B10 samples in TMA (**Figure 3.1c**). The

samples exhibited clear two-way shape memory cycles under the stress-free condition.
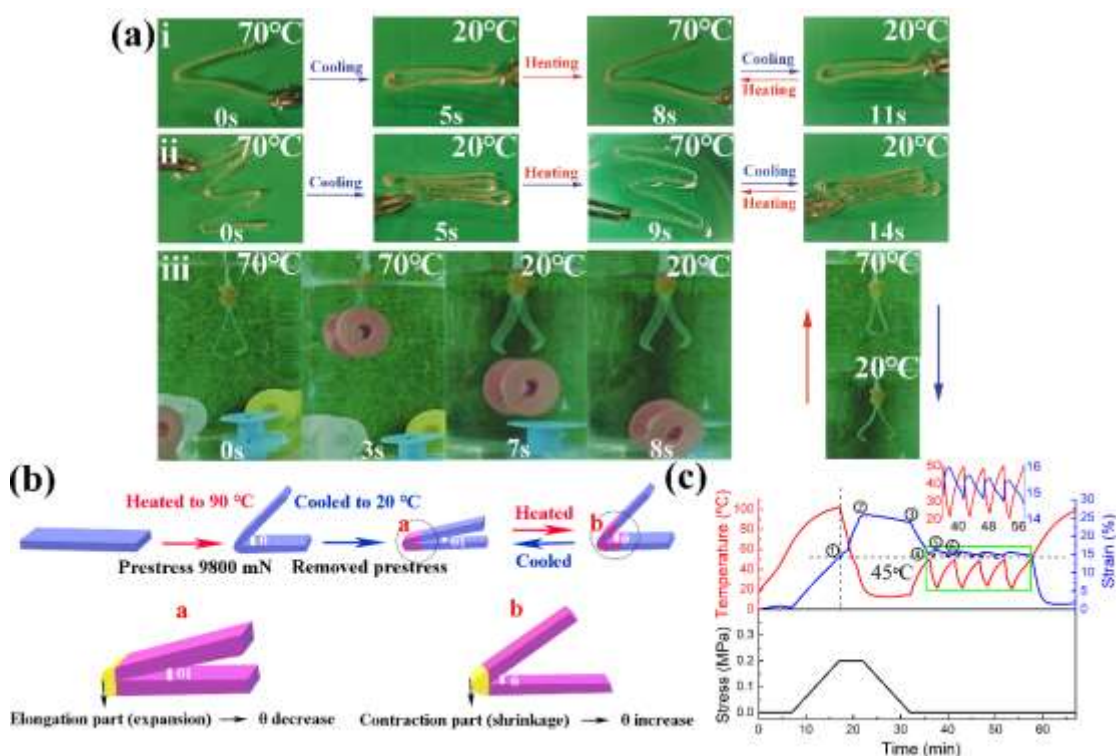
Figure 3.1 (a) Photographs of the "V", "M", and gripper shapes of the PEVA-B10 sample in hot and cold water taken from videos. (b) Schematics of the stress-free PEVA/BPO two-way shape memory behavior design. (c) Stress-free two-way shape memory cycles of the PEVA-B10 sample.

The design of the programming step of the PEVA-B10 sample to achieve the 2W-SME under the stress-free condition is shown in **Figure 3.1b**. The PEVA-B10 film was first deformed to the "V" shape at 90 °C (the programmed shape (S_{prog}) was considered to be the initial shape), cooled to 20 °C under prestress, and then the prestress was removed at 20 °C. The shape reversibly shrank to an angle of θ_1 (a in **Figure 3.1(b)**). When the sample was heated again to 90 °C, the initial "V" shape expanded to an angle of θ (b in **Figure 3.1(b)**) in response to only temperature. The samples elongated during cooling and contracted during heating. Material elongation led to a decrease of θ and shrinking of the "V" shape (yellow part in a in **Figure 3.1b**). Material contraction led

to an increase of θ (yellow part in b in **Figure 3.1b**).

It should be noted that the actuation strain is related to the applied prestress under the stress-free condition, and larger actuation strain can be achieved with larger applied stress. Owing to strain above 50% reaching the maximum value of the TMA machine, a limit of 0.2 MPa was used. The PEVA-B10 sample showed a smaller degree of the stress-free 2W-SME (**Figure 3.1c**) compared with using large prestress (**Figure 3.1a**). The external stimulus of the low temperature and high temperature are specified based on the thermal property of the materials. Here, the crystallization temperature (T_c) and melting temperature (T_m) are the reference temperature, which are the important "switch on" temperature in ensuring sample to achieve their two-way shape memory behavior

### 3.3.1.2 Formation conditions of stress-free 2W-SME

As an example, the formation conditions for the stress-free two-way shape memory behavior of PEVA-B10 at T_{set} = 45 °C are shown in **Figure 3.2b**. PEVA-B10 was preheated to 100 °C and then stretched at 0.2 MPa to the initial prestretching strain ($R_{prestretch}$, ①). The temperature was then decreased to room temperature under fixed prestress, and the sample elongated during the cooling process (①–②). The prestress was released to 0 MPa, and the strain slightly decreased owing to the shape memory fixity(②–③). The sample was then reheated to T_{set} = 35, 45, and 65 °C, and the sample was allow to recover (③–④) to three different R_{rec} values (④), which correspond to $R_{rec} > R_{prestretch}$, $R_{rec} = R_{prestretch}$, and $R_{rec} < R_{prestretch}$, respectively. The sample was cooled to room temperature and reheated to T_{set} again (④–⑤ and ⑤–⑥), which was repeated

for three cycles under the stress-free condition. The actuation strain (ε_a) and recovery

ratio (R_r) show the actuation reversibility under the stress-free condition:

$$\varepsilon_a = (\varepsilon_L - \varepsilon_H) \times 100\% \qquad\qquad \text{Eq. (3.1)}$$

$$R_r = (\varepsilon_L - \varepsilon_{Hrec})/(\varepsilon_L - \varepsilon_{H0}) \times 100\% \qquad\qquad \text{Eq. (3.2)}$$

where ε_{H0} represents R_{rec} (④), ε_L is the strain at low temperature (⑤), ε_{Hrec} is the

strain when the sample is reheated to T_{set} (⑥), and ε_H represents the strain at T_{set} in every

cycle.
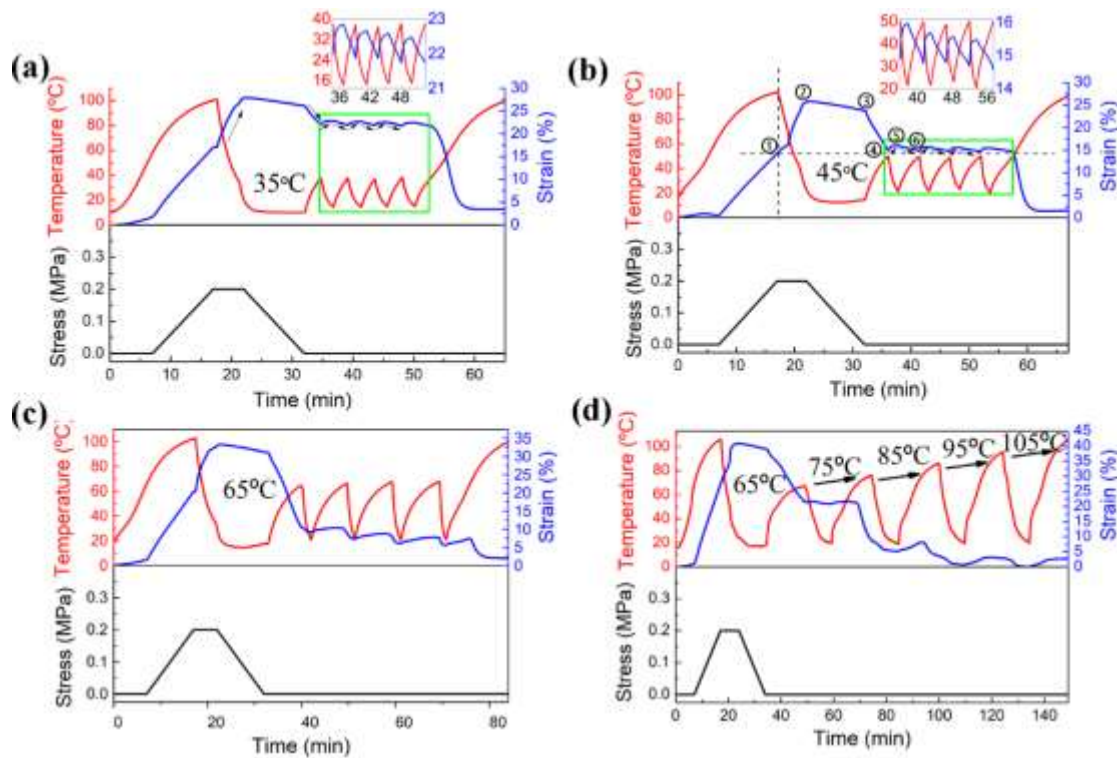
Figure 3.2 Stress-free two-way shape memory behavior of PEVA-B10 and the relationship between the initial prestretching strain, recovery strain, and setting temperature. (a) T_{set} = 35 °C. (b) T_{set} = 45 °C. (c) T_{set} = 65 °C. (d) T_{set} = 65-105 °C.

From **Table 3.1**, the best stress-free 2W-SME was achieved when $R_{rec} = R_{prestretch}$

at 45 °C (**Figure 3.2b**), where the ε_a values were 1.06%, 0.91%, and 0.88% and the R_r

value were 99.9%, 97.3%, and 97.7% in the first, second and third cycles, respectively.

The stress-free 2W-SME was weaker when $R_{rec} > R_{prestretch}$ at 35 °C (**Figure 3.2a**),

where the ε_a value were 0.85%, 0.79%, and 0.71% and the R_r values were 98.5%, 97.9%, and 98.8% in the first, second, and third cycles, respectively. It is interesting that the stress-free 2W-SME totally disappeared when $R_{rec} < R_{prestretch}$ at 65 °C (**Figure 3.2c**). The sample did not exhibit two-way shape memory behavior under the stress-free condition with T_{set} ranging from 65 to 105 °C (**Figure 3.2d**).

Table 3.1 Stress-free two-way shape memory properties under different formation conditions

Condition	Stress-free 2W-SME					
	ε_a (%)			R_r (%)		
	1st cycle	2nd cycle	3rd cycle	1st cycle	2nd cycle	3rd cycle
$R_{rec}=R_{prestretch}$ R_{rec}	1.06	0.91	0.88	99.9	97.3	97.7
$> R_{prestretch}$	0.85	0.79	0.71	98.5	97.9	98.8
$R_{rec} < R_{prestretch}$	—	—	—	—	—	—

It is important to consider the relationship between the initial prestretching strain and the recovery strain, which was the main way to achieve the stress-free 2W-SME. In addition, the stress-free two-way shape memory behavior can be controlled by varying R_{rec} using different T_{set} during the recovery process (③–④). The stress-free 2W-SME cannot be achieved if the recovery shape at T_{set} is larger than S_{prog}. These results may contribute to the use of the stress-free 2W-SME in real smart material applications.

3.3.2 Two-way shape memory behavior under constant stress conditions

Photographs of PEVA-B10 samples lifting a constant weight (2940 mN) at high (95 °C) and low temperature (35 °C) are shown in **Figure 3.3a**. Under constant external

stress, the material contracted when heated above the T_m, whereas the material elongated when the temperature dropped below the T_c. Therefore, reversible shape change can be achieved by changing the temperature under constant stress.
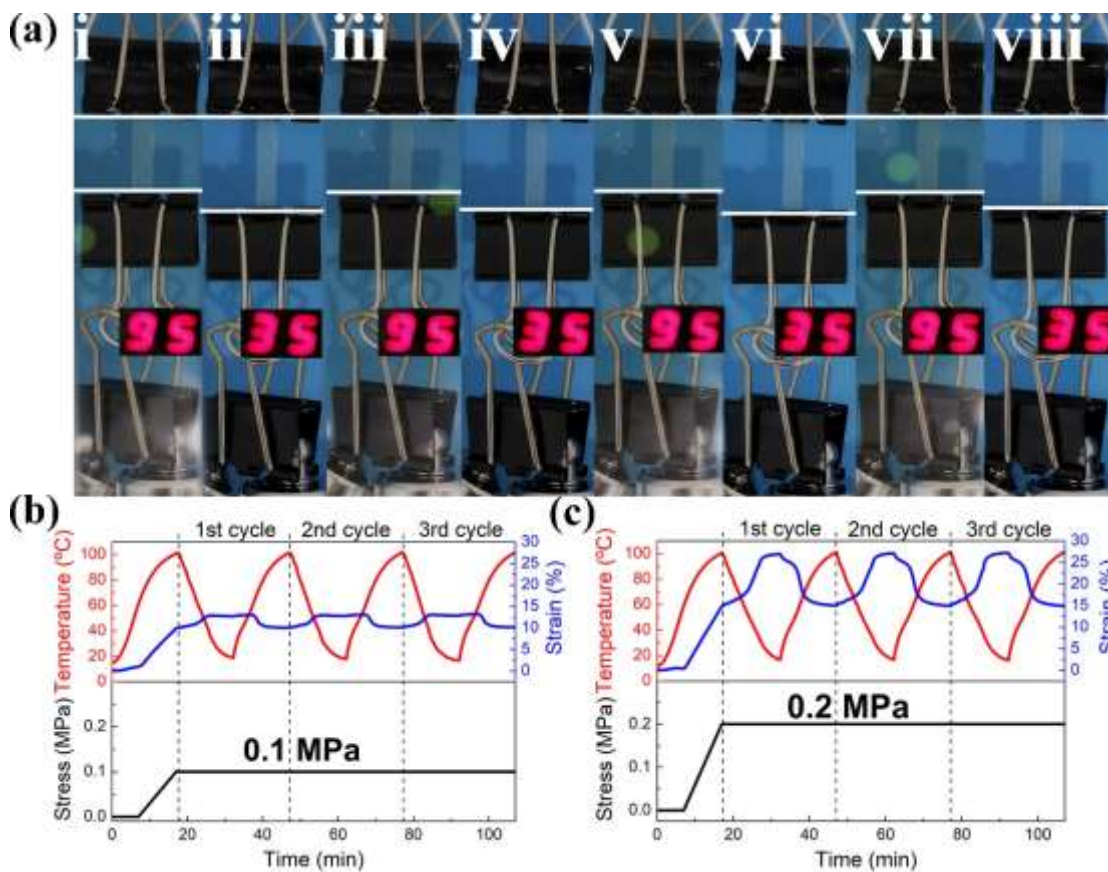
Figure 3.3 (a) Photographs of PEVA-B10 under constant stress of 2940 mN during the heating and cooling processes taken from videos. (b) Two-way shape memory cycles of PEVA-B10 under constant stress of 0.1 MPa. (c) Two-way shape memory cycles of PEVA-B10 under constant stress of 0.2 MPa.

The thermo-mechanical strain cycles of PEVA-B10 with constant stresses of 0.1 MPa (180 mN) and 0.2 MPa (360 mN) are shown in **Figure 3.3b and Figure 3.3c**, respectively. The results shows that larger actuation strain can be achieved with larger applied prestretch external stress. PEVA-B10 showed less two-way shape memory behavior under an applied stress of 0.1 MPa compared with the 0.2 MPa case. The actuation strain increased with increasing external stress. Large stress induced an

increase in the degree of crystallinity and a more oriented crystalline structure formed (**Figure 3.4 and Figure 3.5**). Furthermore, under the same prestress condition of 0.2 MPa, the actuation performance of the sample under constant stress was much more obvious than in the stress-free case (**Figure 3.1c and 3.3c**).

3.3.2.1 Microstructure characterization by 2D-WAXS and DSC analysis
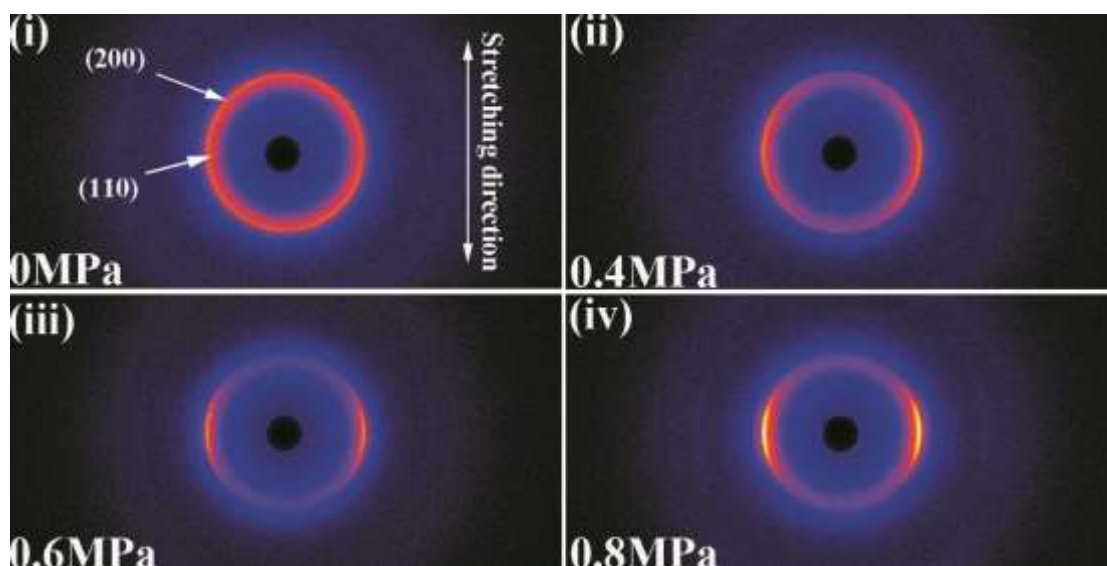
Figure 3.4 2D-WAXS patterns of the PEVA-B10 sample after cooling: (i) unstretched and under stress conditions of (ii) 0.4 MPa, (iii) 0.6 MPa, and (iv) 0.8 MPa. The white arrows indicate the stretching direction.

Table 3.2 T_m and ΔHm values of PEVA-B10 subjected to cooling under various applied stresses

Applied stress (MPa)	T_m (℃)	ΔHm (J/g)
0	70.50	18.09
0.4	71.41	22.03
0.6	71.57	27.58
0.8	75.66	40.38

[a] T_m: melting temperature peak of PEVA

[b] ΔHm: melting enthalpy calculated as the area under the curve of the PEVA melting peak

The nanoscale structural changes of the oriented crystals of PEVA-B10 after cooling under different stress conditions and the related mechanism were investigated by 2D-WAXS. The 2D-WAXS patterns of PEVA-B10 samples undergoing elongation during cooling with different stress conditions are shown in **Figure 3.4**. The unstretched sample exhibited two continuous concentric Debye–Scherrer rings located at $2\theta = 21.4°$ and $23.7°$ corresponding to the (110) and (200) planes of orthorhombic polyethylene, respectively, which are attributed to the random crystalline orientation. In the stretched samples, the discontinuous Debye–Scherrer rings showed a very distinct oriented distribution and the reflection split into four off-meridional patterns and became more intense with increasing stress, suggesting that the preferred orientation of the crystal chains was parallel to the stretching direction.

The DSC second heating scans of PEVA-B10 samples cooled under fixed strain are shown in **Figure 3.5**. The endothermic crystal-melting peak during the second heating run corresponds to the T_m. The T_m and heat of fusion (ΔH_m) values are given in **Table 3.2**. T_m and ΔHm increased with increasing applied stress. This indicates that higher load led to formation of a more ordered crystal structure [48]. Contraction of the PEVA/BPO samples during heating is because of melting of the cystals, and the crosslinked networks porvide a force to allow the sapmles to recover to their original shapes.
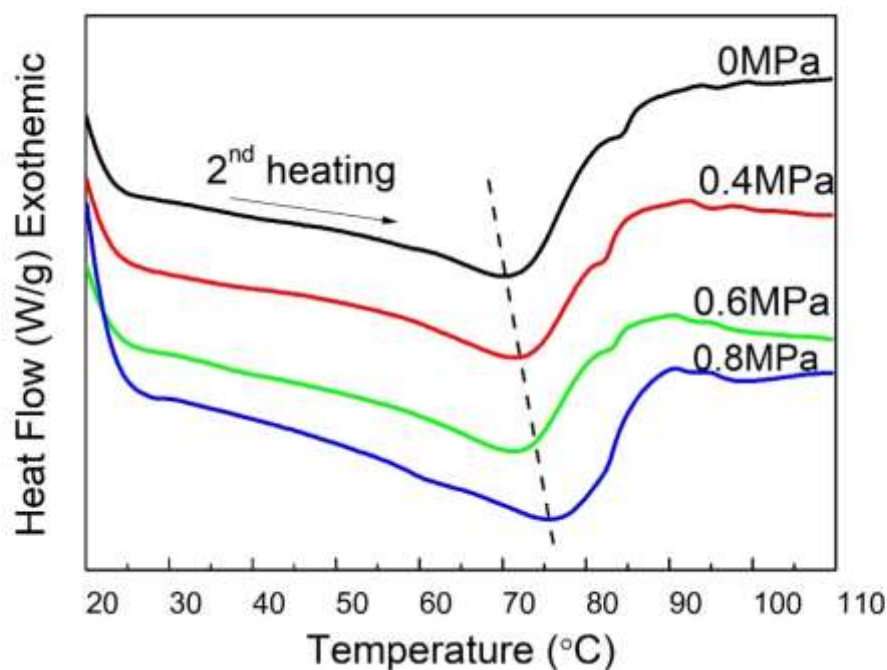
Figure 3.5 Second heating run in the DSC test for PEVA-B10 samples stretched at various stresses (0.4–0.8 MPa) and unstretched PEVA-B10 (0 MPa).
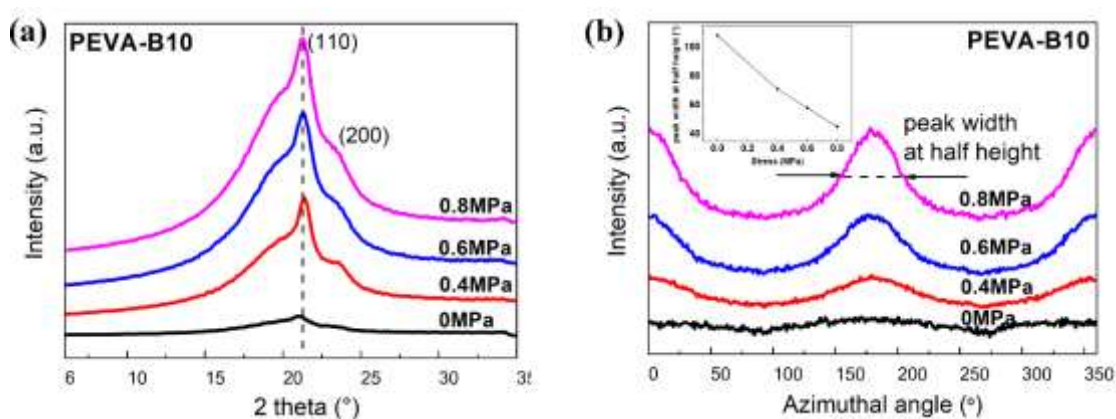
Figure 3.6 (a) 1D-WAXS intensity profiles of PEVA-B10 during cooling with various stress levels. (b) Azimuthal scanning profiles for (110) plane reflection of the PEVA-B10 sample subjected to cooling under different stress levels. The insert shows the relationship between the peak width at half height and the applied stress.

The 2D-WAXS patterns were converted to 1D-WAXS intensity profiles versus the scattering angle (2θ) and azimuthal angle (**Figure 3.6**). No change in the angular position along the 2θ axis was observed, indicating that the orthorhombic crystal structure was not affected by stress (**Figure 3.6a**). The azimuthal angles for (110) plane

81

reflection at $2\theta = 21.4°$ for samples with different stress levels are shown in **Figure 3.6b**. The unstretched sample showed less variation of the intensity with the azimuthal angle than the stretched samples. The intensity peak became narrower with increasing stress, indicating that a more oriented crystalline structure was achieved. The peak width at half height values of the PEVA-B10 samples at different stress levels are shown in the insert of **Figure 3.6b**. A lower value of the peak width at half height is usually caused by a more oriented crystalline structure. Higher applied stress caused larger strain, resulting in a greater amount of crystal orientation and leading to a lower peak width at half height value. 2D-WAXS analysis demonstrated that excellent two-way actuation behavior can be achieved with high applied stress owing to the preferred orientation of crystal chains of the crystalline structure.

3.3.2.2 Long-term thermomechanical cycle analysis

The stability and repeatability of the long-term two-way shape memory performance of PEVA-B10 during 42 cycles are shown in **Figure 3.7**. In the multicycle experiment, the thermomechanical cycles of the PEVA-B10 sample showed good reversibility of the two-way shape memory behavior. No significant changes were observed, and consistency and stability were maintained during the 42 cycles. It can be expected that PEVA-B10 exhibits stable two-way (reversible) shape memory behavior even during long-term thermomechanical cycles.
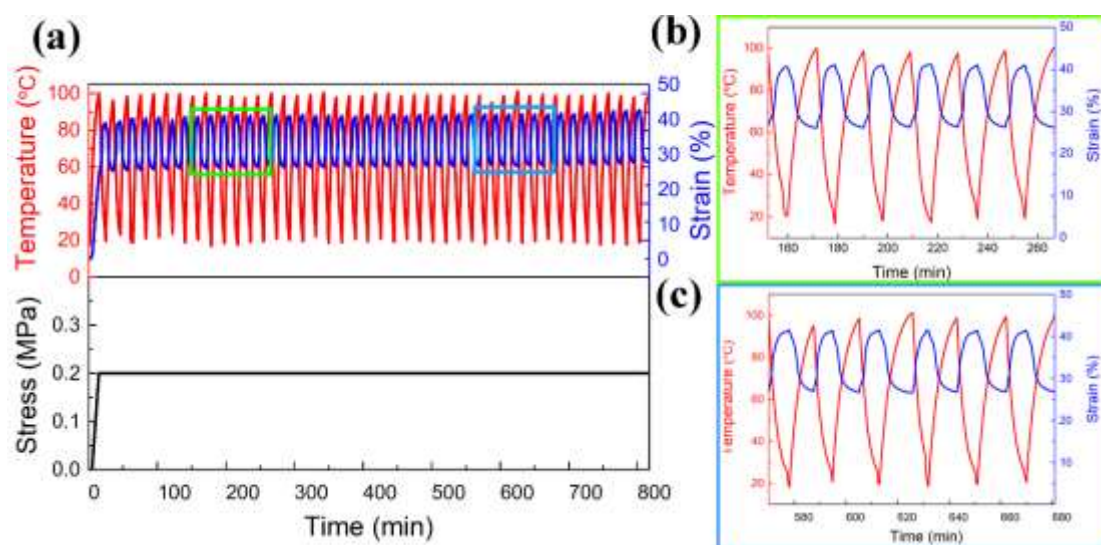
Figure 3.7 (a) Consecutive two-way shape memory cycles of PEVA-B10 for 42 cycles. (b) Two-way shape memory cycles 8–13 (green rectangle in (a)). (c) Two-way shape memory cycles 30-36 (blue rectangle in (a)).

3.3.3 Tunable two-way shape memory driving force and recovery force of PEVA with different BPO contents under constant strain

The two-way shape memory driving force and recovery force properties of PEVA with BPO contents of 0, 2, 4, 6, 8, and 10 wt%, which are designated pristine PEVA, PEVA-B2, PEVA-B4, PEVA-B6, PEVA-B8, and PEVA-10, respectively, are shown in **Figure 3.8a-f**. First, the samples were stretched to strain of 30% at high temperature, and constant strain was maintained throughout the tests. The samples were then cooled to 20 °C and heated to 100 °C again. This was repeated for three cycles to observe the change of the driving force during cooling and recovery force during heating.
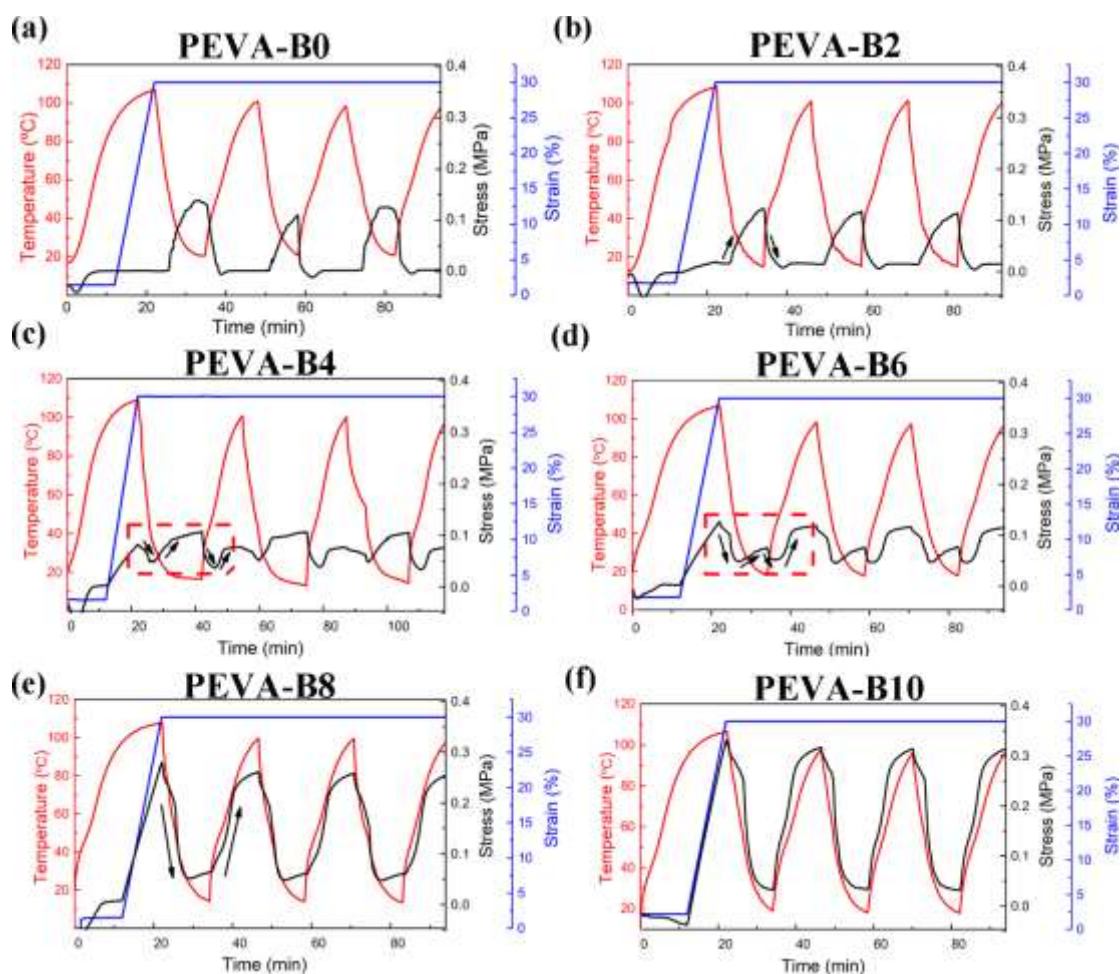
Figure 3.8 Two-way shape memory driving force and recovery force behavior of PEVA with different BPO contents under constant strain. (a) Pristine PEVA. (b) PEVA-B2. (c) PEVA-B4. (d) PEVA-B6. (d) PEVA-B8. (d) PEVA-B10.

Maintaining constant strain, the forces of pristine PEVA and PEVA-B2 slightly increased during cooling and decreased during heating. This behavior can be attributed to the sample becoming rigid during cooling and soft during heating, which occur for most thermoplastic polymers. With increasing BPO content, this behavior showed a weakening trend. From PEVA-B4 to PEVA-B6, the force began to divide into two different trends with an initial decrease and then an increase during cooling and heating (**Figure 3.8c and d**). Furthermore, the actuation and recovery force more obviously formed with a more crosslinked structure. For the PEVA-B8 sample, the driving and

recovery force preliminary formed with the force decreasing during cooling and increasing during heating with only a change in the temperature under the constant strain condition (**Figure 3.8e**). PEVA-B10 showed the strongest two-way shape memory driving force and recovery force behavior (**Figure 3.8f**).

The changing trends of the force were different for pristine PEVA and high crosslink density PEVA-B10. The driving force can be obtained because of promotion of oriented crystal growth inducing sample elongation in the cooling process under load (**Figure 3.4**). The crosslinked structure of the sample leads to contraction when the crystal melts, which provides the recovery force in the heating process (**Figure 3.9a and b**). With constant strain, the highly crosslinked sample can provide a consistent two-way shape memory driving and recovery force, and the magnitude of the force can be controlled by varying the BPO content. These results may contribute to actuator, sensor, and other applications.

3.3.4 High-temperature creep characterization

The high-temperature creep performance of PEVA with different BPO contents is shown in **Figure 3.9a and b)**. The creep strain of PEVA-B1 dramatically increased from 50 to 600 s under constant stress, but the creep strain of the high crosslink density PEVA-B10 sample remained stable (**Figure 3.9a**). Low crosslink density PEVA-B2 and high crosslink density PEVA-B10 were used to investigate the two-way shape memory behavior under constant stress (**Figure 3.9c and d)**. The low crosslink density sample showed a small degree of the 2W-SME, and it did not exhibit good recovery and recyclability. The high crosslink density sample showed highly repeatable

thermomechanical curves, showing its excellent shape memory recovery and highly invertible two-way cyclability.
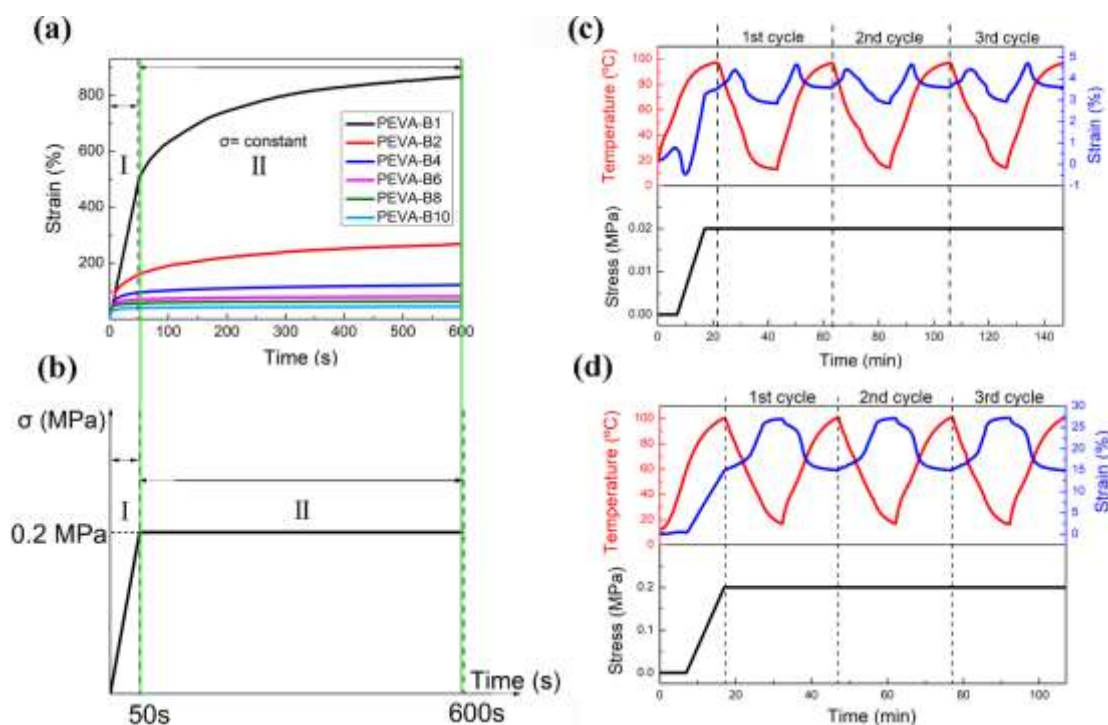
Figure 3.9 (a) and (b) High-temperature creep resistant performance of PEVA with different BPO contents at 90 ℃. (c) Consecutive two-way shape memory cycles for (c) low crosslink density PEVA-B2 and (d) high crosslink density PEVA-B10.

The results for the low crosslink density sample show viscous flow behavior above the melting temperature. However, the high stability of the rubber state with high BPO crosslinking can prevent creep and inhibit plastic flow at high temperature. BPO as a crosslinker plays an important role in allowing the sample to return to its original shape, and the crosslinked network structure provides sufficient force to recover the initial shape. This explains why the high crosslink density sample exhibited ideal shape recovery performance.

4. Conclusion

The 2W-SME of PEVA/BPO has been achieved under both constant stress and

stress-free conditions. The relationship between the initial prestretching strain ($R_{\text{prestretch}}$) and recovery strain (R_{rec}) was the main reason for achievement of the stress-free 2W-SME of PEVA/BPO. Furthermore, three different types of stress-free two-way shape memory behavior were observed during the TMA cycles: the ideal stress-free 2W-SME ($R_{\text{rec}} = R_{\text{prestretch}}$), the weak stress-free 2W-SME ($R_{\text{rec}} > R_{\text{prestretch}}$), and no stress-free 2W-SME ($R_{\text{rec}} < R_{\text{prestretch}}$), which can be controlled by varying R_{rec} using different T_{set} during the recovery process. The two-way shape memory driving force and recovery force behavior of PEVA with different BPO contents under constant strain was investigated, and a clear two-way shape memory driving and recovery force was observed for PEVA-B10. The sample with high BPO content exhibited good high-temperature creep resistant performance. The crystalline regions melted when the temperature reached T_{m}, and the crosslinked network allowed the sample to return to its initial shape. 2D-WAXS and DSC tests indicated that the crystalline structure led to oriented growth of crystals under applied stress, and crystallization led to elongation upon cooling. These results will contribute to actuator, sensor, and artificial intelligence applications.

Reference

[1] Behl. M, Razzaq. M. Y, Lendlein. A. Multifunctional Shape-Memory Polymers. *Adv. Mater.* 2010, *22*, 3388-3410.

[2] Meng. H, Li. G. A review of Stimulus-Responsive Shape Memory Polymer Composites. *Polymer* 2013, *54*, 2199-2221.

[3] Mu. T, Liu. L, Lan. X, Liu. Y, Leng. J. Shape Memory Polymer for Composites. *Compos. Sci. Technol.* 2018, *160*, 169-198.

[4] Liu. C, Qin. H, Mather. P. T. Review of Progress in Shape-Memory Polymers. *J. Mater. Chem.* 2007, *17*, 1543-1558.

[5] Du. L, Xu. Z. Y, Fan. C. J, Xiang. G, Yang. K. K, Wang. Y. Z. A Fascinating Metallo-Supramolecular Polymer Network with Thermal/Magnetic/Light-Responsive Shape-Memory Effect Anchored by Fe_3O_4 Nanoparticles. *Macromolecules* 2018, *51*, 705-715.

[6] Li. W, Liu. Y, Leng. J. Shape Memory Polymer Nanocomposite with Multi-Stimuli Response and Two-Way Reversible Shape Memory Behavior. *RSC Adv.* 2014, *4*, 61847-61854.

[7] Lendlein. A, Schmidt. A. M, Schroeter. M. Langer. R. Shape-Memory Polymer Networks from Oligo (ϵ-caprolactone) dimethacrylates. *J. Polym. Sci., Part A: Polym. Chem.* 2005, *43,* 1369-1381.

[8] Ohki. T, Ni. Q. Q, Ohsako. N, Iwamoto. M. Mechanical and Shape Memory Behavior of Composites with Shape Memory Polymer. *Composites Part A* 2004, *35*, 1065-1073.

[9] Huang. W. M, Yang. B, An. L, Li. C, Chan. Y. S. Water-Driven Programmable Polyurethane Shape Memory Polymer: Demonstration and Mechanism. *Appl. Phys. Lett.* 2005, *86*, 114105.

[10] Lendlein. A, Jiang. H, Jünger. O, Langer. R. Light-Induced Shape-Memory Polymers. *Nature* 2005, *434*, 879.

[11] Liu. Y, Lv. H, Lan. X, Leng. J, Du. S. Review of Electro-Active Shape-Memory Polymer Composite. *Compos. Sci. Technol.* 2009, *69*, 2064-2068.

[12] Yao. Y, Zhou. T, Wang. J, Li. Z, Lu. H, Liu. Y, Leng. J. 'Two way'shape memory composites based on electroactive polymer and thermoplastic membrane. *Compos Part A- Appl S.* 2016, *90*, 502-509.

[13] Zhang. Z. X, Wang. W. Y, Yang. J. H, Zhang. N, Huang. T, Wang. Y. Excellent Electroactive Shape Memory Performance of EVA/PCL/CNT Blend Composites with Selectively Localized CNTs. *J. Phys. Chem. C* 2016, *120*, 22793-22802.

[14] Razzaq. M. Y, Behl, M, Kratz. K, Lendlein. A. Multifunctional Hybrid Nanocomposites with Magnetically Controlled Reversible Shape-Memory Effect. *Adv. Mater.* 2013, *25*, 5730-5733.

[15] Schmidt. A. M. Electromagnetic Activation of Shape Memory Polymer Networks Containing Magnetic Nanoparticles. *Macromol. Rapid Commun.* 2006, *27*, 1168-1172.

[16] Han. X. J, Dong. Z. Q, Fan. M. M, Liu. Y, li. J. H, Wang. Y. F, Zhang. S. pH-induced shape-memory polymers. *Macromol. Rapid Commun.* 2012, *33(12)*, 1055-1060.

[17] Song. J. J, Chang. H. H, Naguib. H. E. Biocompatible Shape Memory Polymer Actuators with High Force Capabilities. *Eur. Polym. J.* 2015, *67*, 186-198.

[18] Kunzelman. J, Chung. T, Mather. P. T, Weder. C. Shape Memory Polymers with Built-in Threshold Temperature Sensors. *J. Mater. Chem.* 2008, *18*, 1082-1086.

[19] Liu. Y, Du. H, Liu. L, Leng. J. Shape memory polymers and their composites in aerospace applications: a review. *Smart Mater. Struct.* 2014, *23(2)*, 023001.

[20] Hu. J, Chen. S. A Review of Actively Moving Polymers in Textile Applications. *J. Mater. Chem.* 2010, *20*, 3346-3355.

[21] Lendlein. A, Langer,. R. Biodegradable, elastic shape-memory polymers for potential biomedical applications. *Science* 2002, *296(5573)*, 1673-1676.

[22] Ward Small. I. V, Singhal. P, Wilson. T. S, Maitland. D. J. Biomedical Applications of Thermally Activated Shape Memory Polymers. *J. Mater. Chem.* 2010, *20*, 3356-3366.

[23] Huang Y. N, Fan L. F, Rong M. Z, Zhang M. Q, Gao Y. M. External Stress-Free Reversible Multiple Shape Memory Polymers. *ACS App. Mater. Interfaces*, 2019, *11(34)*, 31346-31355.

[24] Gao. Y, Liu. W, Zhu. S. Polyolefin thermoplastics for multiple shape and reversible shape memory. *ACS App. Mater. Interfaces*, 2017, *9(5)*, 4882-4889.

[25] Wu. Y, Hu. J, Han. J, Zhu. Y, Huang. H, Li. J, Tang. B. Two-Way Shape Memory Polymer with "Switch-Spring" Composition by Interpenetrating Polymer Network. *J. Mater. Chem. A* 2014, *2*, 18816-18822.

[26] Lu. L, Li. G. One-way Multishape-Memory Effect and Tunable Two-Way Shape

Memory Effect of Lonomer Poly(ethylene-co-methacrylic acid). *ACS Appl. Mater. Interfaces.* 2016, *8*, 14812-148263.

[27] Li. M, Guan. Q, Dingemans. T. J. High-Temperature Shape Memory Behavior of Semicrystalline Polyamide Thermosets. *ACS Appl. Mater. Interfaces.* 2018, *10*, 19106-19115.

[28] Wang. K, Jia. Y. G, Zhu. X. X. Two-Way Reversible Shape Memory Polymers Made of Cross-Linked Cocrystallizable Random Copolymers with Tunable Actuation Temperatures. *Macromolecules* 2017, *50*, 8570-8579.

[29] Xu. Z, Ding. C, Wei. D. W, Bao. R. Y, Ke. K, Liu. Z, Yang. W. Electro and Light Active Actuators Based on Reversible Shape-Memory Polymer Composites with Segregated Conductive Networks. *ACS Appl. Mater. Interfaces.* 2019, *11*, 30332-30340.

[30] Turner. S. A, Zhou. J, Sheiko. S. S, Ashby. V. S. Switchable Micropatterned Surface Topographies Mediated by Reversible Shape Memory. *ACS Appl. Mater. Interfaces.* 2014, *6*, 8017-8021.

[31] Tippets. C. A, Li. Q, Fu, Y. Donew, E, U.; Zhou, J.; Turner, S, A.; Lopez, R. Dynamic Optical Gratings Accessed by Reversible Shape Memory. *ACS Appl. Mater. Interfaces.* 2015, *7*, 14288-14293.

[32] Kolesov. I, Dolynchuk. O, Jehnichen. D, Reuter. U, Stamm. M, Radusch. H. J. Changes of Crystal Structure and Morphology during Two-way Shape-Memory Cycles in Cross-Linked Linear and Short-Chain Branched Polyethylenes. *Macromolecules* 2015, *48*, 4438-4450.

[33] Quitmann. D, Gushterow. N, Sadowski. G, Katzenberg. F, Tiller. J. C. Solvent-Sensitive Reversible Stress-Response of Shape Memory Natural Rubber. *ACS Appl. Mater. Interfaces.* 2013, *5*, 3504-3507.

[34] Chen. S, Hu. J, Zhuo. H, Zhu. Y. Two-way shape memory effect in polymer laminates. *Mater. Lett.* 2008, *62(25)*, 4088-4090.

[35] Ge. Q, Westbrook. K. K, Mather. P. T, Dunn. M. L, Qi. H. J. Thermomechanical behavior of a Two-Way Shape Memory Composite Actuator. *Smart Mater. Struct.* 2013, *22*, 055009.

[36] Westbrook. K. K, Mather. P. T, Parakh. V, Dunn. M. L, Ge, Q, Lee. B. M, Qi. H. J. Two-way reversible shape memory effects in a free-standing polymer composite. *Smart Materials and Structures*, 2011, *20(6)*, 065010.

[37] Zhang. C. S, Ni. Q. Q. Bending Behavior of Shape Memory Polymer based Laminates. *Compos Struct.* 2007, *78*, 153-161.

[38] Wang. Z, Song. W, Ke. L, Wang. Y. Shape Memory Polymer Composite Structure with Two-Way Shape Memory Effects. *Mater. Lett.* 2012, *89*, 216-218.

[39] Tamagawa. H, Kikuchi. K, Nagai. G. Mechanical Characteristics of a Thermo-Responsive Two-Way Shape Change Polymeric Laminate. *Sensor Actuat A-Phys.* 2010, *163*, 356-362.

[40] Qin. H, Mather. P. T. Combined One-Way and Two-Way Shape Memory in a Glass-Forming Nematic Network. *Macromolecules* 2008, *42*, 273-280.

[41] Burke. K. A, Rousseau. I. A, Mather. P. T. Reversible Actuation in Main-Chain Liquid Crystalline Elastomers with Varying Crosslink Densities. *Polymer* 2014, *55*,

5897-5907.

[42] Chung. T, Romo-Uribe. A, Mather. P. T. Two-Way Reversible Shape Memory in a Semicrystalline Network. *Macromolecules* 2008, *41*, 184-192.

[43] Westbrook. K. K, Parakh. V, Chung. T, Mather. P. T, Wan. L. C, Dunn. M. L, Qi. H. J. Constitutive Modeling of Shape Memory Effects in Semicrystalline Polymers with Stretch Induced Crystallization. *J. Eng. Mater. Technol.* 2010, *132*, 041010.

[44] Behl. M, Kratz. K, Zotzmann. J, Nöchel. U, Lendlein. A. Reversible Bidirectional Shape-Memory Polymers. *Adv. Mater.* 2013, *25*, 4466-4469.

[45] Farhan. M, Chaganti. S. R, Nöchel. U, Kratz, K, Lendlein. A. Reversible Shape-Memory Properties of Surface Functionalizable, Crystallizable Crosslinked Terpolymers. *Polym. Adv. Technol.* 2015, *26*, 1421-1427.

[46] Behl, M.; Kratz, K.; Noechel, U.; Sauter, T.; Lendlein, A. Temperature-Memory Polymer Actuators. *PNAS* 2013, *110*, 12555-12559.

[47] Farhan. M, Rudolph. T, Nöchel,. U, Yan. W, Kratz. K, Lendlein. A. Noncontinuously responding Polymeric actuators. *ACS Appl. Mater. Interfaces.* 2017, *9*, 33559-33564.

[48] Pandini. S, Passera, S, Messori. M, Paderni. K, Toselli. M, Gianoncelli. A, Riccò, T. Two-Way Reversible Shape Memory Behavior of Crosslinked Poly (ε-Caprolactone). *Polymer* 2012, *53*, 1915-1924.

[49] Pandini. S, Agnelli. S, Merlettini. A, Chiellini. F, Gualandi. C, Paderni. K, Toselli, M. Multifunctional Electrospun Nonwoven Mats with Two-Way Shape Memory Behavior Prepared from Sol-Gel Crosslinked Poly (ε-Caprolactone). *Macromol*

Mater Eng. 2008, *302*, 1600519.

[50] Li. J, Rodgers. W. R, Xie. T. Semi-Crystalline Two-Way Shape Memory Elastomer. *Polymer* 2011, *52*, 5320-5325.

[51] Qian. C, Dong. Y, Zhu. Y, Fu. Y. Two-Way Shape Memory Behavior of Semi-Crystalline Elastomer under Stress-Free Condition. *Smart Mater. Struct.* 2016, *25*, 085023.

[52] Huang. M, Dong. X, Wang. L, Zhao. J, Liu. G, Wang. D. Two-Way Shape Memory Property and its Structural Origin of Cross-Linked Poly (ε-Caprolactone). *RSC Advances*. 2014, *4*, 55483-55494.

[53] Dolynchuk. O, Kolesov. I, Jehnichen. D, Reuter. U, Radusch. H. J, Sommer. J. U. Reversible Shape-Memory Effect in Cross-Linked Linear Poly (ε-Caprolactone) under Stress and Stress-Free Conditions. *Macromolecules* 2017, *50,* 3841-3854.

[54] Han. J. L, Lai. S. M, Chiu. Y. T, Two-Way Multi-Shape Memory Properties of Peroxide Crosslinked EthyleneVinyl-Acetate Copolymer (EVA)/Polycaprolactone (PCL) blends. *Polym. Adv. Technol.* 2018, *29*, 2010-2024.

[55] Yang. Q; Fan. J, Li. G. Artificial Muscles Made of Chiral Two-Way Shape Memory Polymer Fibers. *Appl. Phys. Lett.* 2016, *109*, 183701.

[56] Zhou. J, Turner. S. A, Brosnan. S. M, Li. Q, Carrillo. J. M. Y, Nykypanchuk. D, Sheiko. S. S. Shapeshifting: Reversible Shape Memory in Semicrystalline Elastomers. *Macromolecules* 2014, *47*, 1768-1776.

[57] Xu. H, Yu. C, Wang. S, Malyarchuk. V, Xie. T, Rogers. J. A. Deformable, Programmable, and Shape-Memorizing Micro-Optics. *Adv. Funct. Mater.* 2013, *23*,

3299-3306.

[58] Hui. J, Xia. H, Chen. H, Qiu. Y, Fu. Y, Ni. Q, Q. Two-Way Reversible Shape Memory Polymer: Synthesis and Characterization of Benzoyl Peroxide-Crosslinked Poly(ethylene-co-vinyl acetate). *Mater. Lett.* 2019, 2*85*, 126762.

Chapter 4

Benzoyl peroxide thermo-crosslinked poly(ethylene-co-vinyl acetate) foam with two-way shape memory effect

4 Benzoyl peroxide thermo-crosslinked poly(ethylene-co-vinyl acetate) foam with two-way shape memory effect

4.1 Introduction

Shape memory polymer foams with three-dimensional (3D) porous structures have been extensively investigated for aerospace, biomedical [1, 2], self-healing [3-5] applications. A wide range of applications [6, 7] can be expected due to the materials' low mass, highly compressible, and self-deployable qualities, such as solar sails, and foldable microcar and airplane wings for specific flight requirements. Numerous methods were used to fabricate porous foam, such as gas foaming [8-11], particulate leaching [12-16], electro-spinning [17], phase separation [18], emulsion templating [19-25], and solid state foaming [26-29].

For the shape memory foam materials, most researches were focused on the one-way shape memory effect(1W-SME), compared with an one-way shape memory polymer foam with the drawback that the programming step requires an external force for each cycle [30-35], which may limit their applications. The two-way shape memory effect (2W-SME) shows full reversibility during exposure to external stimuli in every cycle. The two-way shape memory polymer foams are smart materials that have the advantages of being lightweight and excellent active deformation, which may be potentially applied in a wide range of applications, include--ng lightweight porous

polymeric actuators, sensors, and artificial intelligence. Mather and coworkers proposed shape memory poly(ε-caprolactone)-co-poly(ethylene glycol) foams, their foam with salts could be UV cured and exhibited reversible actuation when compressed [36]. Lendlein and coworkers proposed water-blown polyurethane foams showed a reversible shape memory effect [37]. Despite the importance of two-way shape memory polymer foams, few relevant researchers have focused on this material.

The aim of this chapter is to develop a porous foam with two-way shape memory effect (2W-SME). The poly(ethylene-co-vinyl acetate) (PEVA)/ benzoyl peroxide (BPO) mixture was prepared using a solution method. Samples were foamed via a salt-leaching and thermo-crosslinked technology. The salt-leaching technology resulted in the formation of pores between the pore walls in the PEVA/BPO foam, and the foaming process does not include any chemical blowing agents. Various pore sizes of PEVA/BPO porous foam were obtained using different NaCl particle sizes. The PEVA/BPO foams with various pore sizes exhibited reversible shape changes that allowed contraction during cooling and expansion during heating. The ideal two-way shape memory performance can be clearly observed in the large pore size sample PEVA/BPO-450. The morphology was characterized by scanning electron micron microscopy (SEM) and X-ray microcomputed tomography scanning (μCT) analysis. The compression behavior of PEVA/BPO foam was also investigated. These properties of two-way reversible shape memory PEVA/BPO foams could qualify their use as lightweight porous actuators in artificial intelligence and aerospace applications, among others.

4.2 Experimental

4.2.1 Materials

Poly(ethylene-co-vinyl acetate) (PEVA) with 18 weight percent (wt%) vinyl acetate was purchased from Sigma-Aldrich (Japan). Benzoyl peroxide (BPO, Acros Organics) was purchased from the Nippon Miractran Co., Ltd. (Japan). NaCl particles were purchased from the Wako Pure Chemical Industries, Ltd. (Japan).

4.2.2 Fabrication of two-way shape memory PEVA/BPO foam

Four different sizes of NaCl particles (0–50 μm, 50–110 μm, 110–160 μm, and 160–450 μm; Wako Pure Chemical Industries, Osaka, Japan) were obtained using a ball mill and sieves with different average mesh sizes. Eight grams of PEVA (18 weight percent [wt%] vinyl acetate; Sigma-Aldrich, Tokyo, Japan) containing 2 g BPO (Nippon Miractran, Atsugi, Japan) with four sizes of NaCl particles were completely dissolved in xylene, respectively (**Figure 4.1**). The mixed solution was put in vacuum for 12 h at 85 °C to remove bubbles and then dried at 85 °C for 5 days. Further thermo-crosslinking was performed to cure the sample in a vacuum electric furnace for 7 h at 200 °C and then it was immersed in distilled water to remove the salts (the distilled water was changed every 5 h). Two-way shape memory porous foams were obtained with different pore sizes of 0–50 μm, 50–110 μm, 110–160 μm, and 160–450 μm, which were denoted as PEVA/BPO-50, PEVA/BPO-110, PEVA/BPO-160, PEVA/BPO-450, respectively.
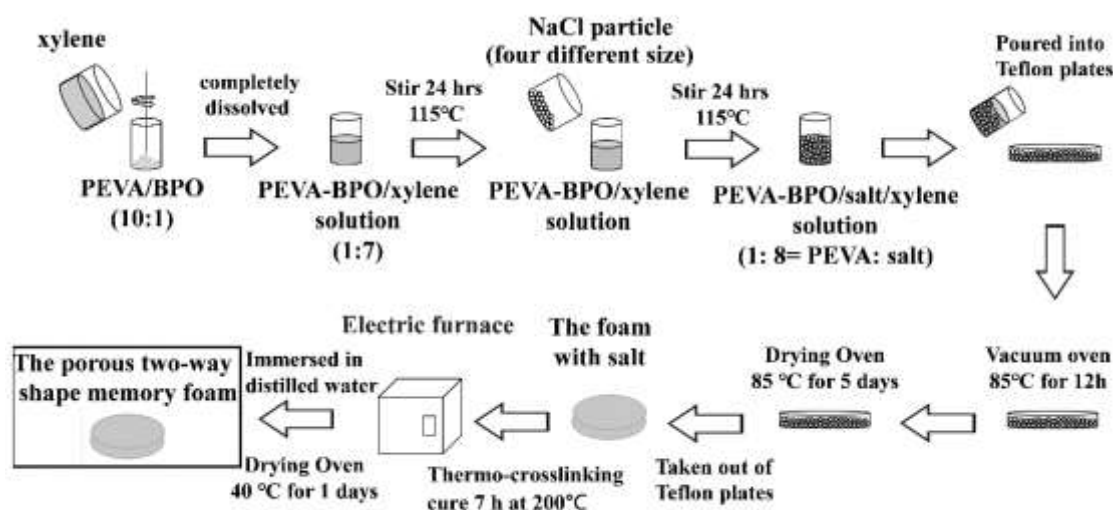
Figure 4.1 Schematic of two-way shape memory PEVA/BPO foam fabrication.

4.2.3 Characterization and evaluation

The pore morphology and 3D structure of the two-way shape memory PEVA/BPO foams were examined by scanning electron microscopy (SEM; SU-1510, Hitachi High-Technologies, Japan) under high vacuum at 15 kV. The samples were first to coated with Pt onto the surface for SEM observation. The average pore size was obtained from SEM image.

The PEVA/BPO foams were scanned using X-ray micro-computed tomography scanning (μCT; Skyscan 1272 Micro-CT, Bruker, Germany) to determine the three-dimensional (3D) structure of PEVA/BPO foam. The foam cut to 6 mm long, 4 mm wide, and 2 mm thick, then placed on a sample tube with a size of 5 mm diameter and scanned with a voltage of 40 kV and 250 μA. The X-ray CT image size was 1224×820 voxels. CTvox software was used for visualization and generation of the 3D images.

The compression behavior of the PEVA/BPO foam was investigated by using the thermomechanical analysis (TMA/SS6100, SII Nano Technology Inc. Japan). Each

sample with different pore size was deformed to 40% compressive strain at a rate of 560 µm/min. Then released at a rate of 560 mm/min.

Two-way shape memory behavior of PEVA/BPO foams was determined by the thermomechanical analysis (TMA/SS6100, SII Nano Technology Inc. Japan) in compression mode. The compression probe was made of quartz glass with a diameter of 3.5 mm, the required diameter of two-way PEVA/BPO foam is in the range from 4 mm to 8 mm, and the cylindrical specimens was placed on sample stage with 12 mm (diameter). The maximum load of TMA machine was 1.4 N and a preload of 10 mN was used. For constant prestrain, the sample was first heated from 25 °C to 85 °C at a rate of 2.5 °C/min, then compressed to 40% compressive strain at a rate of 0.95 mm/min. This compression strain of 40% was maintained as the specimen was cooled to 25 °C and heated to 80 °C again at a rate of 4.5 °C/min, and this step was repeated for three cycles.

The density and porosity were calculated using the following equations:

$$\rho_{porous} = \frac{m_{porous}}{V_{porous}} = \frac{m_{porous}}{\frac{m_{porous}}{\rho_{solid}} + \frac{m_w - m_{porous}}{\rho_w}} = \frac{m_{porous}\,\rho_{solid}\,\rho_w}{m_{porous}\,\rho_w + (m_w - m_{porous})\,\rho_{solid}} \quad (1)$$

$$P = \frac{\rho_{solid} - \rho_{porous}}{\rho_{solid}} \times 100\% \quad (2)$$

where ρ_{porous} is the density of the specimen (g/cm^3), m_{porous} is the weight of the specimen in air (g), V_{porous} is the volume of the specimen (cm^3), m_w is the weight of the water-saturated specimen in air (g), ρ_{solid} is the density of the PEVA (0.94 g/cm^3 at 25 °C), ρ_w is the density of the water (0.99705 g/cm^3 at 25 °C), and P is the porosity of the specimen.

4.3 Results and discussion

4.3.1 The morphology and compression behavior of PEVA/BPO foam
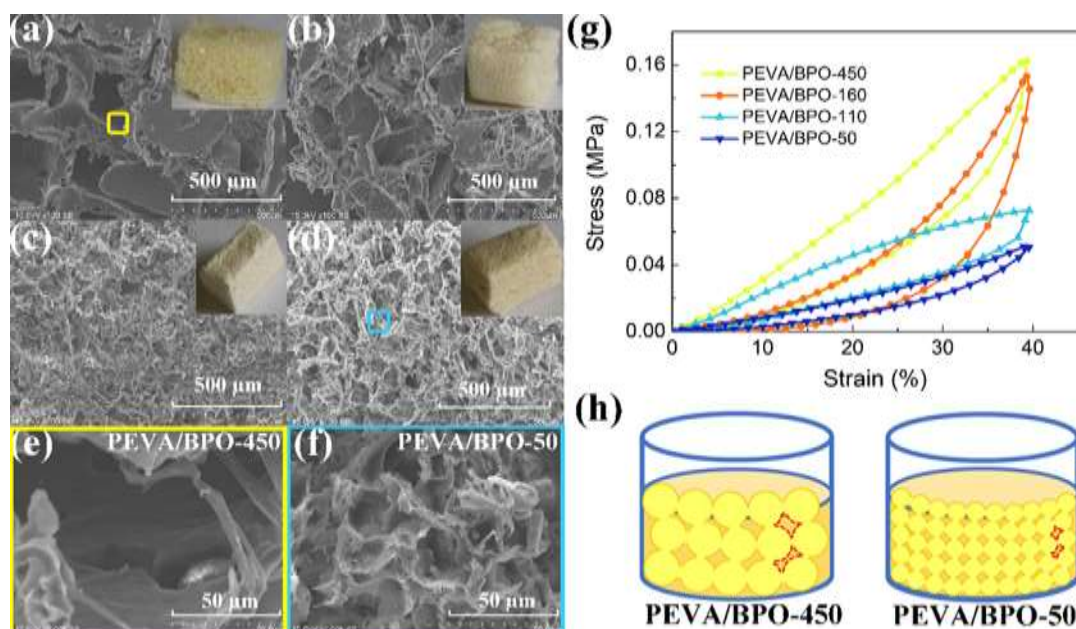
Figure 4.2 SEM photographs of PEVA/BPO foams with various pore sizes: a. PEVA/BPO-450; b. PEVA/BPO-160; c. PEVA/BPO-110; and d. PEVA/BPO-50. The enlarged SEM images are: e. PEVA/BPO-450; f. PEVA/BPO-50. g. compressive stress–strain curves for samples; and h. the formation of the pore wall area between different NaCl particle sizes.

The SEM images of the samples with different pore sizes exhibit an open porous structure with a high degree of pore interconnectivity (**Figure 4.2a–f**). The pore sizes will have a great influence on the two-way shape memory properties; therefore, it was necessary to study the 2W-SME of porous structures in the PEVA/BPO foams. The pore wall areas (red area in **Figure 4.2h**) between pores increased with the increase in the size of NaCl particles. The large pore wall areas can be formed with large pores (PEVA/BPO-450, **Figure 4.2a** and **h**). Each sample was deformed to 40% compressive strain then released at a rate of 560 μm/min, the compressive stress of four samples

were 0.16 MPa, 0.15 MPa, 0.07 MPa, and 0.05 MPa, respectively (**Figure 4.2g**). The PEVA/BPO-450 sample with large pore size exhibited the largest compression resistance, which is probably attributed to the fact that the large pore walls area provided enough space for thermo-crosslinking as a result of crosslinked networks restricting the mobility of the molecular structure. That is, greater crosslinking density led to increased Young's modulus.
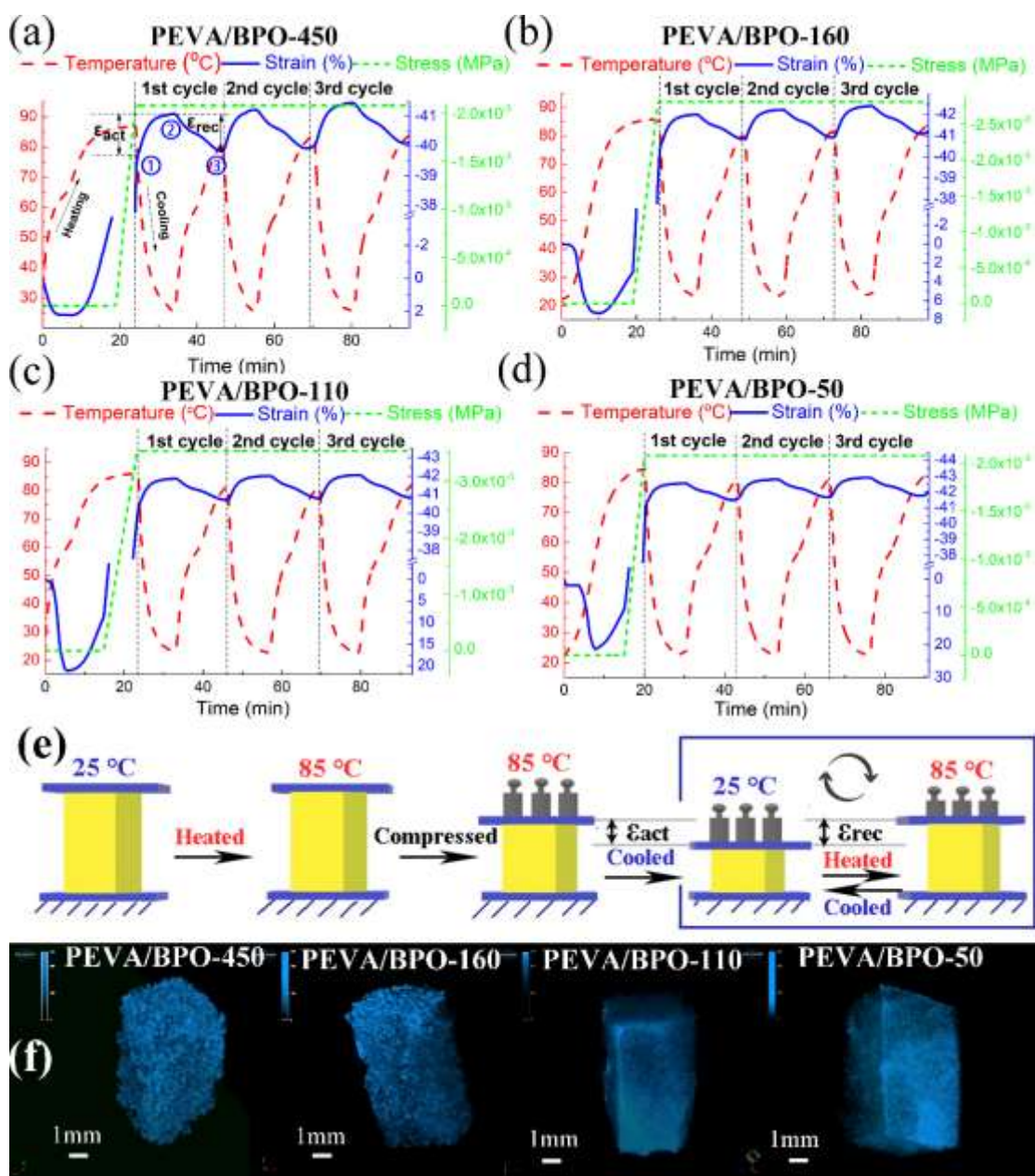
4.3.2 The two-way shape memory behavior and porous structure of PEVA/BPO foam

The sample with a 4–5 mm (diameter) was first heated from 25 °C to 85 °C above the crystalline melt temperature (T_m) at a rate of 2.5 °C/min, which represents the semi-crystalline transformed to amorphous in the foams, and compressed to a 40% compressive strain at a rate of 950 μm/min using a 3.5 mm-diameter compression probe. A constant stress was then maintained throughout the test. The temperature was cooled from high temperatures to 25 °C, and the samples were observed to contract along the compression direction because of the promotion of oriented crystal growth called as actuation strain (ε_{act}) as marked in **Figure 4.3a,** ①–②. The temperature was increased to 80 °C again at a rate of 4.5 °C/min under constant compression stress and the crystalline melt led to the sample expanding to the original shape, which was called recovery strain (ε_{rec}) as result of crosslinking in **Figure 4.3a**, ②–③. This cooling–heating process was repeated for three cycles. The mark of ① in the curve represents the prestretching at high temperatures, ② is the strain deformation at low temperatures,

and ③ is the strain deformation when the sample is reheated to 80 °C in every cycle.

The actuation strain (ε_{act}) and recovery ratio (R_{rec}) are important indicators explaining

the two-way shape memory performance (**Table 4.1**), where the recovery ratio (R_{rec})

which was defined by $R_{rec} = \varepsilon_{rec}/\varepsilon_{act} \times 100\%$.

Figure 4.3 Two-way shape memory behavior of samples with various pore size: a. PEVA/BPO-450; b. PEVA/BPO-160; c. PEVA/BPO-110; d. PEVA/BPO-50; e. two-way shape memory behavior of PEVA/BPO foam under constant compression; f. 3D X-ray μCT image of samples with different pore sizes.

Thermomechanical analysis confirmed the clear 2W-SME of the PEVA/BPO foam, which shows that the strain change during cooling and heating was affected by different porous structures (**Figure 4.3a–d, Table 4.1**). Under the same prestretching strain of 40%, we found that the large pore size sample (PEVA/BPO-450) showed an ideal two-way shape memory performance at the crosslinking temperature of 200 °C (**Table 4.1**). This was probably attributable to the fact that large pore wall areas with large pore sizes formed in the PEVA/BPO foam (**Figure 4.2h**), which provided enough area for crosslinking reactions. The crosslinking reaction restricts crystallization and the molecular chains within the network, which led to increased Young's modulus and restrained the plastic flow at high temperatures. **Figure 4.3 e** shows the two-way reversible shape memory process of PEVA/BPO foams. The pores were classified into four sizes, and the more-intuitive porous structures with different pore wall areas were observed in 3D microstructure images (**Figure 4.3f**).

Table 4.1. Two-way shape memory properties, density, and porosity of the PEVA/BPO foams

Sample	ε_{act} (%)			R_{rec} (%)			ρ (g/cm^3)	Porosity (%)	Pore size (μm)
	1st cycle	2nd cycle	3rd cycle	1st cycle	2nd cycle	3rd cycle			
PEVA/BPO-450	1.60	1.39	1.53	83.88	94.07	88.66	0.1434	84.74	160-450
PEVA/BPO-160	1.57	1.40	1.48	74.61	93.35	88.80	0.1529	83.73	110-160
PEVA/BPO-110	1.44	1.29	1.28	80.43	94.92	97.56	0.1775	81.12	50-110
PEVA/BPO-50	1.48	1.30	1.23	70.61	86.33	92.92	0.1865	80.16	0-50

4.4 Conclusion

Two-way reversible shape memory PEVA/BPO foams with different

interconnected pores were fabricated using a salt-leaching and thermo-crosslinking technology. The different reversible shape changes in various pore sizes of PEVA/BPO foams were investigated upon exposure at low/high temperatures under constant compression conditions. The samples with large pore size exhibited ideal two-way shape memory behavior under the same prestretching strain at the crosslinking temperature of 200 °C. The morphology of porous PEVA/BPO foams was also investigated. Future work is needed to improve the material's two-way shape memory actuation and recovery performance for practical applications of lightweight porous actuators in the artificial intelligence and smart bioengineering fields.

Reference

[1] Metcalfe. A, Desfaits. A. C, Salazkin. I, Yahia. L. H, Sokolowski. W. M, Raymond. J. Cold hibernated elastic memory foams for endovascular interventions. *Biomaterials*, 2003, *24(3)*, 491-497.

[2] De Nardo. L, Alberti. R, Cigada. A, Yahia. L. H, Tanzi. M. C, Farè. S. Shape memory polymer foams for cerebral aneurysm reparation: effects of plasma sterilization on physical properties and cytocompatibility. *Acta biomaterialia*, 2009, *5(5)*, 1508-1518.

[3] Li. G, Uppu. N. Shape memory polymer based self-healing syntactic foam: 3-D confined thermomechanical characterization. *Compo. Sci. Technolo*. 2010, *70(9)*, 1419-1427.

[4] Li. G, Nettles. D. Thermomechanical characterization of a shape memory polymer based self-repairing syntactic foam. *Polymer*, 2010, *51(3)*, 755-762.

[5] Van Meerbeek. I. M, Mac Murray. B. C, Kim. J. W, Robinson. S. S, Zou. P. X, Silberstein. M. N, Shepherd. R. F. Morphing Metal and Elastomer Bicontinuous Foams for Reversible Stiffness, Shape Memory, and Self-Healing Soft Machines. *Adv. Mater*. 2016, *28(14)*, 2801-2806.

[6] Hasan. S. M, Nash. L. D, Maitland. D. J. Porous shape memory polymers: Design and applications. *J. Polym. Sci. Pol. Phys*. 2016, *54(14)*, 1300-1318.

[7] Fabrizio. Q, Loredana. S, Anna. S. E. Shape memory epoxy foams for space applications. *Mater. Lett*. 2012, *69*, 20-23.

[8] Singhal. P, Rodriguez. J. N, Small. W, Eagleston. S, Van de Water. J, Maitland. D.

J, Wilson. T. S. Ultra low density and highly crosslinked biocompatible shape memory polyurethane foams. *J. Polym. Sci. Pol. Phys.* 2012, *50(10)*, 724-737.

[9] Kim. H. J, Park. I. K, Kim. J. H, Cho. C. S, Kim. M. S. Gas foaming fabrication of porous biphasic calcium phosphate for bone regeneration. *Tissue. Eng. Regen. Med.* 2012, *9(2)*, 63-68.

[10] Parks. K. L, Beckman. E. J. Generation of microcellular polyurethane foams via polymerization in carbon dioxide. II: Foam formation and characterization. *Polym. Eng. Sci.* 1996, *36(19)*, 2417-2431.

[11] Di Maio. E, Mensitieri. G, Iannace. S, Nicolais. L, Li. W, Flumerfelt. R. W. Structure optimization of polycaprolactone foams by using mixtures of CO2 and N2 as blowing agents. *Polym. Eng. Sci.* 2005, *45(3)*, 432-441.

[12] Gaillard. C, Despois. J. F, Mortensen. A. Processing of NaCl powders of controlled size and shape for the microstructural tailoring of aluminium foams. *Mater. Sci. Eng. A*, 2004, *374(1-2)*, 250-262.

[13] El-Kady. A. M, Rizk. R. A, El-Hady. B. M. A, Shafaa. M. W, Ahmed. M. M. Characterization, and antibacterial properties of novel silver releasing nanocomposite scaffolds fabricated by the gas foaming/salt-leaching technique. *JGEB*, 2012, *10(2)*, 229-238.

[14] Okamoto. M, John. B. Synthetic biopolymer nanocomposites for tissue engineering scaffolds. *Prog. Polym. Sci.* 2013, *38(10-11)*, 1487-1503.

[15] Janik. H, Marzec. M. A review: Fabrication of porous polyurethane scaffolds. *Mater. Sci. Eng. C.* 2015, *48*, 586-591.

[16] Okamoto. M, John. B. Synthetic biopolymer nanocomposites for tissue engineering scaffolds. *Prog. Polym. Sci.* 2013, *38(10-11)*, 1487-1503.

[17] Tseng. L. F, Mather. P. T, Henderson. J. H. A programmable shape-changing scaffold for regenerative medicine. In *2012 38th Annual Northeast Bioengineering Conference (NEBEC)* (pp. 227-228), 2012, IEEE.

[18] Nam. Y. S, Yoon. J. J, Park. T. G. A novel fabrication method of macroporous biodegradable polymer scaffolds using gas foaming salt as a porogen additive. *Journal of Biomedical Materials Research: An Official FFB, JSB, and The Australian Society for Biomaterials and the Korean Society for Biomaterials*, 2000, *53(1)*, 1-7.

[19] Lo. H, Kadiyala. S, Guggino. S. E, Leong. K. W. Poly (L-lactic acid) foams with cell seeding and controlled-release capacity. *J. Biomed. Mater. Res.* 1996, *30(4)*, 475-484.

[20] Livshin. S, Silverstein. M. S. Crystallinity in cross-linked porous polymers from high internal phase emulsions. *Macromolecules*, 2007, *40(17)*, 6349-6354.

[21] Lissant. K, editor. Emulsions and emulsion technology. CRC Press, 1974.

[22] Bartl. V. H, Von Bonin W. Über die Polymerisation in umgekehrter Emulsion. Macromol. Chem. Phys. 1962, *57(1)*, 74-95.

[23] Cameron. N. R. High internal phase emulsion templating as a route to well-defined porous polymers. *Polymer*, 2005, *46(5)*, 1439-1449.

[24] Kimmins. S. D, Cameron. N. R. Functional porous polymers by emulsion templating: recent advances. *Adv. Funct. Mater.* 2011, *21(2)*, 211-225.

[25] Zhang. H, Cooper. A. I. Synthesis and applications of emulsion-templated porous materials. *Soft Matter*. 2005, *1(2)*, 107-113.

[26] Quadrini. F, Santo. L, Squeo. E. A. Solid-state foaming of nano–clay-filled thermoset foams with shape memory properties. *Polym-Plast Technol Eng*. 2012, *51(6)*, 560-567.

[27] Kumar. V, Weller. J. E. A process to produce microcellular PVC. *Int. Polym. Proc*. 1993, *8(1)*, 73-80.

[28] Kumar. V, Weller. J. Production of microcellular polycarbonate using carbon dioxide for bubble nucleation. *J. Eng. Ind*. 1994, *116(4)*, 413-420.

[29] Chow. T. S. Molecular interpretation of the glass transition temperature of polymer-diluent systems. *Macromolecules*, 1980, *13(2)*, 362-364.

[30] Hearon. K, Singhal. P, Horn. J, Small IV. W, Olsovsky. C, Maitland. K. C, Maitland. D. J. Porous shape-memory polymers. *Polym Rev*. 2013, *53(1)*, 41-75.

[31] Chung. S. E, Park. C. H. The thermoresponsive shape memory characteristics of polyurethane foam. *J. Appl. Poly. Sci*. 2010, *117(4)*, 2265-2271.

[32] Zhang. D, Petersen. K. M, Grunlan. M. A. Inorganic–organic shape memory polymer (SMP) foams with highly tunable properties. *ACS Appl. Mater. Interfaces*. 2012, *5(1)*, 186-191.

[33] Squeo.E. A, Quadrini. F. Shape memory epoxy foams by solid-state foaming. *Smart Mater. Struct*. 2010, *19(10)*, 105002.

[34] Santo. L, Quadrini. F, Squeo. E. A, Dolce. F, Mascetti. G, Bertolotto. D, Zolesi. V. Behavior of shape memory epoxy foams in microgravity: experimental results of

STS-134 mission. *Microgravity Sci. Tec.* 2012, *24(4)*, 287-296.

[35] Santo. L. Shape memory polymer foams. Prog. Aerosp. Sci. 2016 ,Feb 1;81:60-5.

[36] Baker. R. M, Henderson. J. H, Mather. P. T. Shape memory poly (ε-caprolactone)-co-poly (ethylene glycol) foams with body temperature triggering and two-way actuation. *J. Mater. Chem. B*. 2013, *1(38)*, 4916-4920.

[37] Zharinova. E, Heuchel. M, Weigel. T, Gerber. D, Kratz. K, Lendlein. A. Water-blown polyurethane foams showing a reversible shape-memory effect. *Polymers*, 2016, *8(12)*, 412.

Chapter 5

Conclusions

5 Conclusions

This dissertation has synthesized and investigated the two-way reversible shape memory polymers using thermal crosslinking reaction which exhibits the full two-way shape memory reversibility following exposure to external stimuli of temperature. The finding in this study in this study is expected to have a contribution to their application as soft material actuators and artificial muscles in various fields.

In chapter 1, general introduction of shape memory polymers (SMPs), two-way shape memory polymers (2W-SMPs) and shape memory polymer foams were introduced in three sections which indicated shape memory type, structures, synthesis and their applications.

In chapter 2, we synthesized two-way (reversible) chemically crosslinked semi-crystalline shape memory PEVA/BPO polymers with various crosslinking densities from poly(ethylene-co-vinyl acetate) (PEVA) with various contents of benzoyl peroxide (BPO) by thermally crosslinking reaction via micro twin-screw extruder and hot-pressing machine. PEVA containing various contents of BPO —i.e., 0wt% to 14wt%, indicated by PEVA-B0 to PEVA-B14 were prepared. The network properties and the two-way shape memory behavior of PEVA/BPO samples were determined by the gel content. The gel content increased markedly from 69.77% to 91.25% with the increment of the BPO content from 1 wt% to 4 wt%, whereas it increased slowly from 91.25% to 95.82% as the BPO content increased from 4 wt% to 12 wt%. The developed materials were capable of reversible shape change, and the "switch on" temperature triggering shape change within a reasonable range. The recovery ratio (R_{rec}) increased markedly

as the BPO content increased from 4 wt% to 10 wt%. The PEVA-B10 (PEVA with 10 wt% BPO) sample had optimal actuation performance and an excellent recovery ratio of over 99%. The non-crosslinked sample (PEVA-B0) did not recover during the heating, and did not exhibit two-way shape memory behavior. PEVA-B1 demonstrated weak two-way shape memory behavior and did not exhibit good thermomechanical recyclability. These results indicate that the crosslinking using BPO plays an important role in ensuring samples return to their original shape, and the PEVA/BPO compositions with high crosslinking densities had significantly elevated recovery ratios. As a result, the developed PEVA/BPO materials were adequately soft and had good mechanical properties, even at large deformation.

In chapter 3, the two-way shape memory effect (2W-SME) of PEVA/BPO has been achieved under both constant stress and stress-free conditions. We found that the relationship between the initial prestretching strain ($R_{prestretch}$) and recovery strain (R_{rec}) was the main reason for achievement of the stress-free 2W-SME of PEVA/BPO polymers. Furthermore, three different types of stress-free two-way shape memory behavior were observed during the TMA cycles: the ideal stress-free 2W-SME ($R_{rec} = R_{prestretch}$), the weak stress-free 2W-SME ($R_{rec} > R_{prestretch}$), and no stress-free 2W-SME ($R_{rec} < R_{prestretch}$), which can be controlled by varying R_{rec} using different T_{set} during the recovery process. More importantly, the two-way shape memory driving force and recovery force, as the one of key indicators for two-way shape memory materials, was investigated, and it significantly changed depending on the BPO content. An ideal two-way shape memory driving and recovery force was observed for PEVA-B10. The

sample with a high BPO content showed excellent high-temperature creep resistant performance. A highly crosslinked structure can suppress viscous flow and provides sufficient force to allow the sample to recover its initial shape after crystal melting. Therefore, the PEVA/BPO samples were able to contract during heating. 2D-WAXS and DSC tests indicated that the crystalline structure led to oriented growth of crystals under applied stress, and crystallization led to elongation upon cooling.

In chapter 4, a porous PEVA/BPO foam with 2W-SME was innovated. PEVA/BPO mixture was prepared using solution method, and then samples were foamed via a salt-leaching and thermo-crosslinked technology. The salt-leaching technology resulted in the formation of pores between the pore walls in the PEVA/BPO foam. This technology has the advantages of easy process and control of the porous structure, and the foaming process does not include any chemical blowing agents. Various pore sizes of PEVA/BPO porous foam were obtained using different NaCl particle sizes. The two-way shape memory properties of PEVA-BPO foam were investigated using the thermomechanical analysis (TMA). The PEVA/BPO foams with various pore sizes exhibited reversible shape changes that allowed contraction during cooling and expansion during heating. The ideal two-way shape memory performance can be clearly observed in the large pore size sample PEVA/BPO-450. The morphology was characterized by scanning electron micron microscopy (SEM) and X-ray micro-computed tomography scanning (μCT) analysis. The compression behavior of PEVA/BPO foam was also investigated. This finding of the two-way shape memory PEVA/BPO foams may contribute to their applications as lightweight actuators in

artificial intelligence, artificial filed and smart bioengineering.

As a total conclusion, a novel two-way PEVA/BPO shape memory polymers using thermal crosslinking reaction were successfully developed. BPO as a common crosslinker can endow the two-way shape memory PEVA/BPO polymers with the ability of actuation and shape recovery. The high crosslinking density sample with high content of BPO had optimal actuation performance and excellent shape recovery ratio. PEVA and BPO are both non-toxic and suitable for application in human body. The two-way PEVA/BPO shape memory polymers, which show the full reversibility in heating and cooling, will provide multiple options for practical applications, such as soft actuators, sensors, and artificial intelligence applications.

Accomplishments

List of publications

Journal of publications

[1] **Jin Hui**, Hong Xia, Hairong Chen, Yiping Qiu, Yaqin Fu, Qing-Qing Ni. Two-way reversible shape memory polymer: synthesis and characterization of benzoyl peroxide-crosslinked poly (ethylene-co-vinyl acetate). *Materials Letters* (2019), doi: https://doi.org/10.1016/j.matlet.2019.126762. (Accepted 30 September 2019).

[2] **Jin Hui**, Hong Xia, Yaqin Fu, Yiping Qiu, Qing-Qing Ni. Two-way reversible shape memory properties of benzoyl peroxide crosslinked poly(ethylene-co-vinyl acetate) under different stress conditions. *Macromolecular materials and Engineering* (2020), doi: https://doi.org/10.1002/mame.201900825. (Accepted 21 February 2020)

[3] **Jin Hui**, Hong Xia, Yaqin Fu, Yiping Qiu, Qing-Qing Ni. Benzoyl peroxide thermo-crosslinked poly (ethylene-co-vinyl acetate) foam with two-way shape memory effect. *Materials Letters* (2020), https://doi.org/10.1016/j.matlet.2020.127343. (Accepted 10 January 2020).

International Conference

[1] **<u>Jin Hui</u>**, Qing-Qing Ni. Two-way reversible shape memory polymer: synthesis and characterization of benzoyl peroxide crosslinked poly(ethylene-co-vinyl acetate). 2019 International Workshop on Materials and Design (MatDes 2019), Oxford, United Kingdom, March 29-April 1, 2019. (Oral presentation).

[2] **<u>Jin Hui</u>**, Qing-Qing Ni. Two-way reversible shape memory polymer: synthesis and characterization of benzoyl peroxide crosslinked poly(ethylene-co-vinyl acetate). The Composites and Advanced Materials Expo 2019 (CAMX 2019), Anaheim, California, USA, September 23-26, 2019. (Poster presentation).

Domestic Conference

[1] **<u>Jin Hui</u>**, Qing-Qing Ni. Development and Application of Two-way reversible shape memory polymer: Benzoyl peroxide crosslinked poly(ethylene-co-vinyl acetate). SYMPOSIUM OF ADVANCED COMPOSITES (SAC) 2019, Sapporo, Hokkaido, Japan, October 18-22, 2019. (Poster presentation).

Acknowledgements

It would not have been possible to write this doctoral thesis without the help and support of the many kind people around me during my PhD study at Shinshu University.

Above all, I would like to thanks to my parents, for their love, financial support and encouragement throughout these four years. Without their support, it was hard for me to go through many tough times to getting PhD degree in Japan. I am so grateful to them.

Thank you to my supervisor, Prof. Qing-Qing Ni, for providing guidance and feedback throughout this research.

I am deeply grateful to the China Scholarship Council (CSC) to give me three years financial support, allows me don't worry about making a living so I can more concentrate to do my research.

My gratitude also goes to Shinshu University for providing me good experimental facility and peaceful campus environment. Special thanks to international fiber engineering course and Prof. Masuhiro Tsukada, for giving me English proofreading support and offering me a lot of opportunities to attend the international conference, allows me to broaden my views and helps to improve my research.

I would like to extend my gratitude to several more people for their support for this research, especially to thank Mr. Yusuke Okada, Ms. Ayako Nishida, Ms. Sachiko Yoshioka, Mr. Masaaki Takeda, Ms. Mariko Usami, for valuable technical advice, helps for solving research problems and offer experimental equipment's support.

Special thanks are given to Prof. Yiping Qiu and Prof. Lan Yao at Donghua

University, for many invaluable advices, encouragement and guiding my way through this unpredictable PhD journey.

I have to thank all my colleagues in research group for the willing help and giving me nice advices, which have contributed to the improvement of the thesis.

During the period of four years, I would like to thank my friends for always listening and giving me words of encouragement, thanks for their faith in me, thanks to be there.

I want to thanks to everyone who have been taking care of me during my PhD period in Japan.

July, 2020

Ueda, Japan